

# POLITECNICO DI TORINO

MECHANICAL ENGINEERING (Master's Degree)



*Design and behavior of a 3D-printed QZS (quasi zero stiffness)  
vibration isolator*

*Tutor:*

**Prof. ANASTASIO DARIO**

*Student:*

**Cheng Peihong**

*Co-tutor:*

**Prof. DAGA ALESSANDRO PAOLO**

---

# Abstract

Engineering applications have conventionally aimed to avoid phenomena related to mechanical instabilities or buckling, as they can bring undesired nonlinear effects or even failure. In recent years however the research in this field has experienced an inversion of direction making use of such phenomena to improve the performance of solids and structures. In this context, the adoption of pre-compressed slender beam elements is one of the most common solutions. A typical application is the development of quasi-zero stiffness (QZS) vibration isolators, that bring a high static stiffness and an extremely low dynamic stiffness.

Generally, the QZS characteristics can be obtained by coupling a negative stiffness effect with a positive one. When considering beam elements, the application of a compressive axial force can lead to a mechanical instability and to a negative stiffness region in the force-displacement characteristics.

This thesis studies the quasi-static behavior of such elements by comparing experimental measurements with a mathematical model (base on the force analysis). To this end, a 3D-printed V-shaped structure is considered, comprising two pre-compressed beam elements and a controllable pre-load. The regulation of the pre-load allows the V-structure to undergo tensile or compressive forces, thus altering its characteristics. In particular, the restoring force of the system can show regions of negative or quasi-zero stiffness when compressive forces are applied.

# **Acknowledgments**

This project was completed under the continuous guidance of my tutor Prof. ANASTASIO DARIO and Prof. DAGA ALESSANDRO PAOLO. From the beginning to the end of the project, both transferred me patient guidance and careful care permitting me to not lose my direction and motivation rather finding scientific attitude and rigorous scientific spirit.

Thank you for giving me such a unique opportunity!

# Contents

<b>1 INTRODUCTION</b>	<b>6</b>
1.1 THE DEVELOPMENT AND DILEMMA OF QZS VIBRATION ISOLATOR	6
1.2 SIMPLE QZS AND NEGATIVE STIFFNESS STRUCTURE	7
1.2.1 prestressed spring structure	7
1.2.2 prestressed beam structure	9
1.2.3 curved beam structure	10
1.2.4 curved shell structure	10
1.3 FLEXURE HINGES	12
1.4 SIMULATION OF STRUCTURE	15
1.4.1 using solidworks simulation	15
1.4.2 using ansys simulation	17
1.4.2 simulation comparison	20
<b>2 DESIGN MODEL OF THE STRUCTURE</b>	<b>24</b>
2.1 SINGLE V-SHAPE BEAM	24
2.1.1 determine geometric parameters	24
2.1.2 structure simulation result comparison	25
2.1.3 estimation of the negative stiffness range	34
2.2 DOUBLE V-SHAPE BEAM	36
2.2.1 determine geometric parameters	36
2.2.2 structure simulation result comparison	37
2.2.3 problem of double v-shape beam	40
<b>3 ANALYTICAL MODEL OF THE V-SHAPE BEAM</b>	<b>42</b>

---

3.1 CLASSICAL OBLIQUE SPRING MODEL .....	42
3.2 V-SHAPE BEAM FORCE ANALYSIS .....	45
3.2.1 force analysis.....	45
3.2.2 consideration on the torsional stiffness $K_t$ (flexure hinges).....	49
3.2.3 compression process simulation.....	49
3.2.4 displacement process simulation.....	56
<b>4 EXPERIMENT .....</b>	<b>84</b>
4.1 DESIGN THE EXPERIMENT MODEL .....	84
4.2 3D-PRINTING PROCESS .....	91
4.2.1 3d-printing for v-shape beam .....	91
4.2.2 3d-printing for support part .....	95
4.3 MEASUREMENT .....	97
<b>5 RESULTS AND DISCUSSION .....</b>	<b>100</b>
5.1 FORCE DEFLECTION RESULT COMPARISON .....	100
5.2 NEGATIVE STIFFNESS COMPARISON .....	105
<b>6 CONCLUSION.....</b>	<b>110</b>
<b>7 REFERENCES.....</b>	<b>111</b>

---

# 1 Introduction

## 1.1 The development and dilemma of QZS vibration isolator

In engineering systems, vibration isolators are frequently employed to isolate important items from external vibration stimulation. In ideal case of vibration isolators (a mass  $m$  connect by a spring  $k$  on a rigid support), isolation will not occur until a frequency of  $\sqrt{2k/m}$  ([1]). Thus, a low natural frequency is preferred for the vibration isolators in order to ensure efficient isolation. This kind of low natural frequency vibration isolator also known as a quasi-zero stiffness (QZS) isolator.

The quasi-zero stiffness (QZS) effect can be generally achieved by combining negative stiffness and positive stiffness ([1], [2], [7]), by a combination of mechanical components like springs or beam. The most common way is to combine oblique springs in order to generate a region of low static stiffness or even quasi-zero stiffness ([1], [9]). In addition to the oblique spring component, prestressed or buckled beams can also be used to achieve negative stiffness.

Prior studies ([1], [2]) on the QZS isolator have mostly concentrated on the large-scale individual structure required to support a car seat or shield the engine from outside disturbances. In contrast, the development of miniaturized and small-scaled QZS mechanisms remains a challenging topic. As a result, a structure or material that possesses QZS capabilities and is the same size as precision instruments or microdevices will be well suited for vibration isolation as a coating or supporting component. Metamaterials and meta-structures have been suggested and achieved in the field of energy absorption and vibration isolation in recent years due to the rapid development of 3D printing technology ([9]). The theory to achieve energy absorption for metamaterials and meta-structures is considered to be the negative stiffness acquired from unit cell via buckling or snap-through. The meta-structures will have the requisite shock protection or energy absorption performance by properly connecting the unit cells with negative stiffness properties in series ([4], [9]). As curved and inclined beams are simple to construct using 3D printing technology, they are now the major emphasis in cell configuration design ([4], [9]). It provides a new idea for the investigation of structures utilized for vibration isolation in micromachinery.

The purpose of this work is to investigate the static and dynamic properties of a V-shaped beam arrangement using FE modeling techniques and experimental measurements. First, a simplified analytical model of the V-shape beam is established to determine its geometric parameters. The possibility of adopting flexure hinges to optimize the curved beam is also discussed in this first part. FE analyses are then conducted to assess the behavior of the device with different configurations, and the results are compared with the predictions of the analytical models. Once a final design is selected, the V-shape beam mechanism is 3D-printed by fused deposition modeling (FDM) on a UltiMaker 3 out of generic polylactic acid (PLA) with custom setting. Isotropic material properties are assumed based on FDM printed PLA with a layer raster angle of  $0^\circ$ . A Young's modulus of  $3.12 \text{ GPa}$  and an ultimate tensile stress of  $50.23 \text{ MPa}$  are used with Poisson's ratio of 0.3 ([7]). Eventually, experimental measurements are conducted to analyze the real behavior of the prototype.

## 1.2 Simple QZS and negative stiffness structure

### 1.2.1 Prestressed spring structure

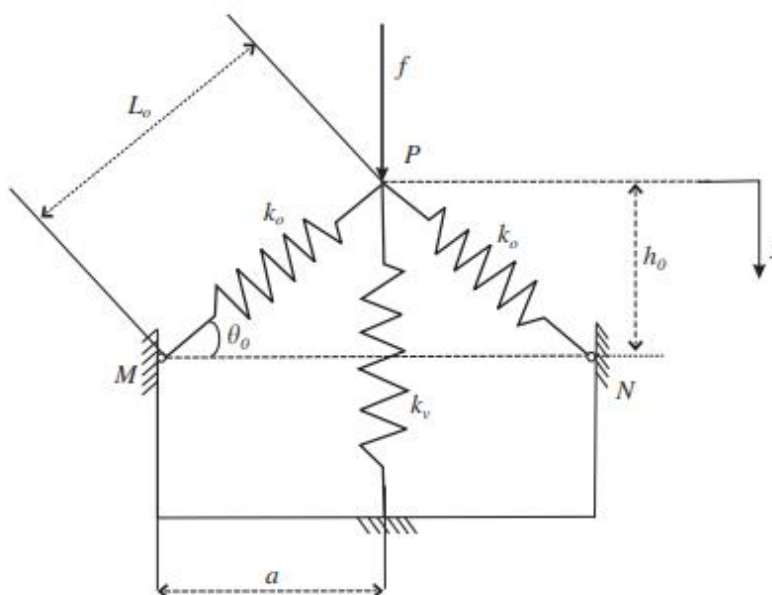


Fig1.2.1.1 Schematic representation of the simplest QZS system [1]

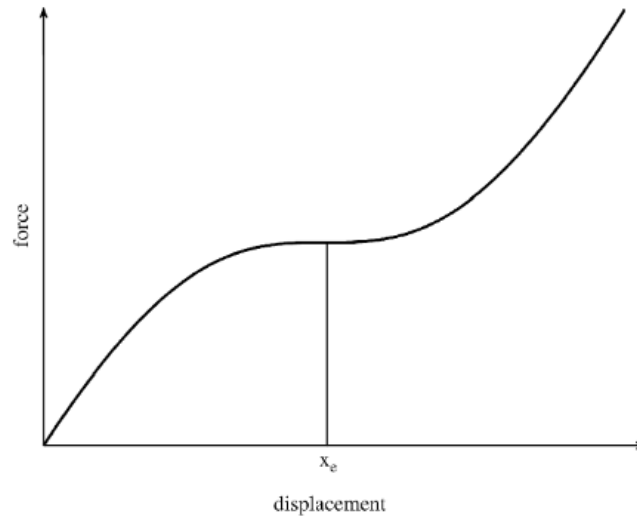


Fig1.2.1.2 Typical force-displacement characteristic of the simplest QZS system [1]

The simplest quasi-zero stiffness structure is shown in Fig1.2.1.1 [1]. The system is designed so that the spring contract when the system is loaded with a mass ( $m$ ), causing the vertical spring ( $k_v$ ), to bear the static load and the oblique springs ( $k_o$ ), to be in the horizontal position. This is the state of static equilibrium, and the movement around this state is what is most important. When the spring system is employed in this way, the negative stiffness of the oblique springs in the vertical direction balances the positive stiffness of the vertical spring. Properly design the vertical and horizontal spring is critical ([1]), the spring exhibit linear behavior when the vertical displacement in a certain range (Fig 1.2.1.2).

## 1.2.2 Prestressed beam structure

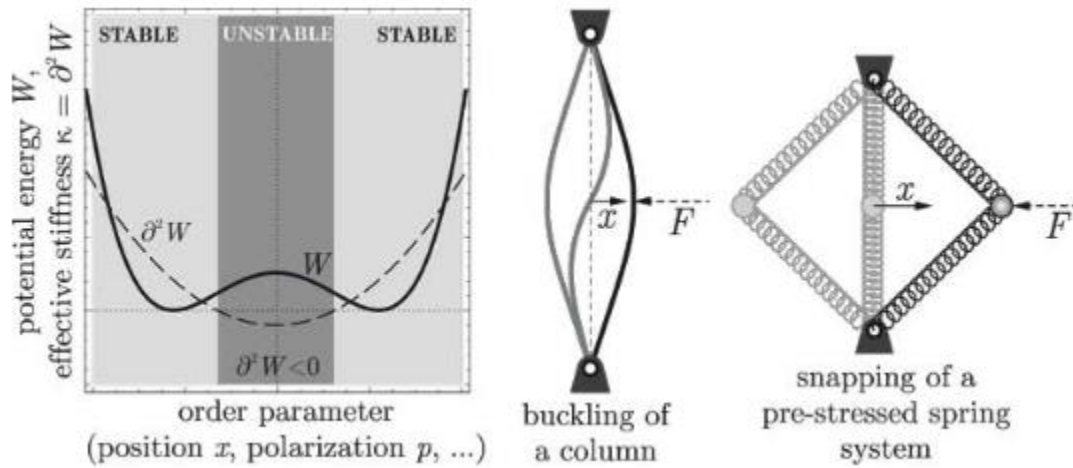


Fig 1.2.2.1 Example systems showing instabilities that correspond to local energy maxima, including prestressed buckled beams and springs [2]

The beam buckling can be considered as equivalent of the previously discussed oblique springs model, by implementing compression of the beam, the structure becomes bistable (Fig 1.2.2.1 [2]) along the displacement direction  $x$ . Moving the middle or one end of the beam (along the direction  $x$ ), the behavior of system is the same as the oblique springs model in a certain range of compression. In order to achieve negative stiffness, the preloading (compression) of the beam is compulsory.

### 1.2.3 Curved beam structure

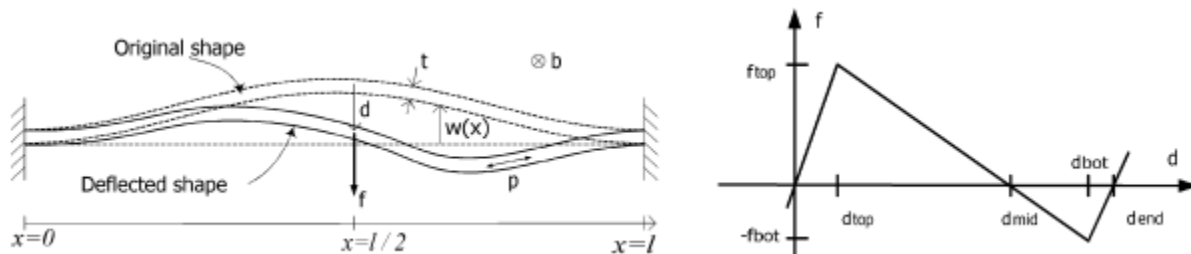


Fig 1.2.3.1 Geometry and force-displacement characteristic for curved beam deflection analysis [3]

Prof. Jin introduces a monolithic mechanically-bistable mechanism that does not rely on residual stress for its bistability ([3]). Two curved centrally clamped parallel beams, referred as "double curved beams," are a common implementation of this mechanism. The mechanism exhibits the negative stiffness between  $d_{top}$  to  $d_{bot}$  (Fig 1.2.3.1 [3]) without prestress.

### 1.2.4 Curved shell structure

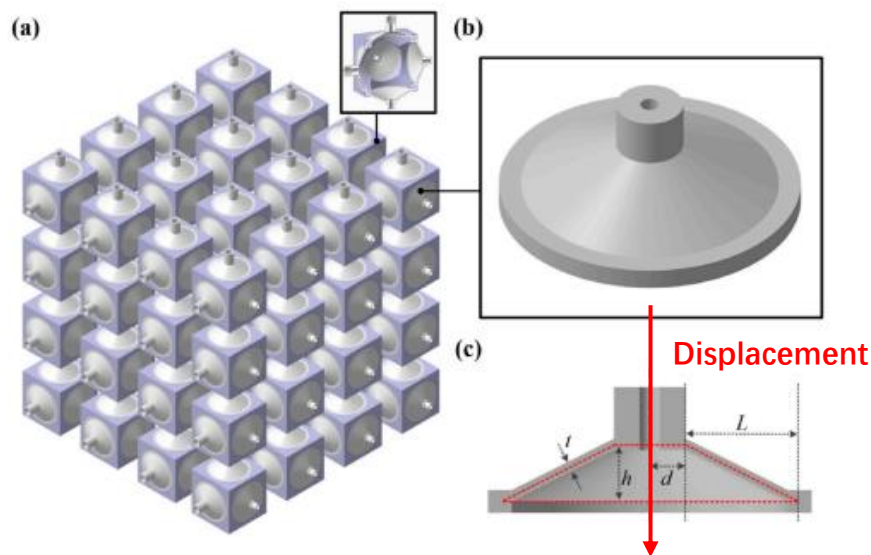


Fig 1.2.3.3 Schematic diagram of tri-directional NS mechanical metamaterial and section view of its unit cell [4]

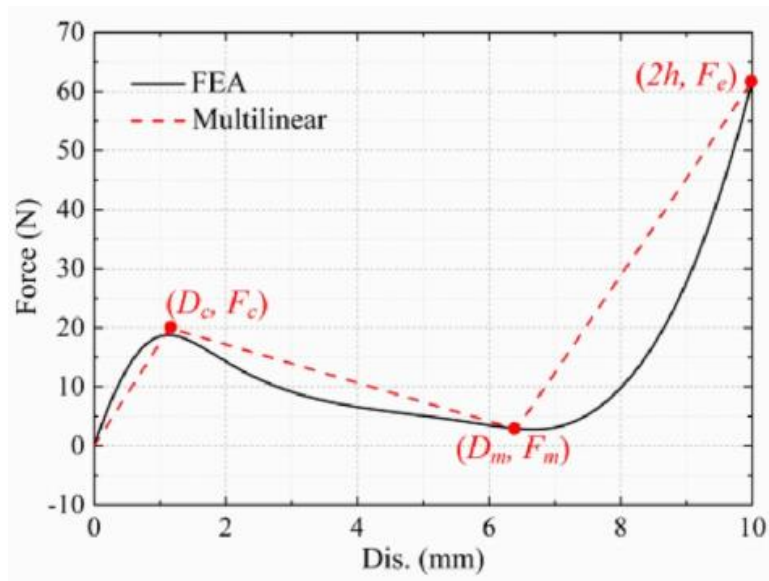


Fig 1.2.3.4 force-displacement characteristic of unit cell [4]

Prof. TAN have introduced a new type of truncated-conical shell systems ([4]), it has similar property as sinusoidal curved beam (Fig 1.2.3.4 [4]). Multiple shell element can be assembled together to compose one large part (Fig 1.2.3.3 [4]). By better arranging the meta-structure, the entire component can achieve the negative stiffness in multiple directions. Although this structure has many advantages, sufficient displacement ( $d_{bot} \geq x \geq d_{top}$  [3] or  $D_m \geq x \geq D_c$  [4]) must be applied in order to achieve the negative stiffness region. This is challenging for the material, and it also limit the useful working condition.

## 1.3 Flexure hinges

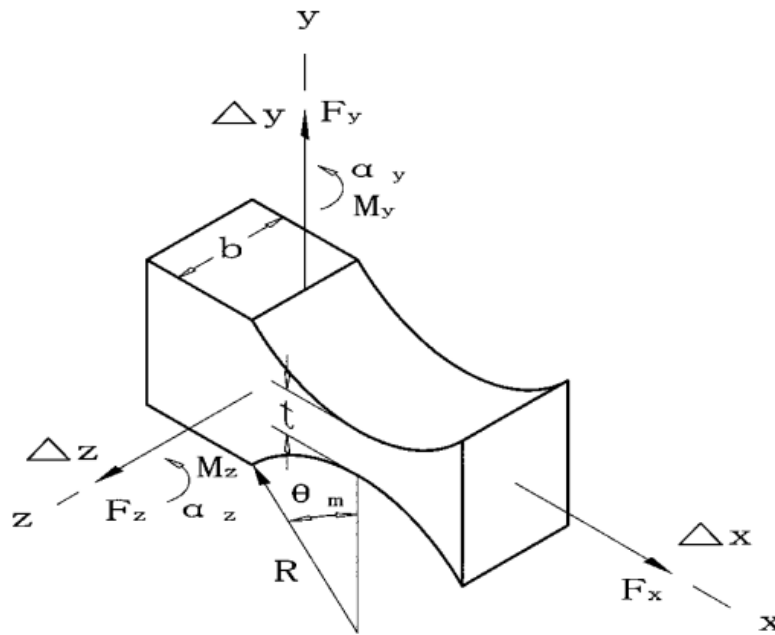


Fig 1.3.1 Hinge dimensions and various forces and moments which cause deflections [5]

A flexure hinge consists of a flexible, slender region between two adjacent rigid parts that undergo relative limited rotation in a mechanism and is the important constituent of lumped compliant mechanisms ([10]). In 1965, Prof.J.M.Paros and L.Weisbord discovered the mathematic model to estimate the flexure hinges which have been widely used in applications such as gyroscopes, accelerometers, balance scales ([5]). Base on reference [5], the stiffness of flexure hinges characterized by elastic modulus of material ( $E$ ), and by following geometrical properties (Fig 1.3.1): thickness ( $b$ ), height ( $h$ ), length ( $l$ ), mid-thickness ( $s$ ), and radius ( $R$ ). It reads:

$$\alpha_z / M_z \approx 9\pi R^{0.5} / 2Ebt^{2.5} \quad (\text{Eq 1.3.1 [5]})$$

This equation only properly works when  $t/2R \ll 1$  and  $t \ll h$  ([5]).

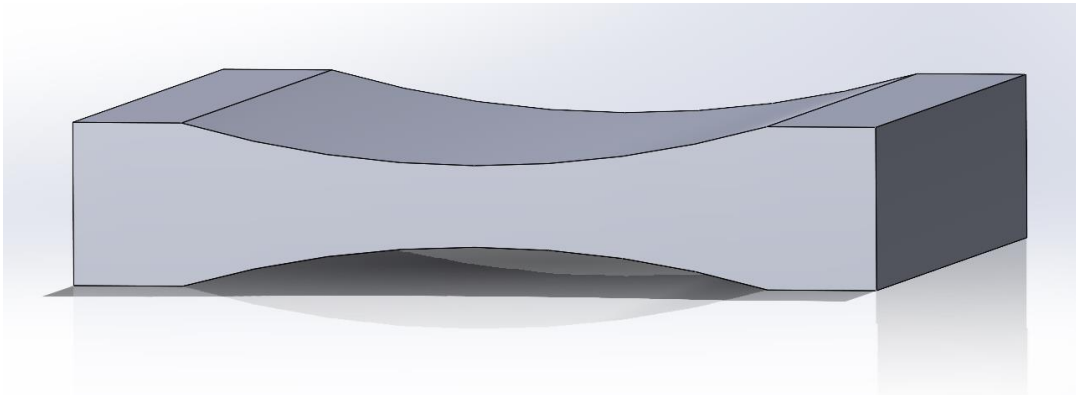


Fig 1.3.2 Flexure hinges CAD model (SolidWorks)

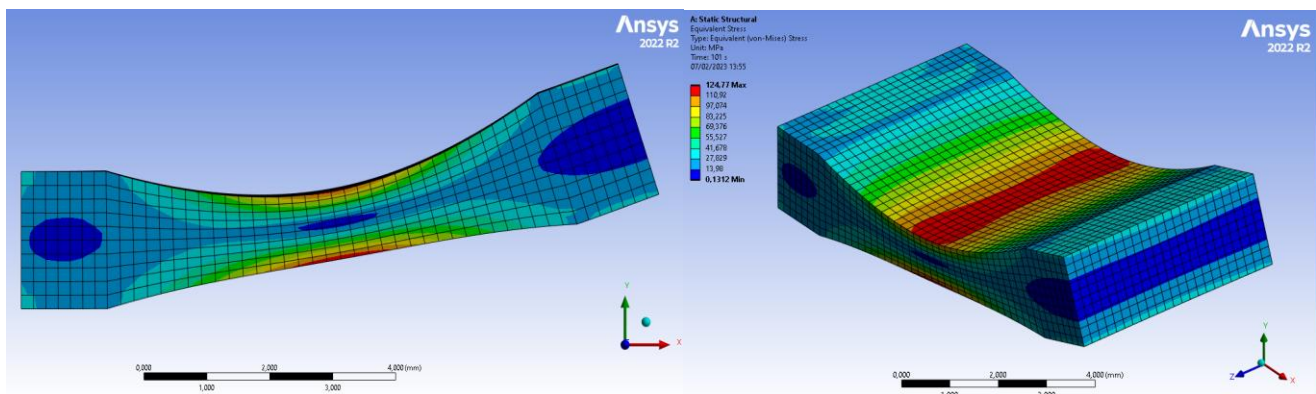


Fig 1.3.3 Flexure hinges FE simulation (Ansys)

Fig 1.3.2 show the flexure hinges with  $t = 1 \text{ mm}$ ,  $h = 2 \text{ mm}$ ,  $R = 13.528 \text{ mm}$ ,  $b = 5 \text{ mm}$ , by using the Eq 1.3.1 [5], the torsional stiffness can be computed as  $K_t = M_z / \alpha_z = 300 \text{ Nmm/rad}$ . Compare the Ansys show the FEM result (Fig 1.3.3; Fig 1.3.4) with Paros-Wesibord model ( $K_t = 300 \text{ Nmm/rad}$ ), there is a certain error appear. Although the error of the simplified equation (Eq 1.3.1) relative to the Ansys simulation result within 1~15% for  $t/R = 0.074$  and the error can be significantly increase by setting higher  $t/R$  value [6], but the effect on the final result is negligible, it will be further discussed in next chapter.

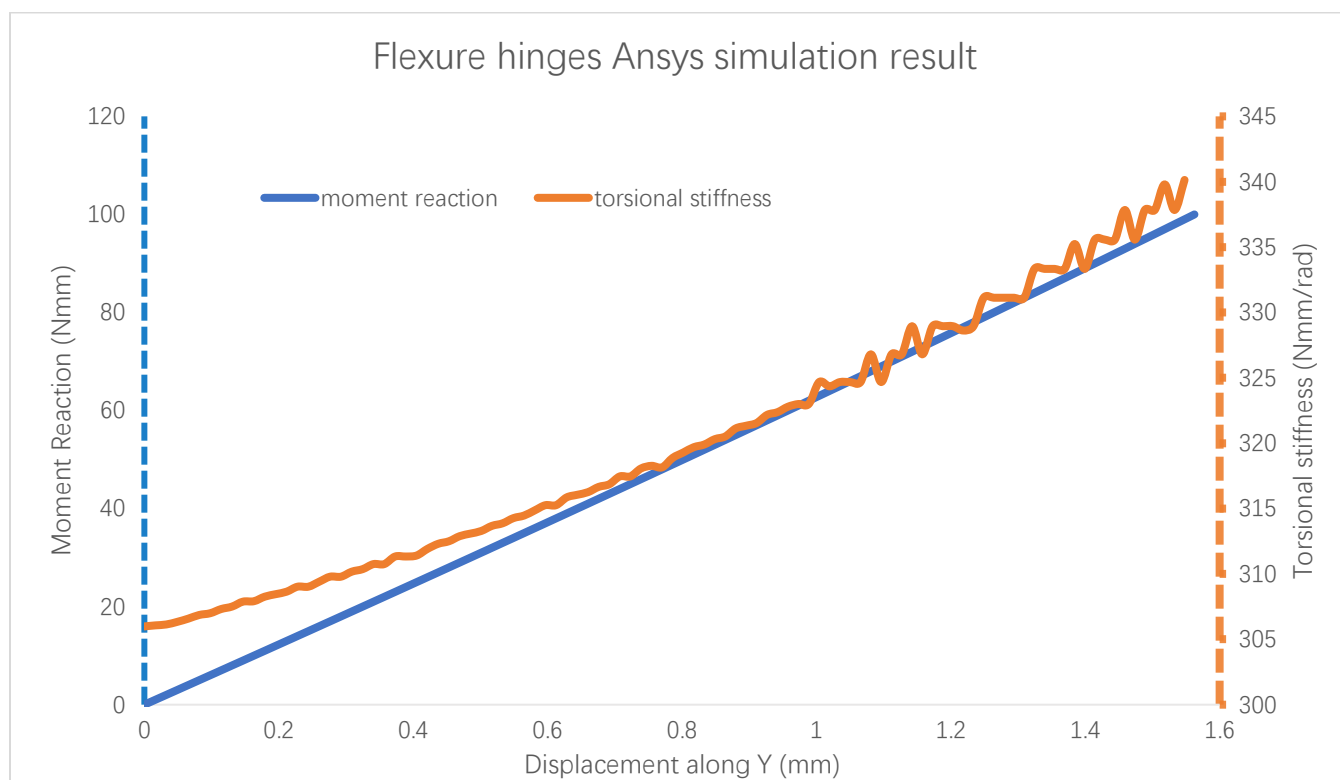


Fig 1.3.4 Moment reaction and torsional stiffness

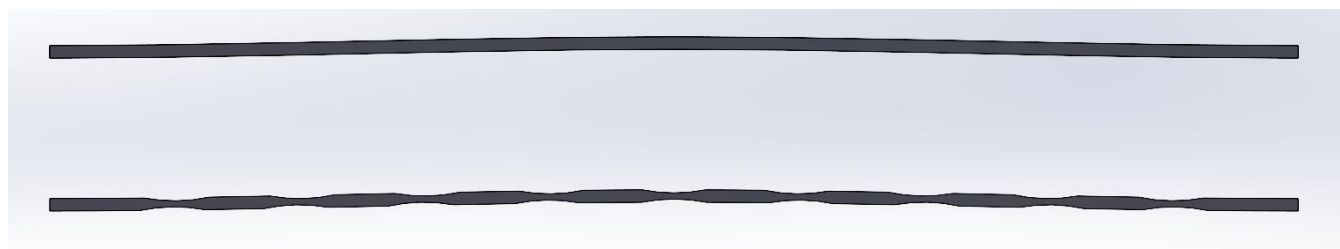


Fig 1.3.5 Beam with flexure hinges

As for one beam part, the beam can be considered as multiple number of rigid part and double multiple number of flexure hinges connection under bending or torsion. The sinusoidal beam with flexure hinges (10 DOF) and without flexure hinges has shown in Fig 1.3.3. The number of DOF means the number of part consider as rigid.

## 1.4 Simulation of structure

### 1.4.1 Using SolidWorks simulation

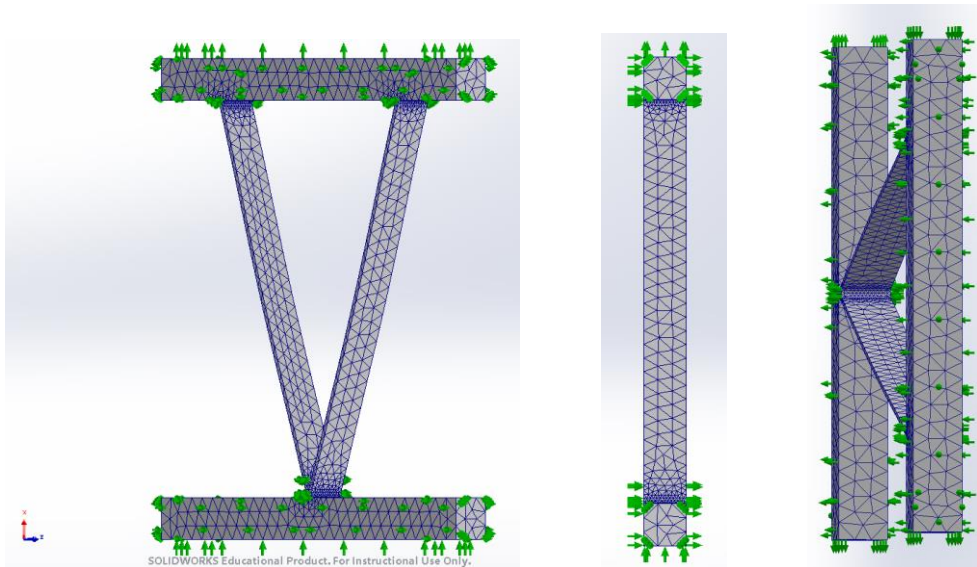


Fig 1.4.1.1 Boundary condition in SolidWorks

SolidWorks is a powerful modeling software. It not only has extremely high operability in 3D modeling, but also has its own simulation plug-in to simulate static and dynamic behaviors. In the simulation interface, it can easily define constraints on each face of the part (Fig 1.4.1.1). The mesh setting is relative with solving efficiency and accuracy, and it is quite relevant, but based on the small part of simple behavior, the difference is not clearly.

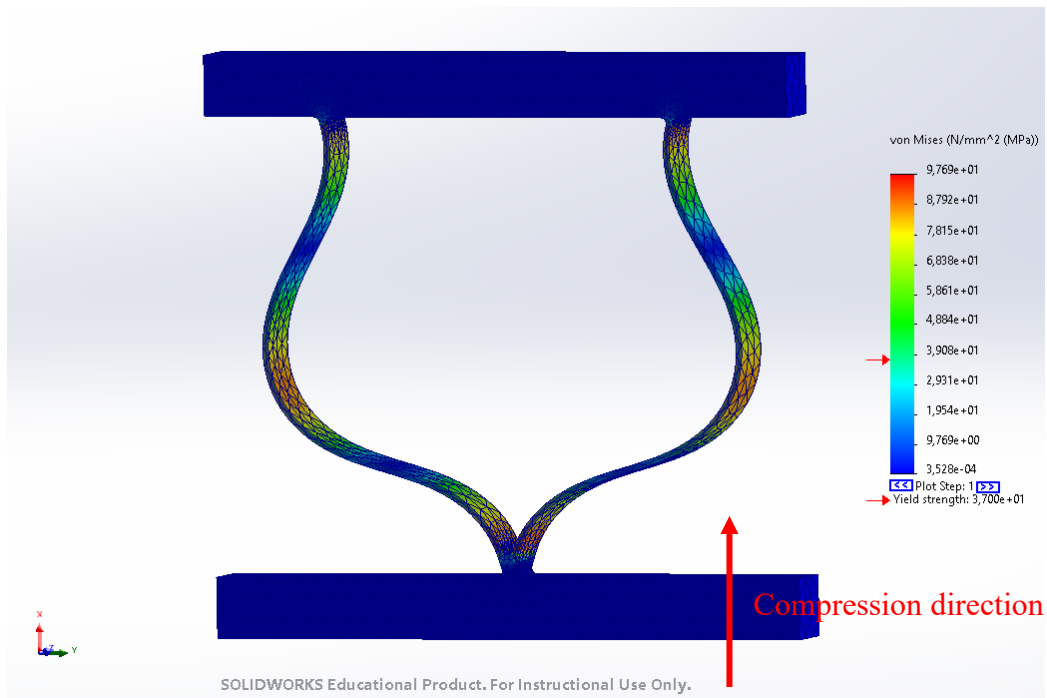


Fig 1.4.1.2 Compression process simulation in SolidWorks

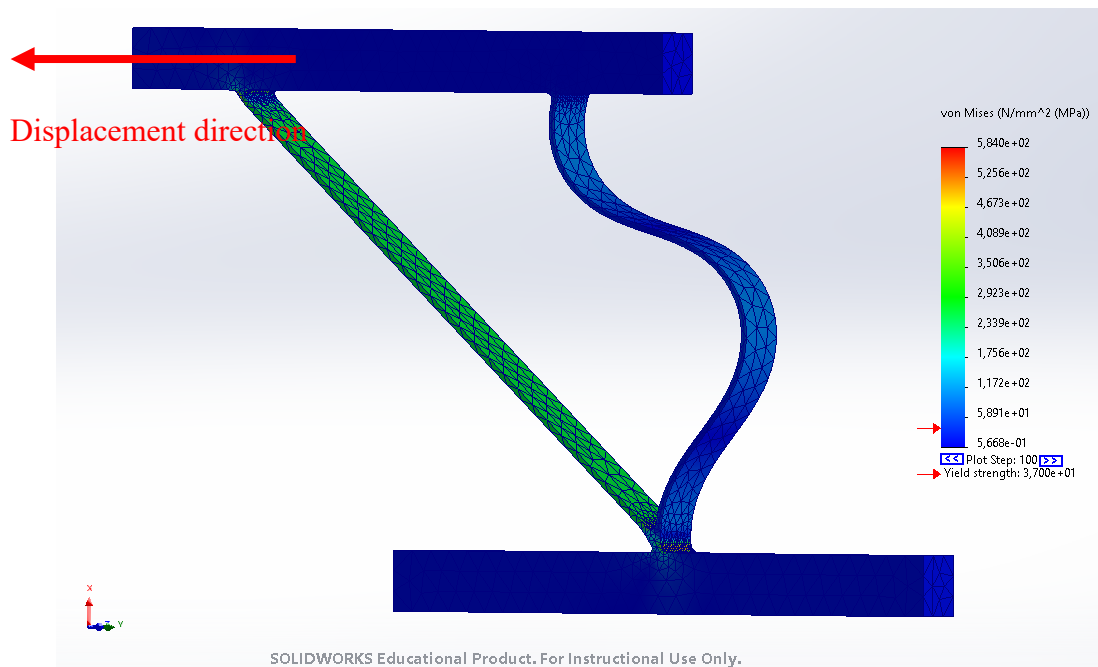


Fig 1.4.1.3 Displacement process simulation in SolidWorks

By setting the fixture correctly, the bottom surface can be compressed in the X direction, and the whole structure will enter the prestressed state (Fig 1.4.1.2). Then by changing the displacement of the upper surface, the desired behavior can be obtained (Fig 1.4.1.3).

### 1.4.2 Using Ansys simulation

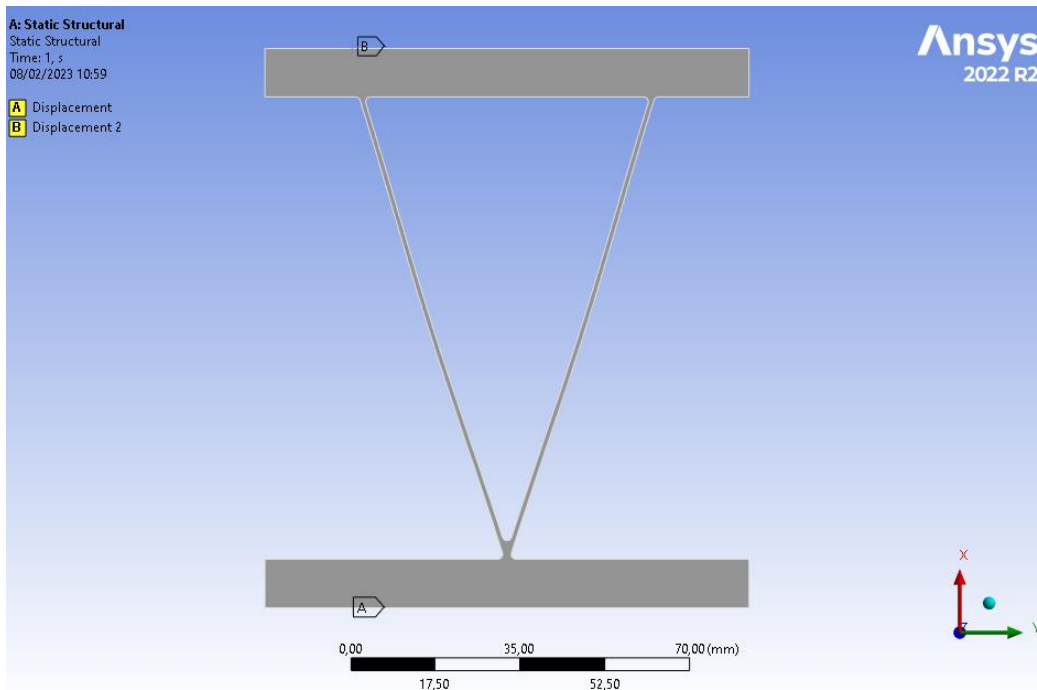


Fig 1.4.2.1 Boundary condition setting in Ansys

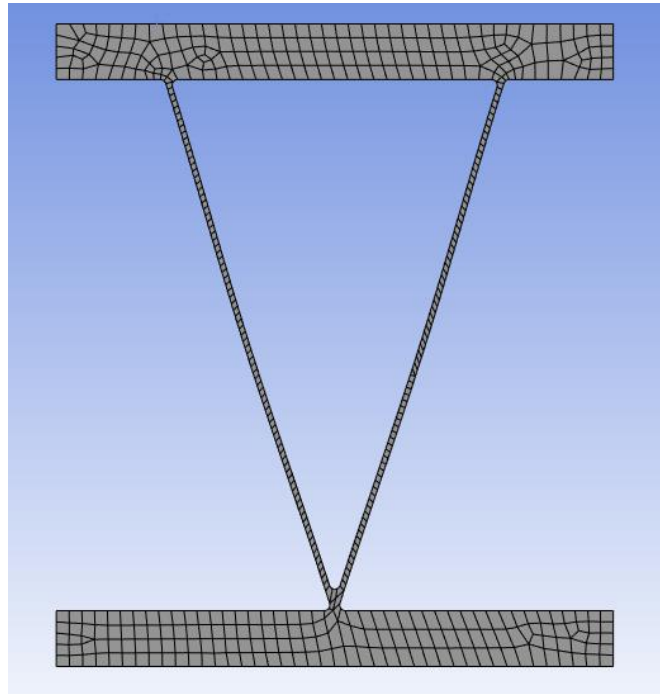


Fig 1.4.2.2 Ansys model meshing

Ansys is a very powerful finite element simulation software. In this thesis, Ansys Workbench is used as the operating platform, and Ansys Mechanical APDL is used as the solver target. Mesh size directly determines the time spent on solving, so choosing an appropriate mesh size to keep the solution time within 1 hours can not only ensure a certain accuracy, but also save time for another operation.

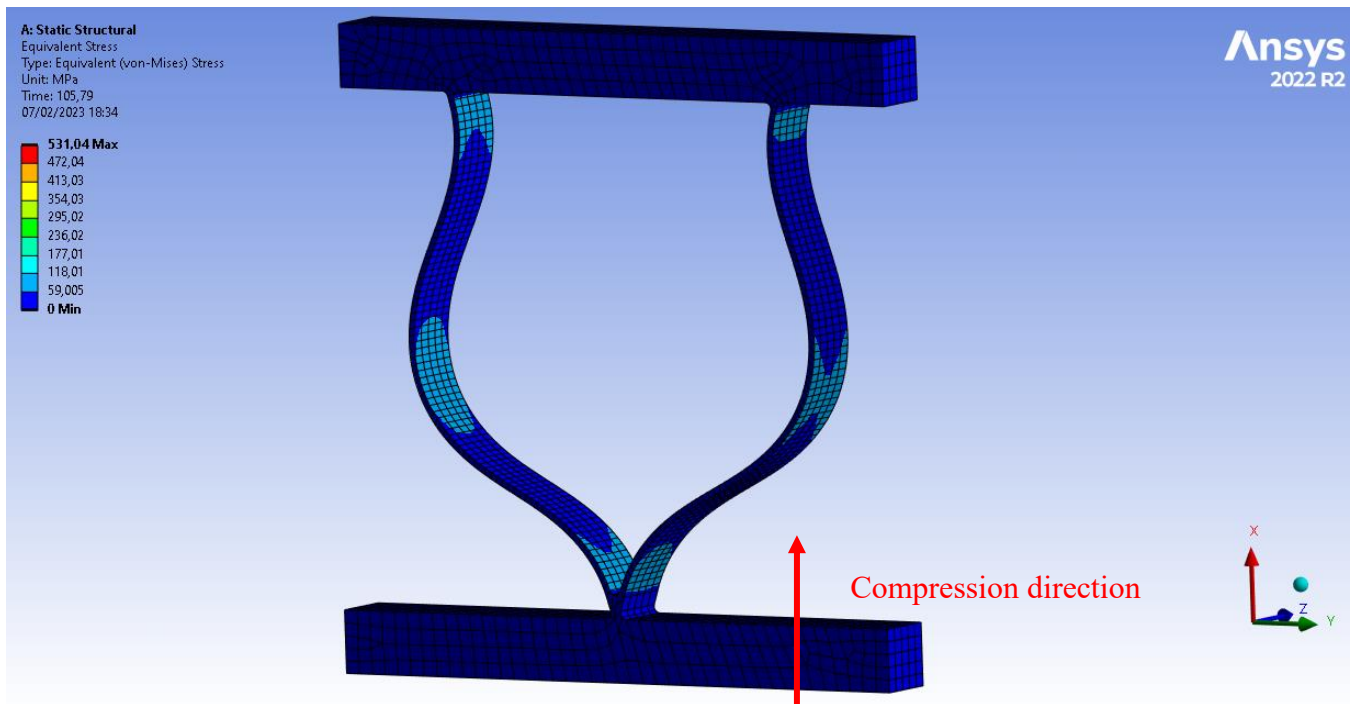


Fig 1.4.2.3 Compression process simulation in Ansys

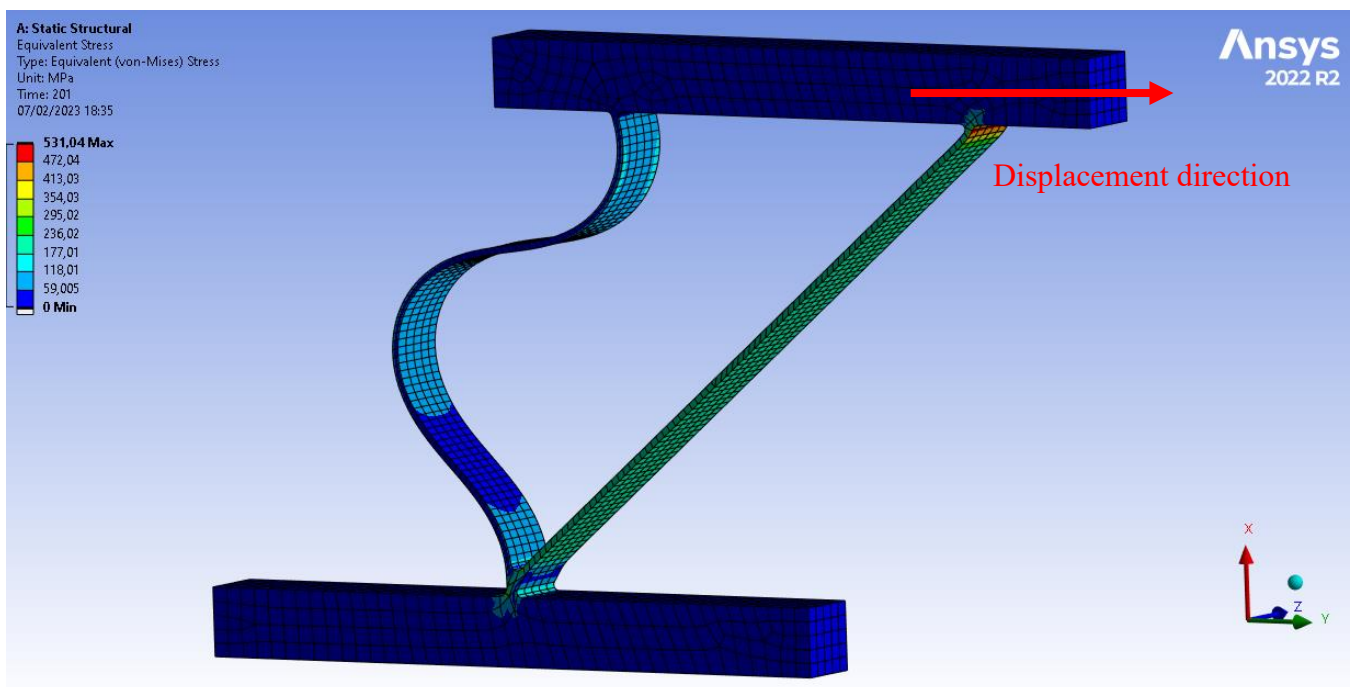


Fig 1.4.2.4 Displacement process simulation in Ansys

Using Ansys to simulate this structure and setting the same boundary condition as SolidWorks: First, setting lower surface moving along X direction while another surface remain steady (Fig 1.4.2.3), then moving upper surface along Y direction (Fig 1.4.2.4).

### 1.4.2 Simulation comparison

For design the structure, must confirm which software are suitable to simulate the structure. Consider given the same geometry parameter of V-shape beam to compare two software simulation result. Specially in the region of unstable.

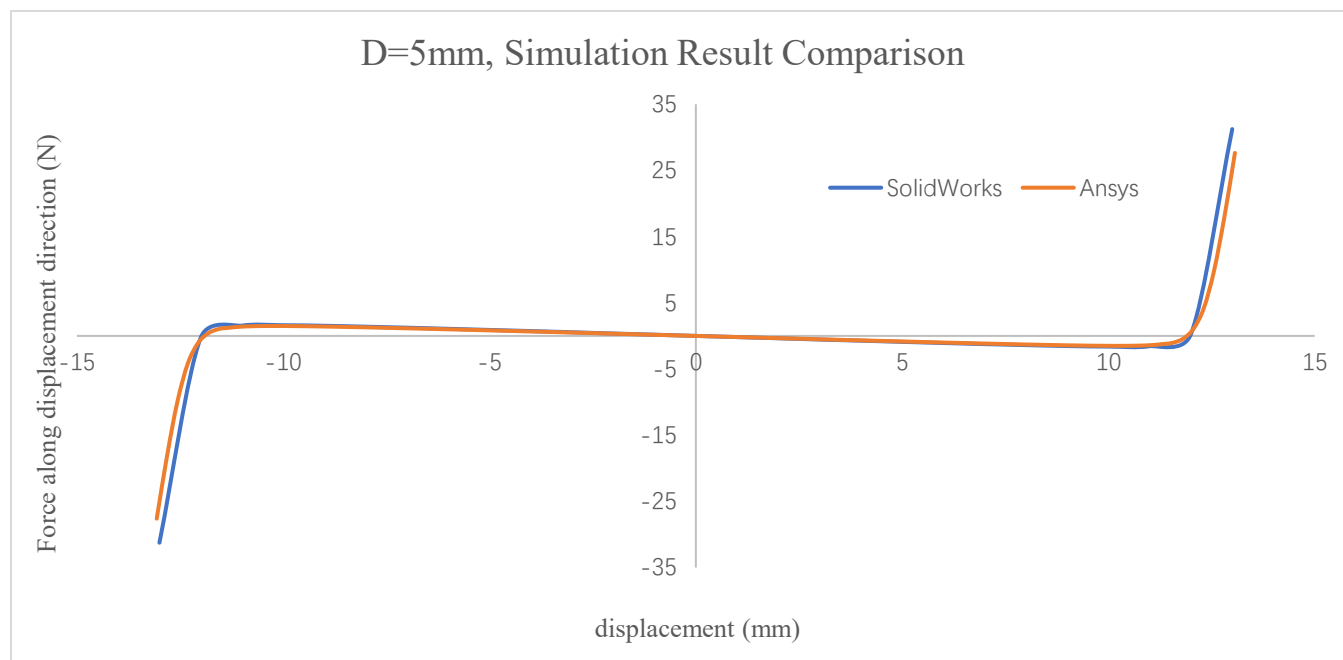


Fig 1.4.2.1 *Preloading* = 5 mm, result comparison

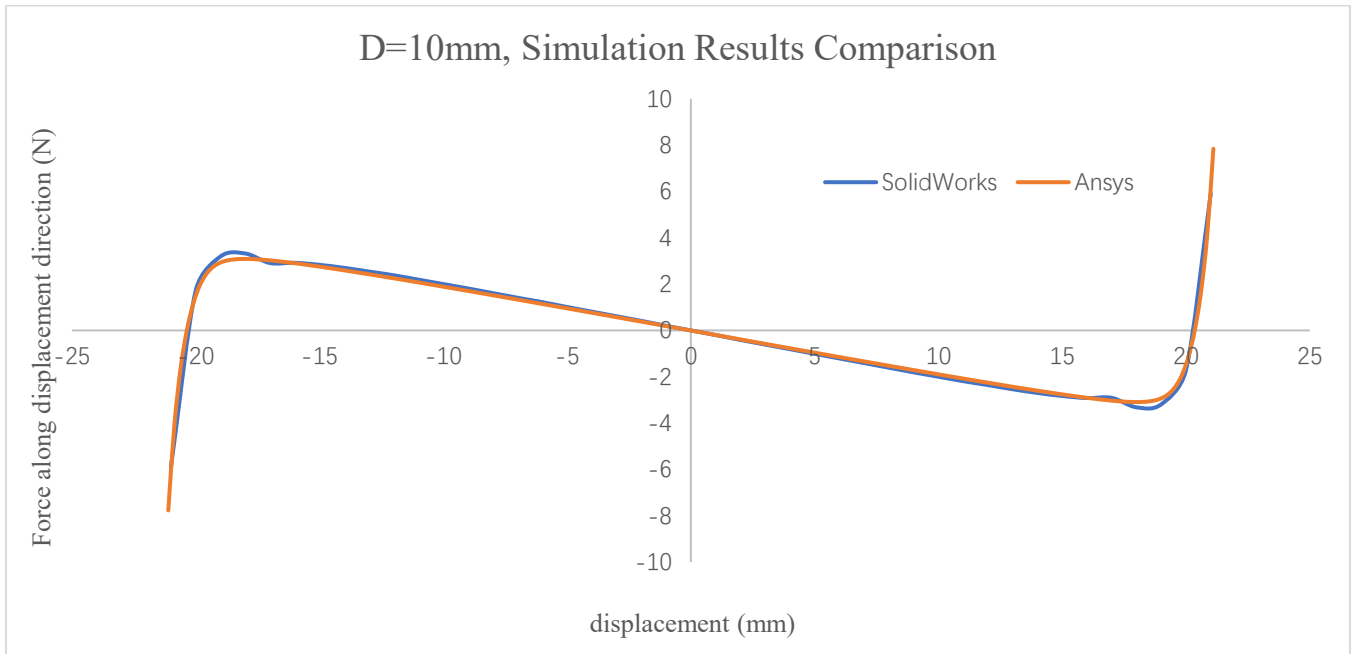


Fig 1.4.2.2 *Preloading* = 10 mm, result comparison

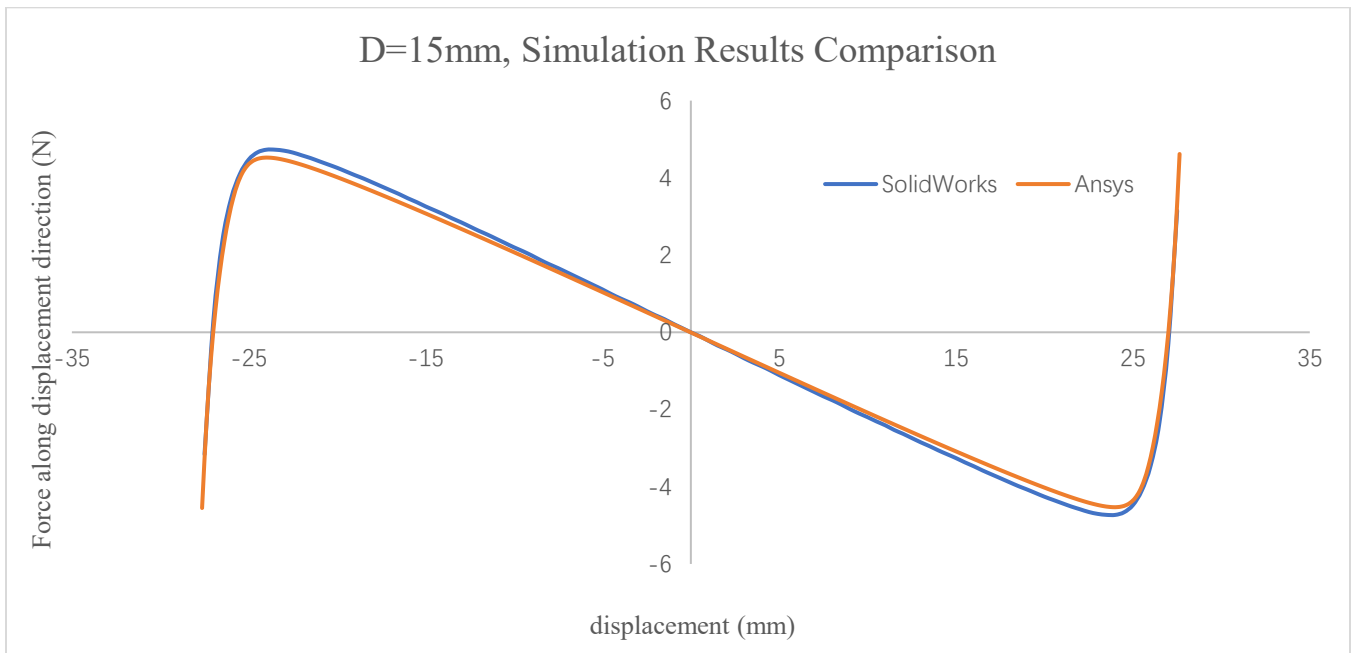


Fig 1.4.2.3 *Preloading* = 15 mm, result comparison

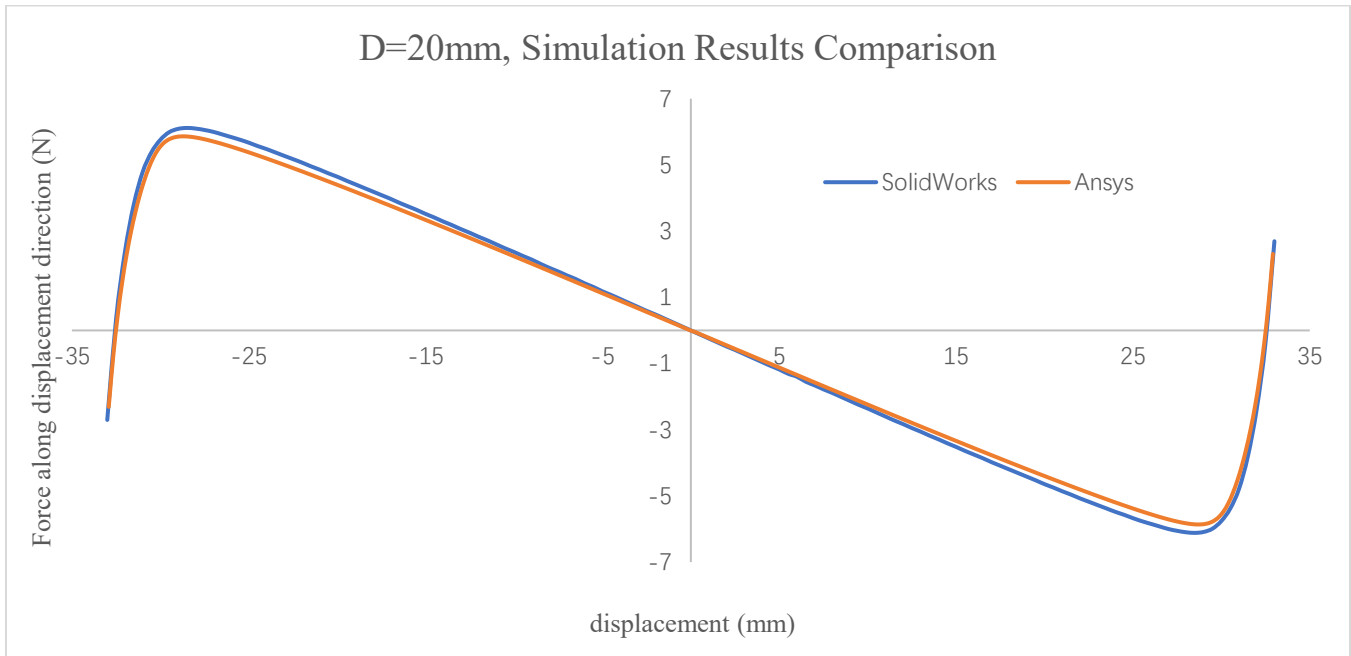


Fig 1.4.2.4 *Preloading = 20 mm*, result comparison

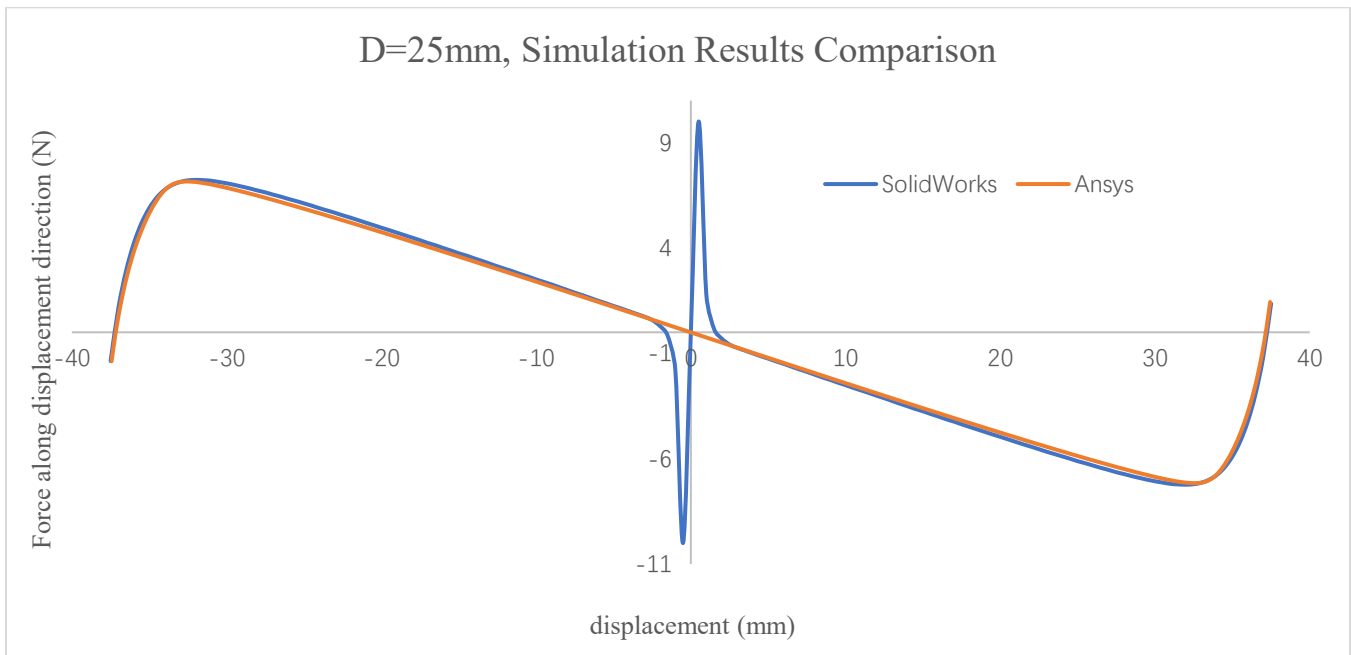


Fig 1.4.2.5 *Preloading = 25 mm*, result comparison

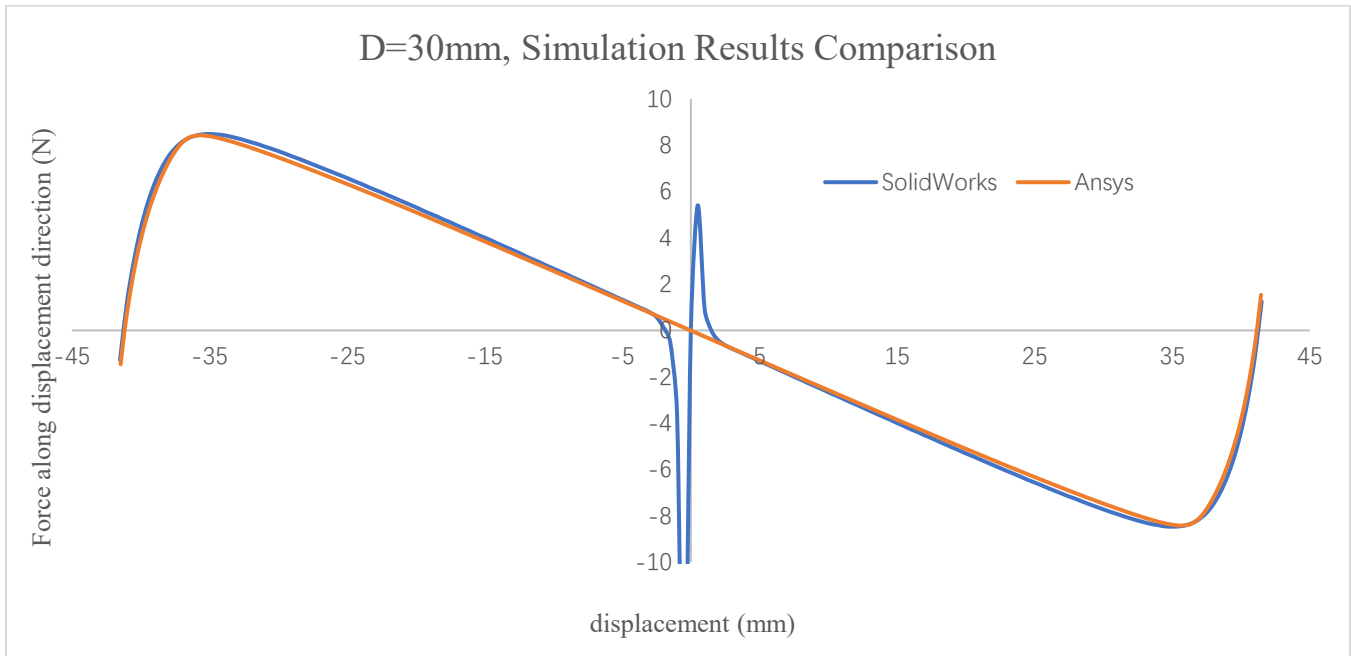


Fig 1.4.2.6 *Preloading* = 30 mm, result comparison

The two software show the same results for  $D = 5, 10, 15, 20 \text{ mm}$ , but once the preloading increase to  $25 \text{ mm}$ , the solver of SolidWorks struggles to handle the unstable point ( $u = 0 \text{ mm}$ ), and the only way to proceed with the simulation is to decrease the singularity estimation factor. Ansys on the other hand, it doesn't have this issue. Therefore, Ansys will be used for next stage of design instead of SolidWorks.

## 2 Design model of the structure

### 2.1 Single V-shape beam

#### 2.1.1 Determine geometric parameters

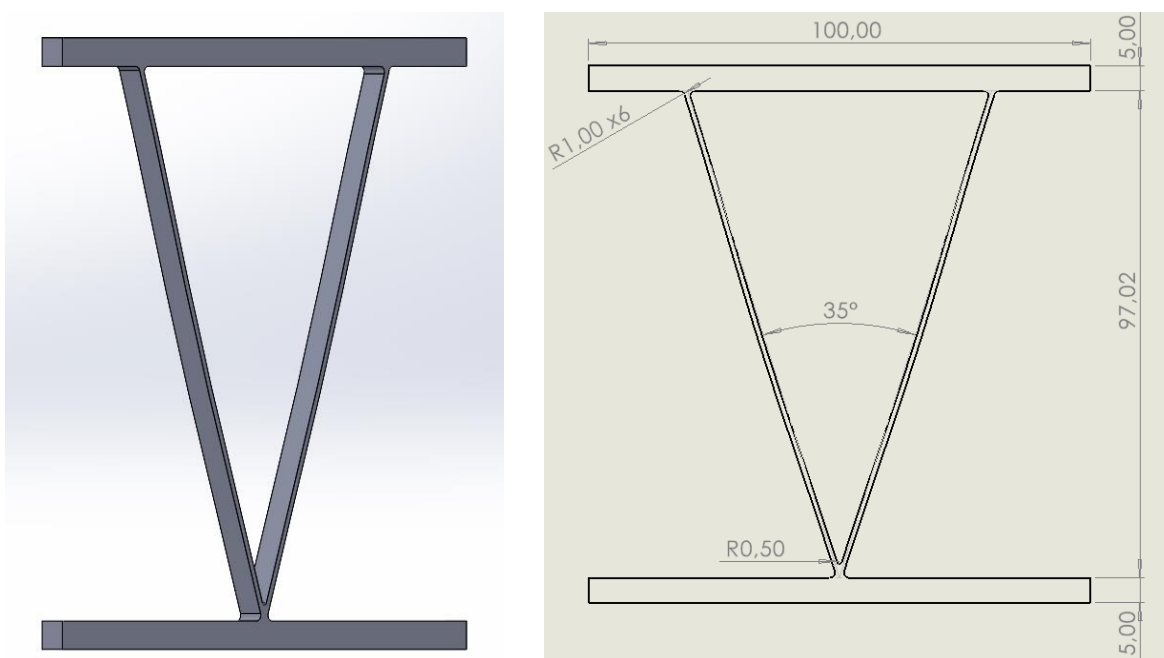


Fig 2.1.1.1 Base design of V-shape beam

The structure designed in this thesis is shown in Fig 2.1.1.1, and it is formed by two slightly curved thin beams and two stiffer walls. The angle between two beams is  $35^\circ$  in this structure, so the structure will be referred to as “V-shape beam” in following. Different values of thickness are taken in consideration, namely  $1\text{ mm}$ ,  $1.2\text{ mm}$ , and  $1.5\text{ mm}$ . The total length of beam is  $100\text{ mm}$  and the width is  $5\text{ mm}$ . The upper and lower walls have been designed to bear the compression without any large deformation.

The shape of curved beam is given by:

$$w(x) = \frac{A}{2} \left[ 1 - \cos \left( 2\pi \frac{x}{L} \right) \right] \quad (\text{Eq 2.1.1})$$

Where  $A$  is the amplitude or initial apex of the beam, equal to  $A = 0.7 \text{ mm}$ .  $L$  is the total length of beam, and  $x \in [0, L]$ . By using the Eq 2.1, the buckling direction can be under control. For the wall and beams connection region, a fillet is added with radius  $1 \text{ mm}$  to reduce the stress concentration. For two curved beams connection region, consider  $0.5 \text{ mm}$  as fillet radius.

### 2.1.2 Structure simulation result comparison

Using Ansys Workbench Static Structure work part to simulate the V-shape beam behavior, the simulation setting as follow:

1. Building the CAD model by using SolidWorks and import the geometry to Ansys. Adding the generic PLA into the Ansys Engineering Data, the generic PLA material property are showing in Chapter 1.1.
2. Setting the mesh resolution as 6.
3. Define the number of steps as 201, and close the auto stepping.
4. Open the Large Deflection and set the Weak Spring as Program Controlled (Fig 2.1.2). For Nonlinear Control, open the Force Convergence and Displacement Convergence (Fig 2.1.2). The other setting remains default.
5. Setting lower surface (A, Fig 2.1.2) only moving along Y direction form 0-101 steps; setting upper surface (B, Fig 2.1.2) keep steady form 0-101 steps and only moving along X direction form 101-201 steps (Fig 2.1.3).
6. For Solution, adding Force Reaction, and set the boundary condition for displacement (A, Fig 2.1.2) and displacement 1 (B, Fig 2.1.2). To avoid changing boundary condition due to large deflection, better adding the Deformation for displacement (A, Fig 2.1.2) and displacement 1 (B, Fig 2.1.2).
7. Solve the simulation.

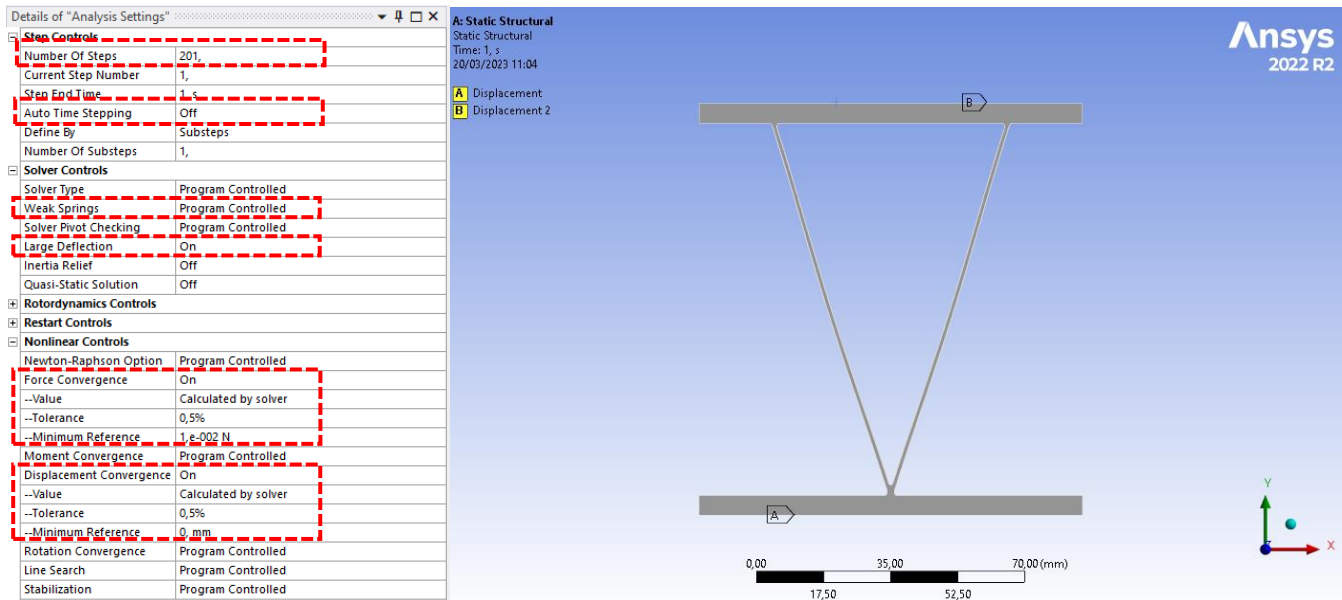


Fig 2.1.2 Ansys simulation setting

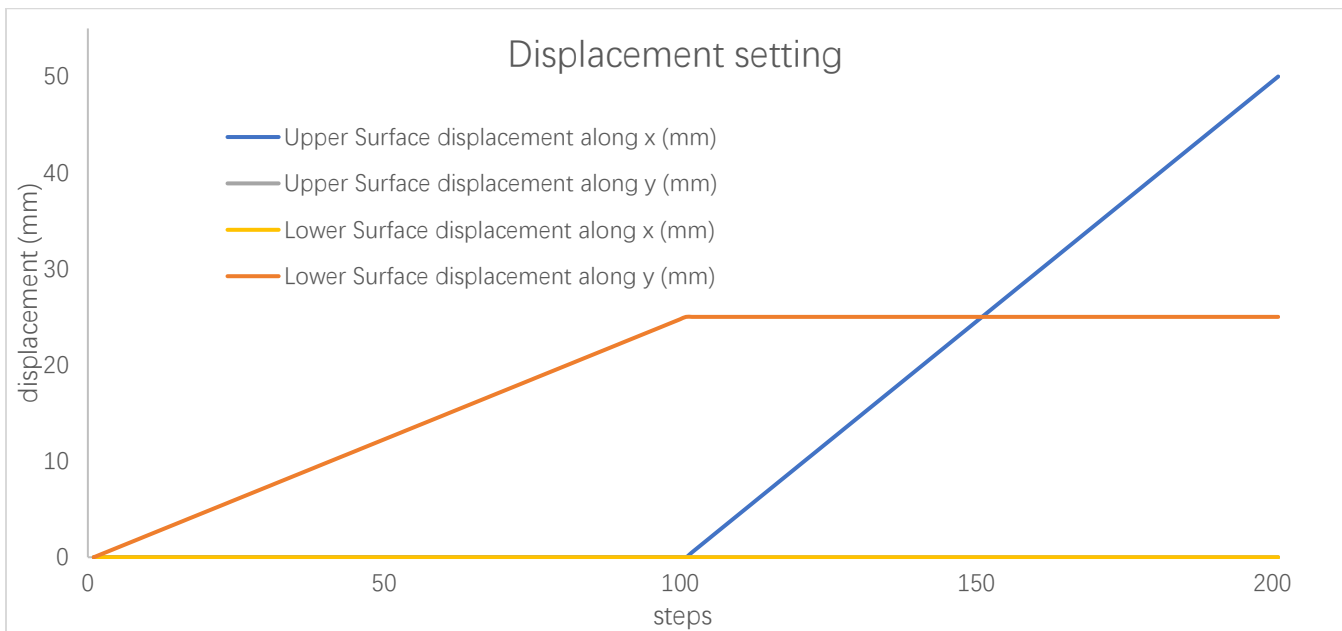


Fig 2.1.3 Ansys simulation displacement setting (Example:  $D = 25 \text{ mm}$ )

Since the whole structure is symmetrical, no matter the upper surface displacement (B, Fig 2.1.2)  $u = 0 \sim 50 \text{ mm}$  or  $u = -50 \sim 0 \text{ mm}$ , the obtained simulation results are the same (Chapter 1.4.2). In order to

save time, only the setting of  $u = 0 \sim 50\text{mm}$  is used for simulation. The Solution will show the  $R$  (along X direction) and  $F$  (along Y direction) are shown in Fig 2.1.2.1. The displacement of surfaces (A and B) will also show in Solution.

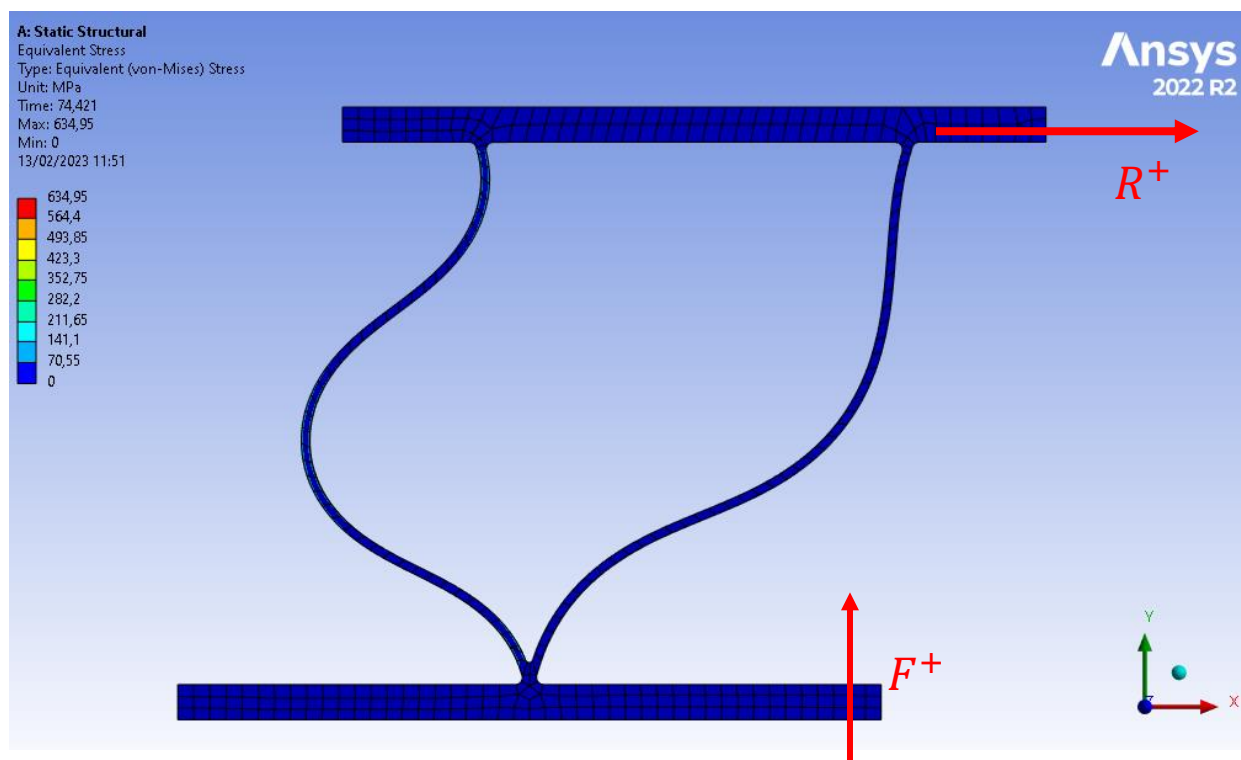


Fig 2.1.2.1

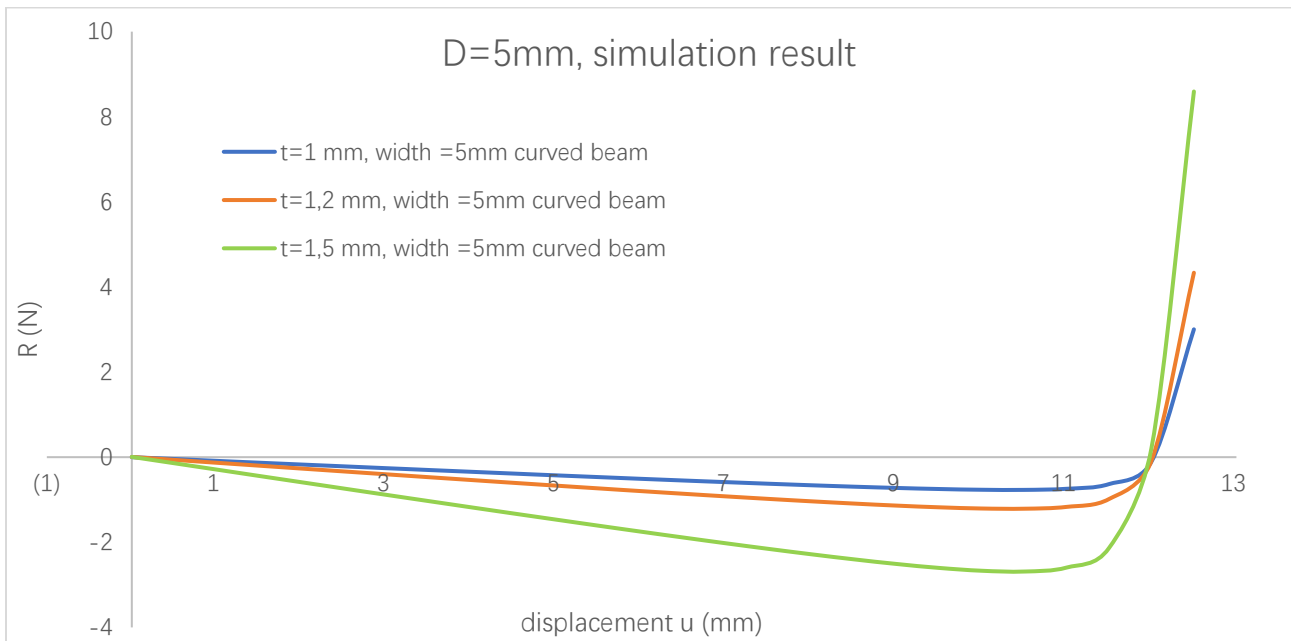


Fig 2.1.2.2 *Preloading = 5 mm*, R result comparison

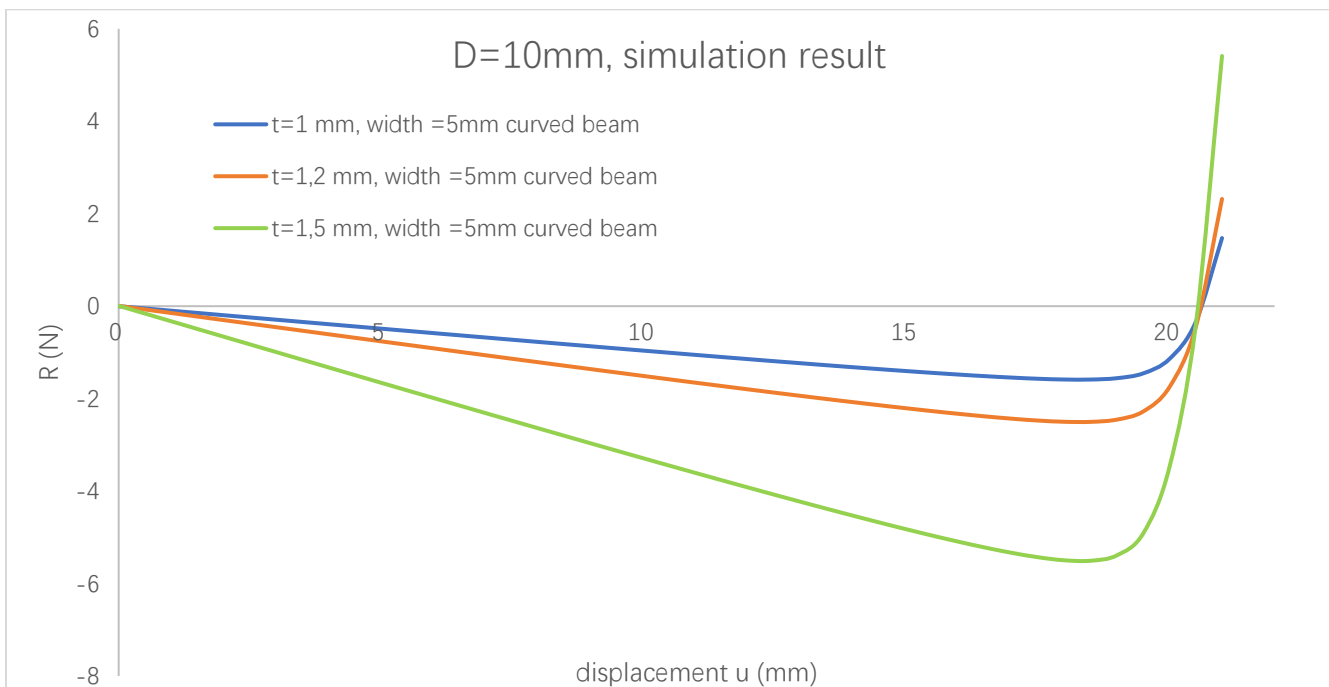


Fig 2.1.2.3 *Preloading = 10 mm*, R result comparison

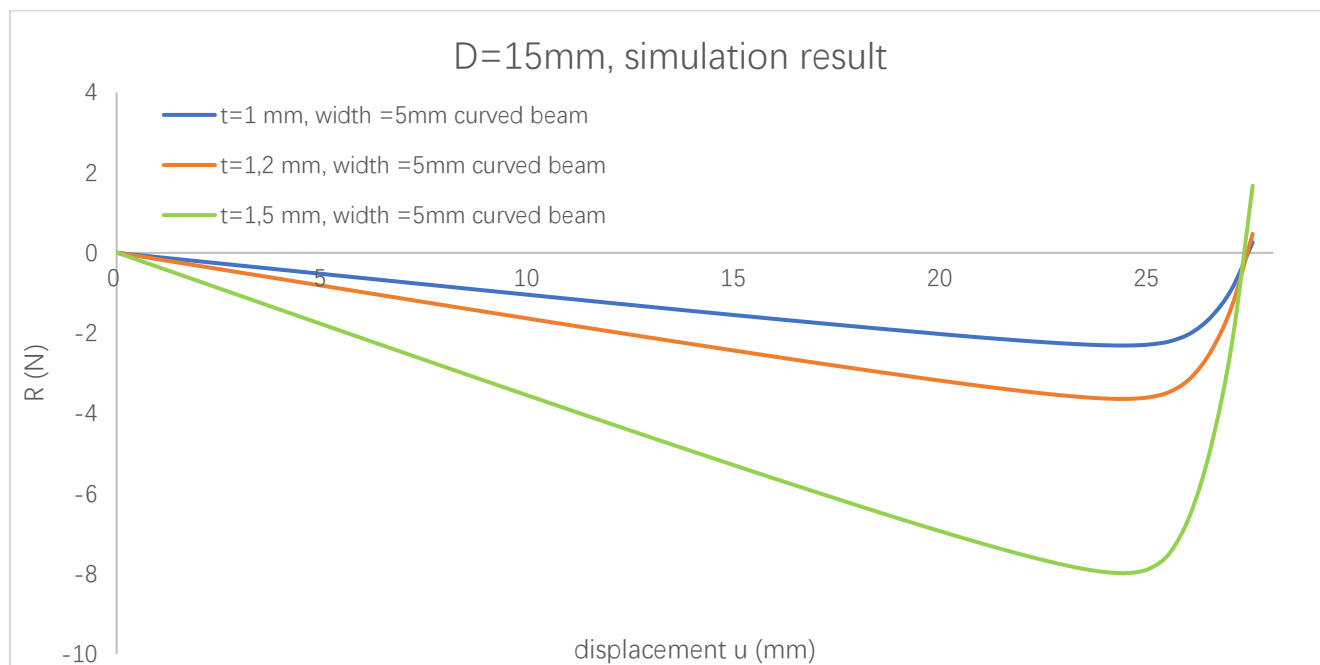


Fig 2.1.2.4 *Preloading* = 15 mm, R result comparison

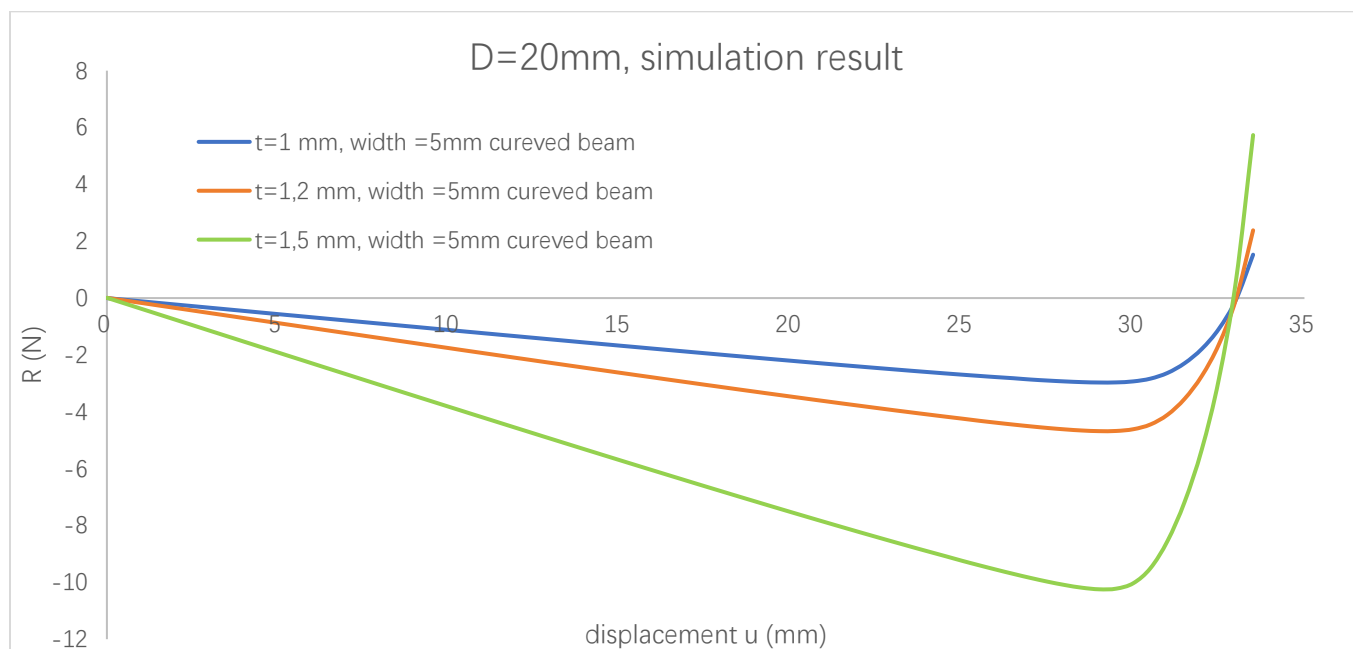


Fig 2.1.2.5 *Preloading* = 20 mm, R result comparison

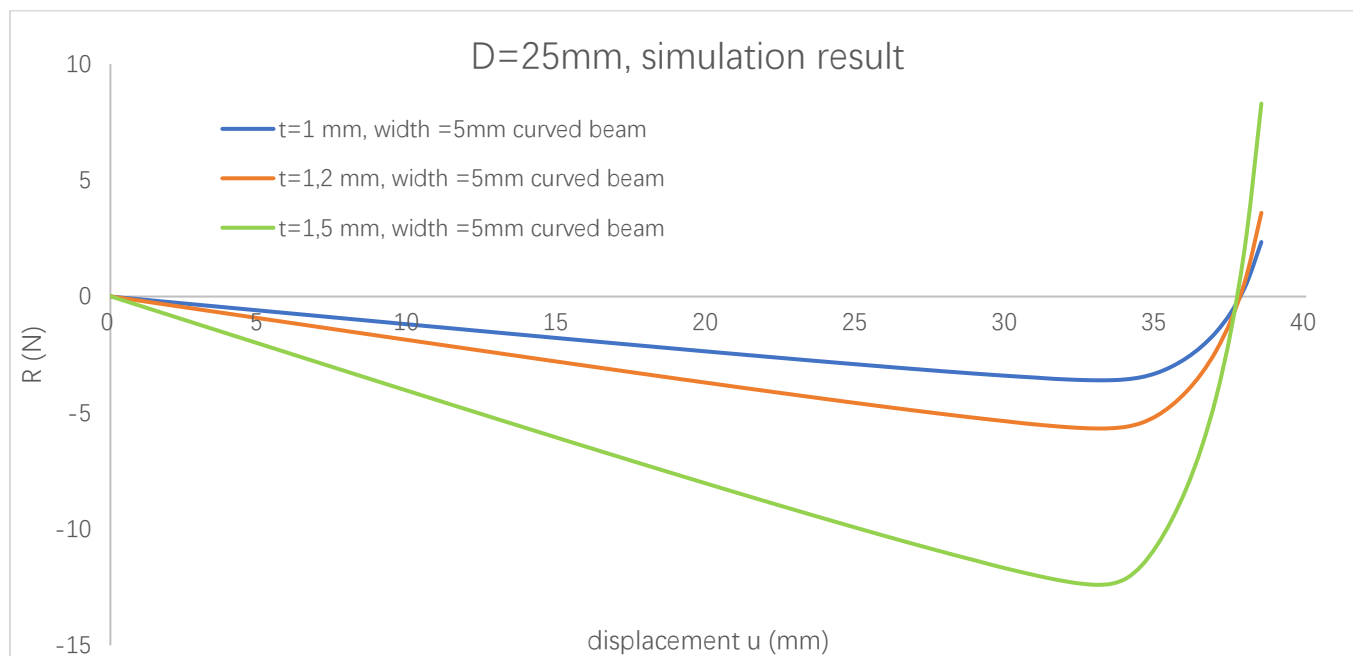


Fig 2.1.2.6 *Preloading* = 25 mm, R result comparison

Based on simulation results (Fig 2.1.2.2; Fig 2.1.2.3; Fig 2.1.2.4; Fig 2.1.2.5; Fig 2.1.2.6), by increasing the thickness of the beam, the maximum negative force (or negative stiffness) increases as well. Conversely the range of negative stiffness with respect to the displacement remain the same when the preloading distance is same. Obviously, as the preloading distance increases, the region of negative stiffness also increases. In practice, it is necessary to consider the material characteristics to avoid plastic deformation during compression. Although a thicker beam can achieve a relatively higher negative stiffness region, it corresponds to a greater vertical force in compression (Fig 2.1.2.7; Fig 2.1.2.8; Fig 2.1.2.9; Fig 2.1.2.10; Fig 2.1.2.11).

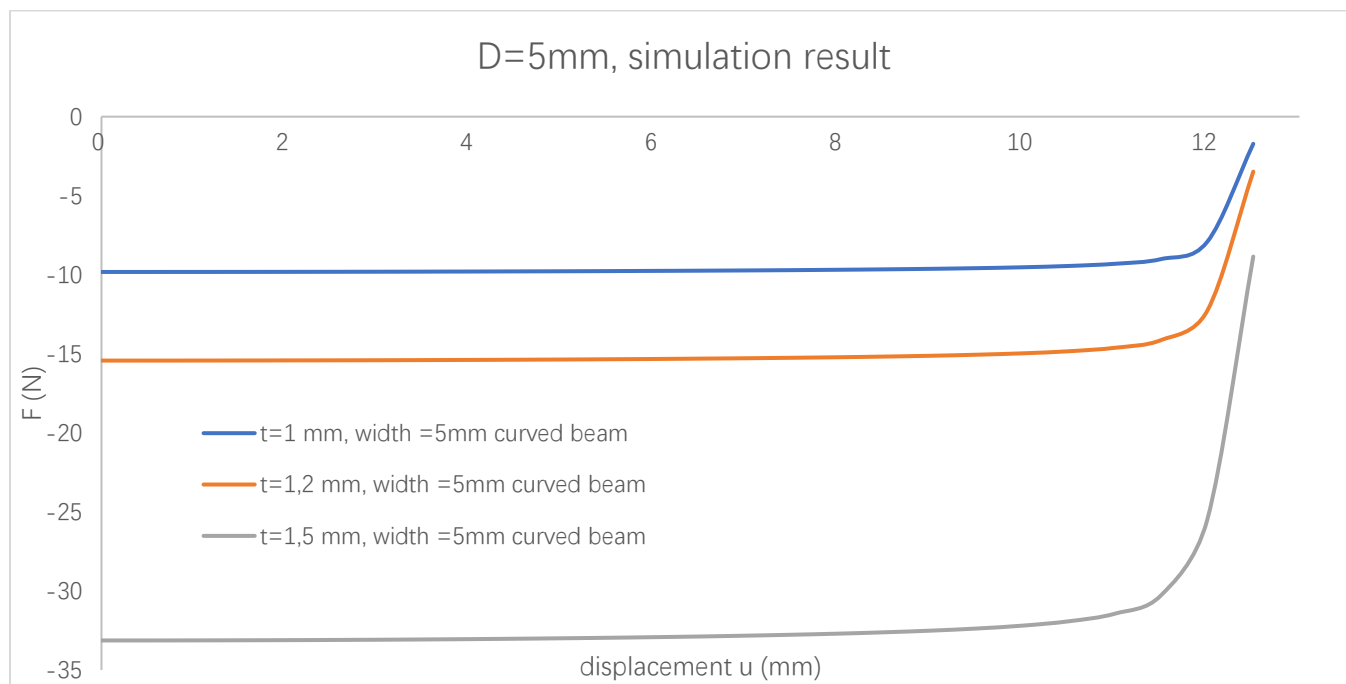


Fig 2.1.2.7 Preloading = 5 mm, F result comparison

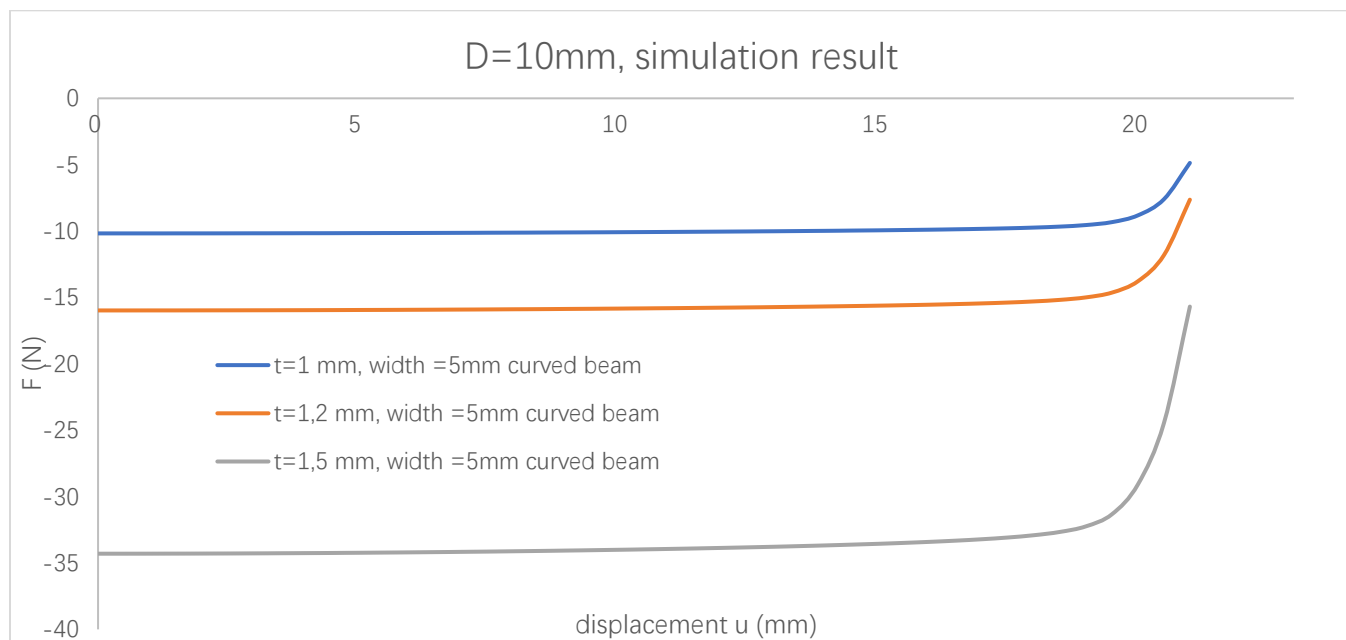


Fig 2.1.2.8 Preloading = 10 mm, F result comparison

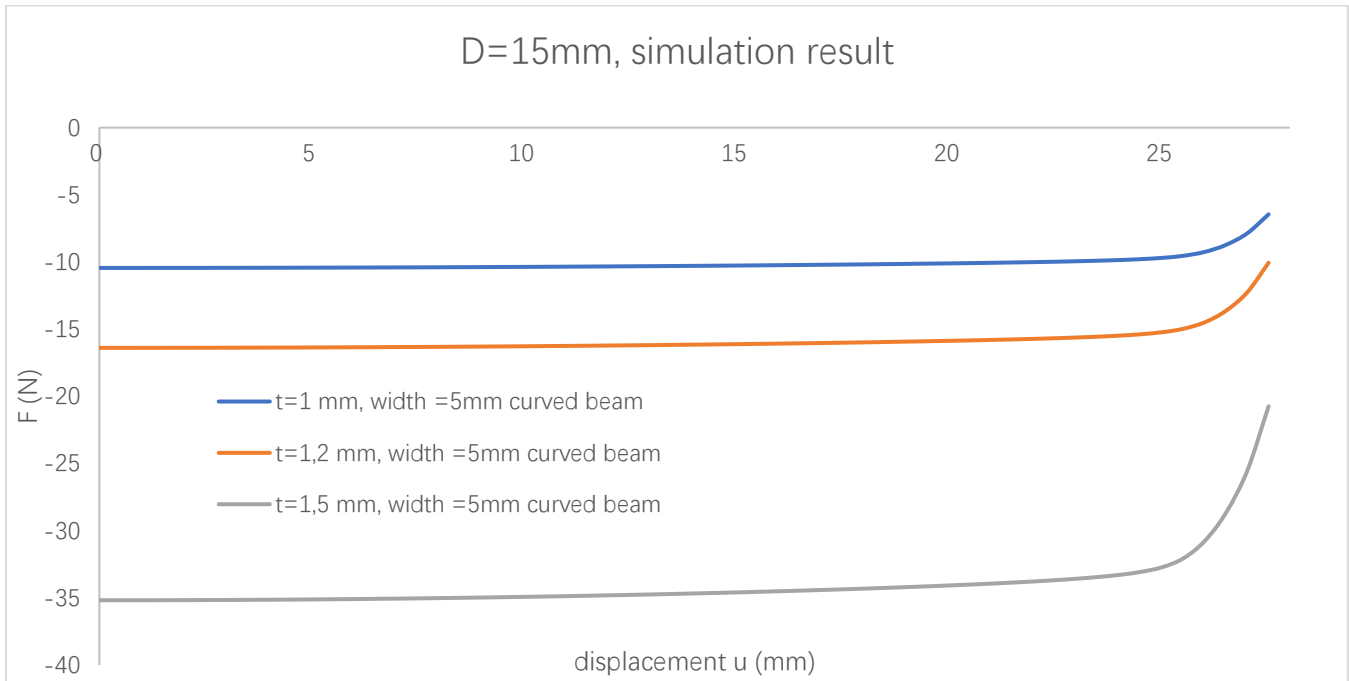


Fig 2.1.2.9 *Preloading = 15 mm*, F result comparison

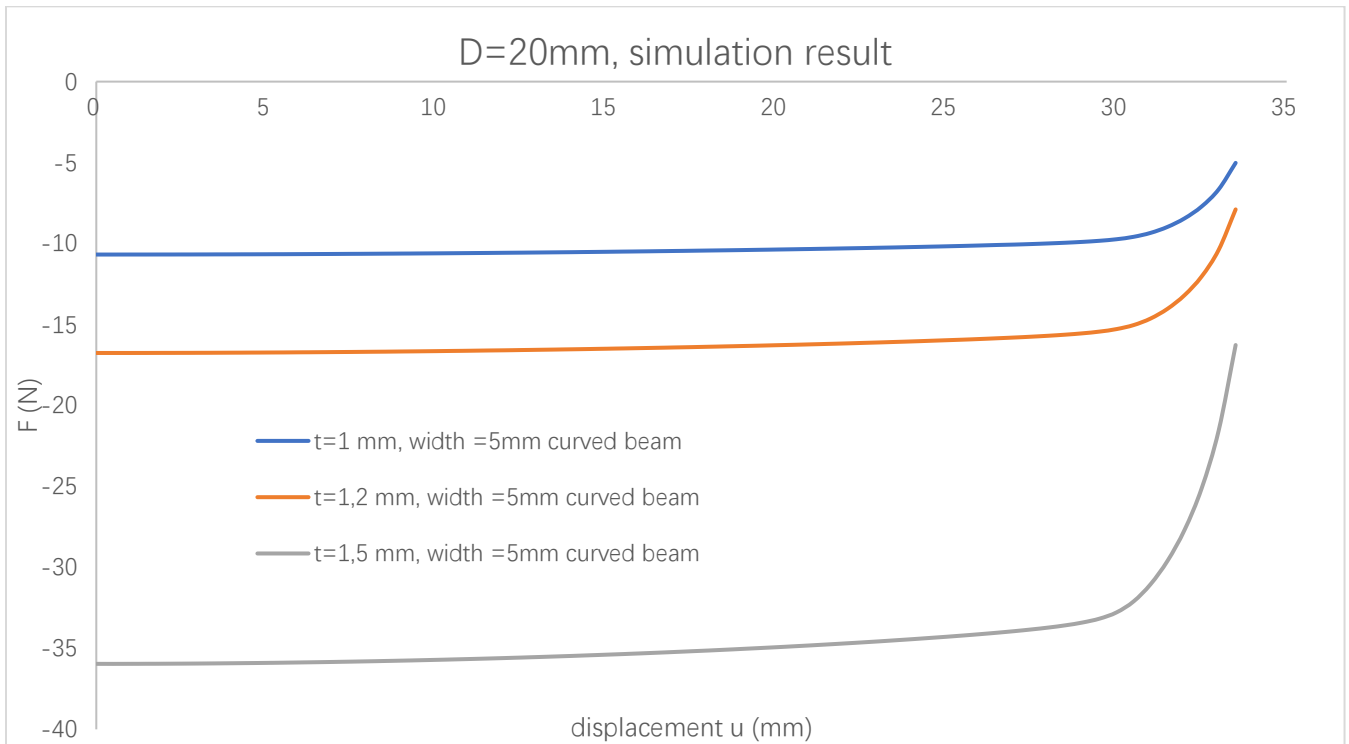


Fig 2.1.2.10 *Preloading = 20 mm*, F result comparison

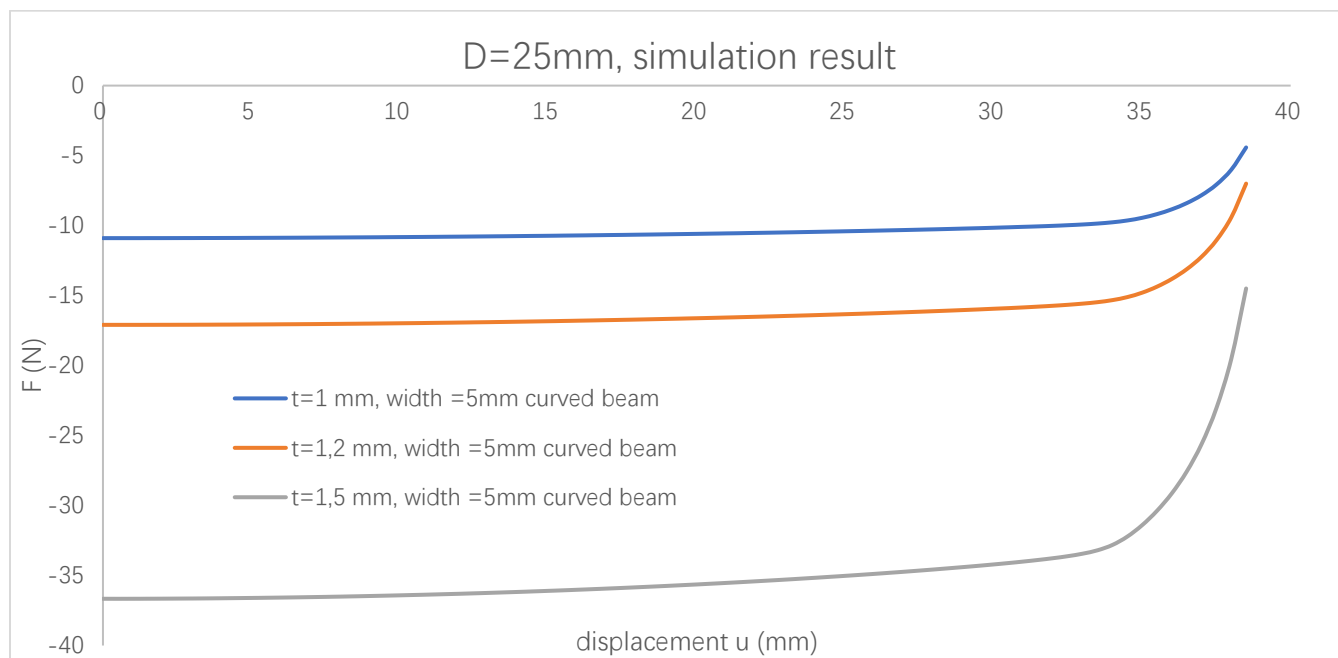


Fig 2.1.2.11 *Preloading = 25 mm*, F result comparison

### 2.1.3 Estimation of the negative stiffness range

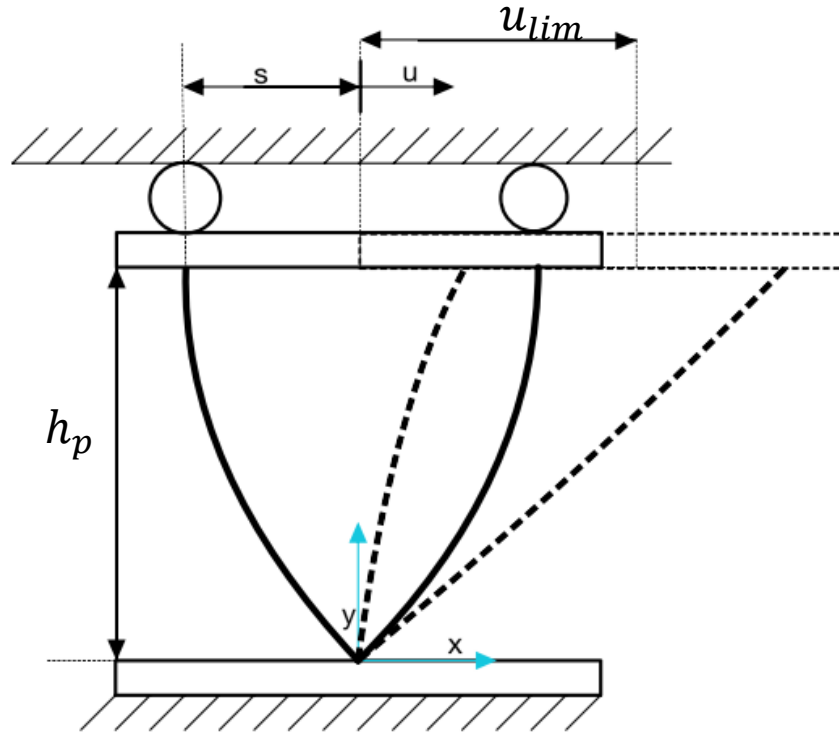


Fig 2.1.3.2 Schematic diagram of V-shape beam geometry limitation

The limitation of the displacement ( $u$ ) can be linked to of a geometry limitation given by the maximum extensions of the beams. This read:

$$u_{lim} = \left( \sqrt{L^2 - \left( L \times \cos\left(\frac{\alpha}{2}\right) - D \right)^2} - s \right) \times 80\% \quad (\text{Eq 2.1.3.1 [7]})$$

Where  $L$  is the free length of beam, and  $\alpha$  is the angle between the two curved beams ( $35^\circ$ ),  $s$  is half distance between the beam on the upper surface ( $s = \frac{L \times \sin(\alpha/2)}{2}$ ). Due to the symmetry of the structure, so the total displacement covering the negative stiffness region is:

$$\text{total negative stiffness range} = u_{lim} \times 2$$

$$\text{(Eq 2.1.3.2)}$$

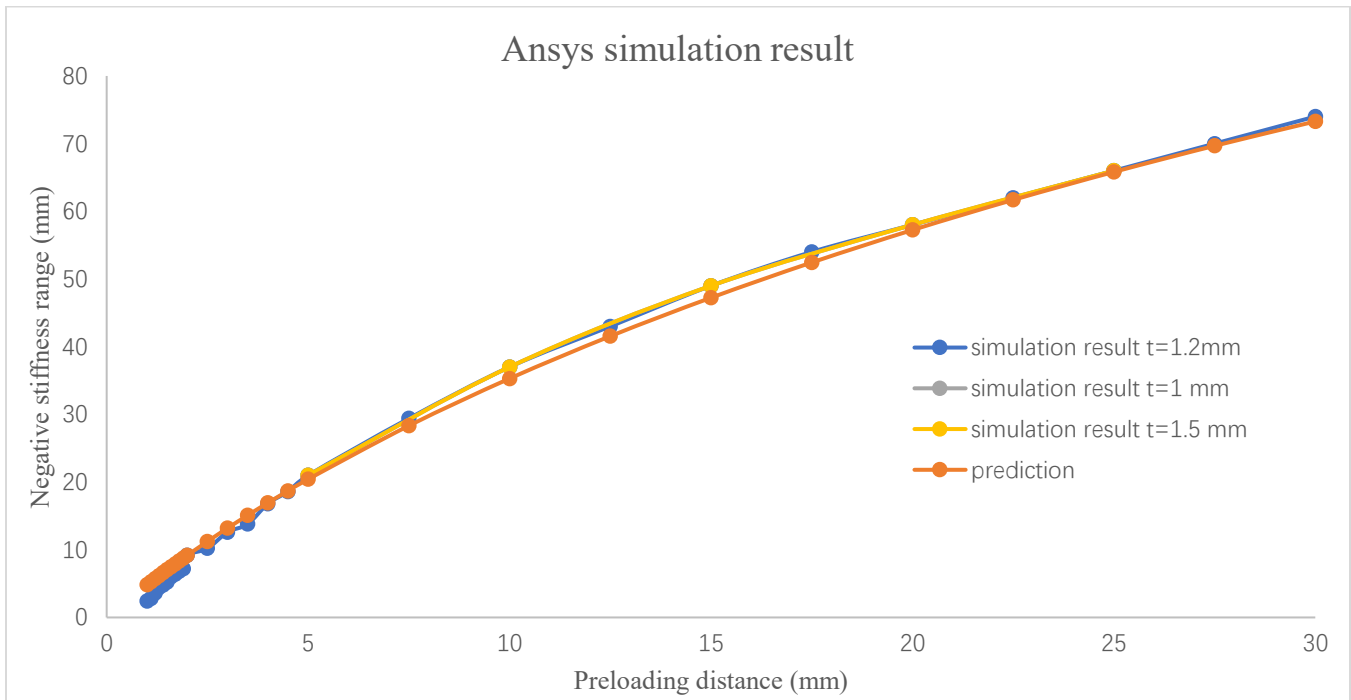


Fig 2.1.3.2 Negative stiffness range comparison

Comparing the prediction of the negative stiffness range with the simulation results of Ansys a low deviation is observed (Fig 2.1.3.2). After comparing beams with different thicknesses, the results show that the negative stiffness range has no relationship with the thickness of the beam, as already seen in Fig 2.1.2.6.

## 2.2 Double V-shape beam

### 2.2.1 Determine geometric parameters

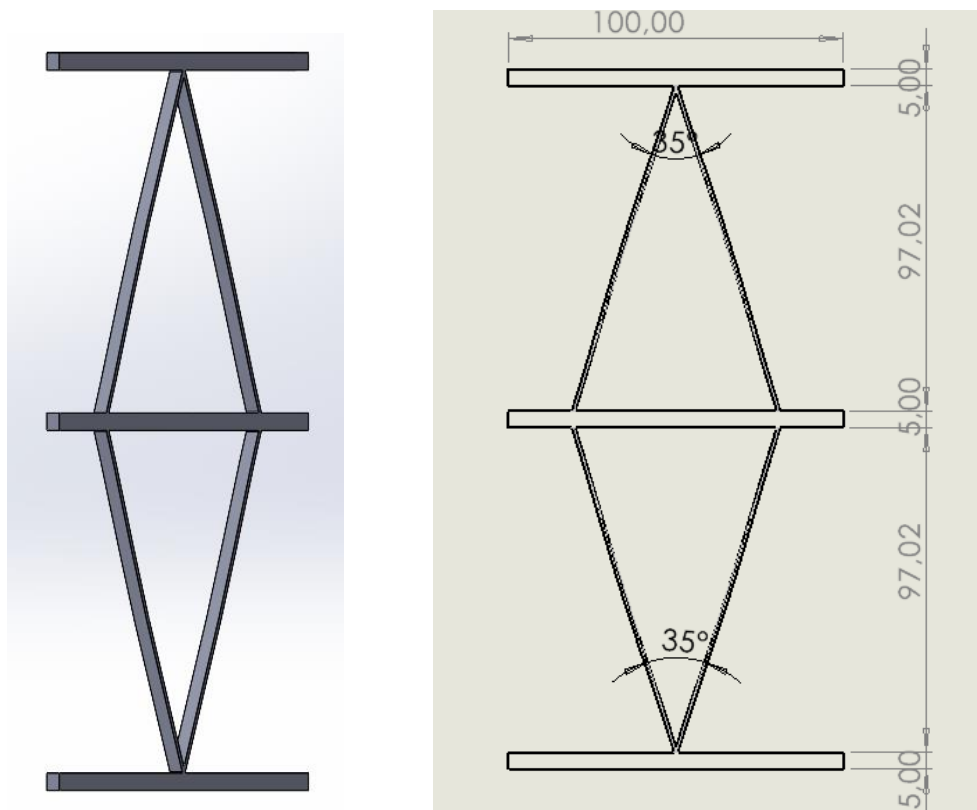


Fig 2.2.1.1 Double V-shape beam drawing

Another possible configuration is Double V-shape beam (Fig 2.2.1.1). The geometry parameter remains same as single V-shape beam, but with two V-shape beams. The width is  $5\text{mm}$ . During the simulation or experiment, only the upper and lower surface will be fixed, the middle surface will move freely along X direction which means we don't need to adding other component to bear the compression. It is a benefit for design the support to fix the upper and lower surface. But if the symmetrical of structure cannot be guaranteed, the middle surface will not keep at the steady position during the compression.

## 2.2.2 Structure simulation result comparison

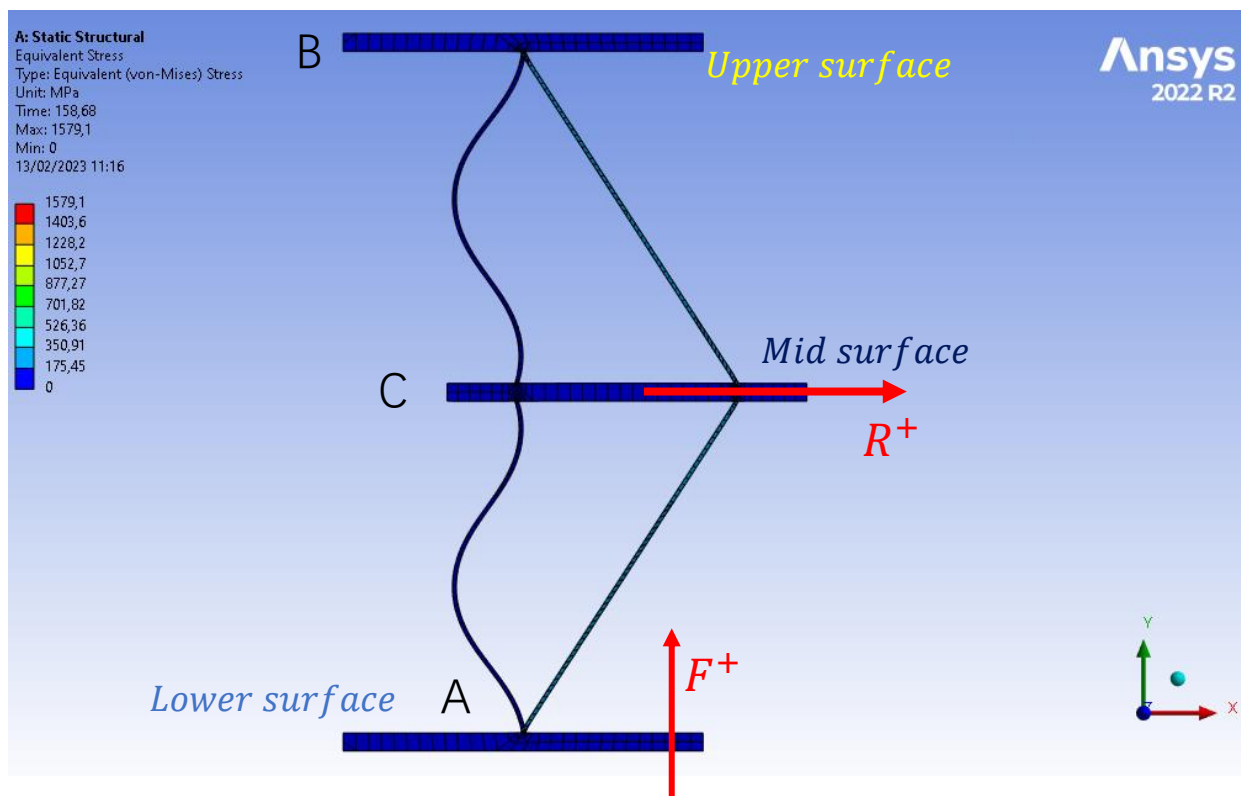


Fig 2.2.2.1 Ansys simulation setting for Double V-shape beam

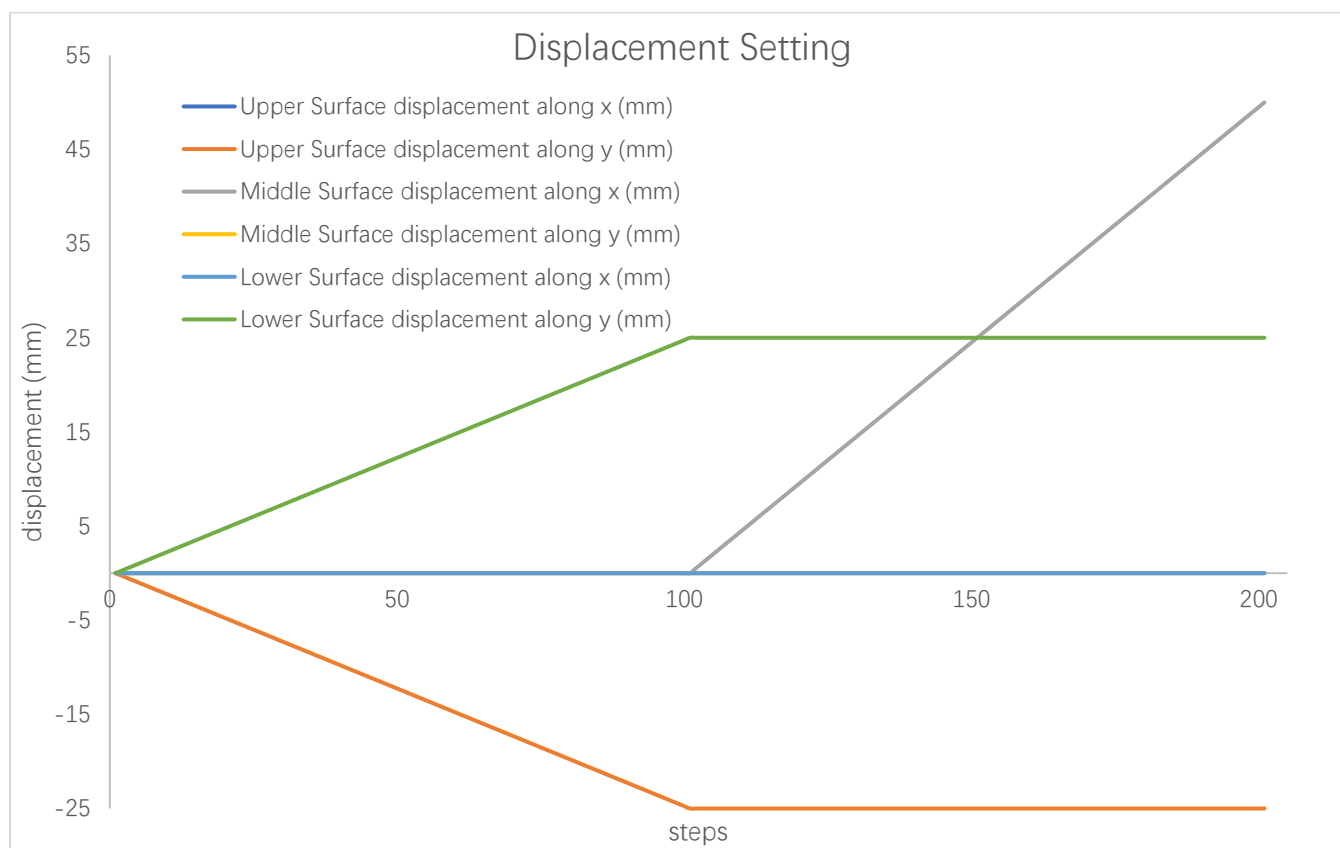


Fig 2.2.2.2 Displacement setting for Double V-shape beam

Using the same simulation setting (chapter 2.1.2) for Double V-shape beam simulation. But instead of setting two boundary, Double V-shape beam need adding one more surface (C, Fig 2.2.2.1). The detail of displacement setting is:

1. Setting lower surface moving along Y direction and upper surface moving opposite direction for 0-101 steps. And set the middle surface moving along X direction for 101-201 steps (Fig 2.2.2.2).
2. Adding the Force Reaction for each surface displacement.

By setting the upper surface and lower surface compressed along Y axis, the mid surface moving along X axis (Fig 2.2.2.1), and by doing quasi-static simulation under 5, 10, 15, 20, 25 mm preloading with beam thickness is 5mm and the results are compared in the following.

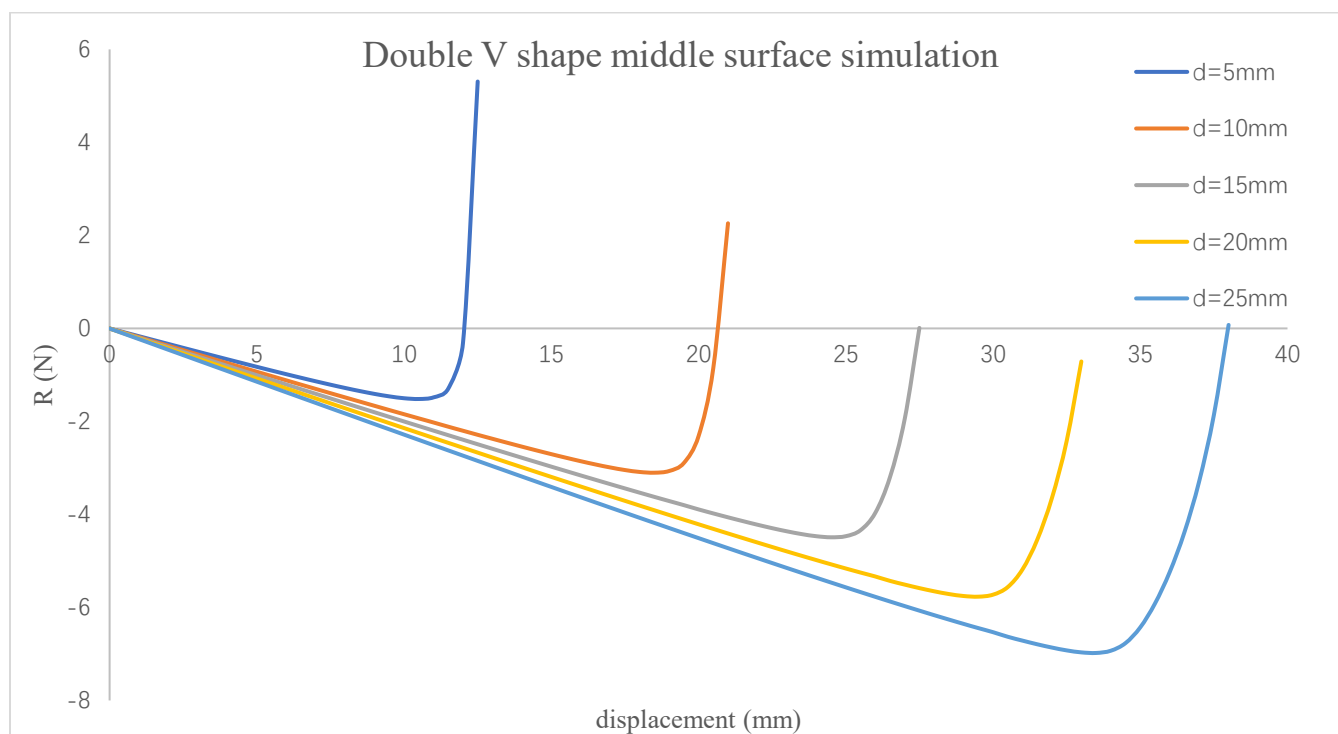


Fig 2.2.2.2

The simulation results show that the negative stiffness range increases for increasing preloading values. This result is consistent with single V-shape beam simulation, but in the Double V-shape beam case the minimum negative forces are twice than the single V-shape beam. This implies that the negative stiffness values are also doubled.

### 2.2.3 Problem of Double V-shape beam

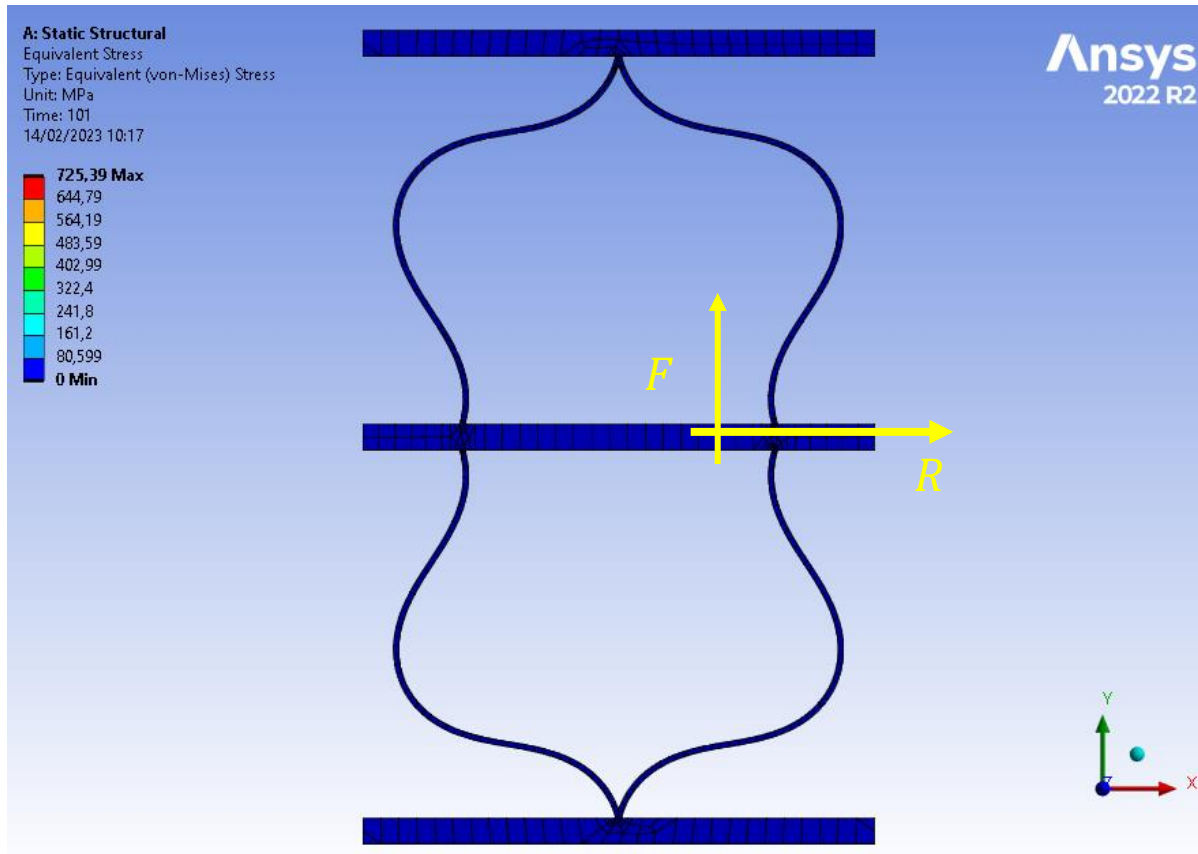


Fig 2.2.3.1

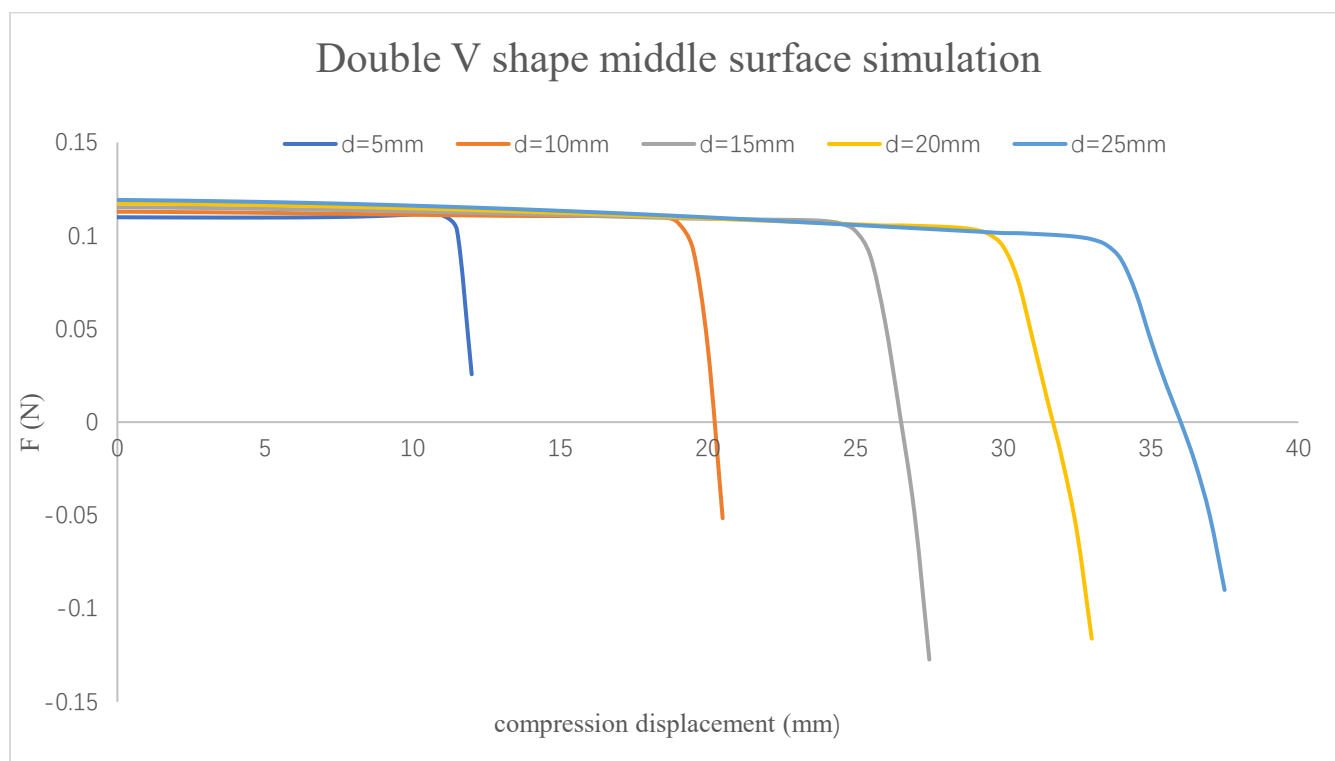


Fig 2.2.3.2

By setting the displacement of upper and lower surface as same value for each step (Fig 2.2.2.2), the double V-shape beam vertical force ( $F$ ) should be remain at 0 during compression, but even in simulation, the result shows that the vertical force ( $F$ ) is not 0. This non-zero vertical force ( $F$ ) suggests that the middle surface tends to be unstable, and thus difficult to be properly guided along the desired motion direction. This is main due to the geometry tolerance of CAD model (obviously, in this thesis, the upper part beams thickness is smaller than the lower part beams thickness). The small geometry tolerance will lead the structure unbalance. It will get more worse in practice.

In practice, the beam may will be printed in different thickness (maybe just few micron) due to small error of 3D printer. These will cause unbalance of the structure and will lead the middle surface under asymmetrical distributed compression, so the middle surface will not move along the desired motion direction (X direction) which will cause experiment failure.

## 3 Analytical model of the V-shape beam

### 3.1 Classical oblique spring model

The classic negative stiffness is based on the oblique spring model. The basis of the model is that negative stiffness is created by axially preloading an ordinary compression spring from its initial length  $L_0$  to compressed length  $L_p$  as shown in Fig 3.1.1 [1], where  $h_0$  is the initial height,  $h_p$  is the height under compression,  $u$  is displacement. So, the preloading distance can be considered as  $d = h_0 - h_p$ .

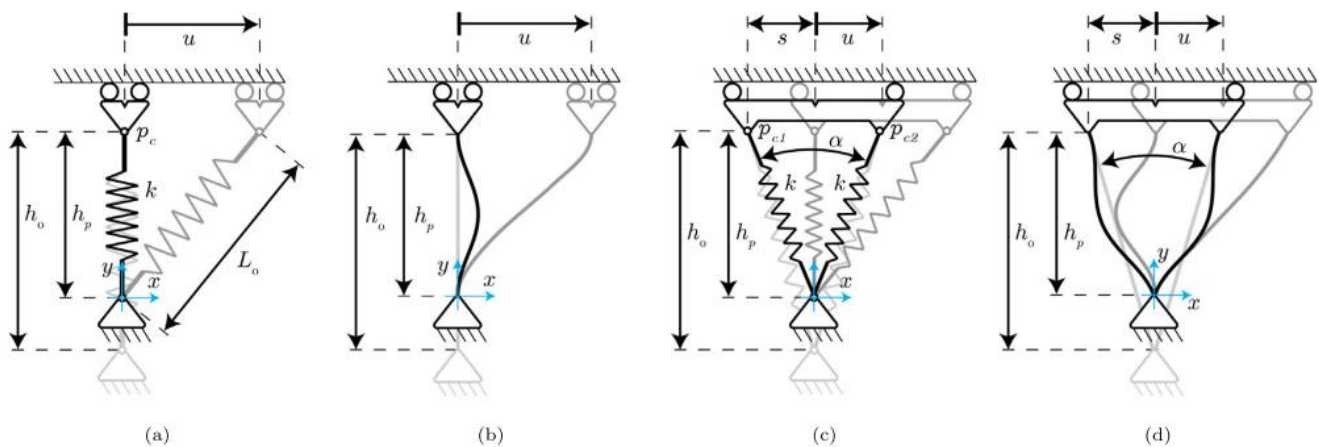


Fig 3.1.1 Schematic diagram of spring model [7]

The potential energy of spring is  $E = \frac{1}{2} \times k \times \sqrt{(h_p^2 + u^2)} - L_0$  (Fig 3.1.1a [1]). Consider the continuum beam compression and bending behavior same as spring (Fig 3.1.1b [1]).  $k$  is spring stiffness. The potential energy of the V-shaped springs (Fig 3.1.1c [1]) is:

$$E = \frac{1}{2} \times k \times \sqrt{(h_p^2 + (s - u)^2)} - L_0 + \frac{1}{2} \times k \times \sqrt{(h_p^2 + (s + u)^2)} - L_0 \quad (\text{Eq 3.1.1})$$

The force and stiffness along the displacement can be describe as:

$$F = \frac{dE}{du} ; K = \frac{dF}{du} \quad (\text{Eq 3.1.2})$$

For the given materials, consider the spring stiffness  $k = 5 \text{ N/mm}$  and  $\alpha = 35^\circ$ . In order to avoid the problem of determining geometric parameters, it is appropriate to use non-dimensional form. Based on reference [2], the non-dimensional form can be write as:

$$E_{nd} = E / \left( \frac{1}{2} \times k \times L_0^2 \right) ; F_{nd} = F / (k \times L_0) ; K_{nd} = K / k \quad (\text{Eq 3.1.3})$$

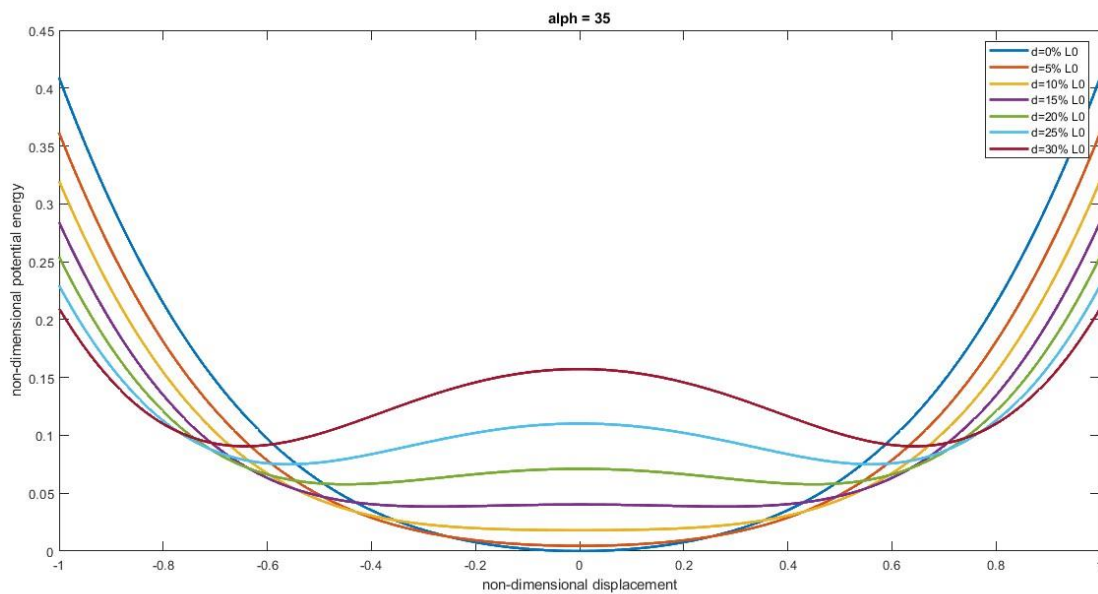


Fig 3.1.2a non-dimensional potential energy of V-shape beam

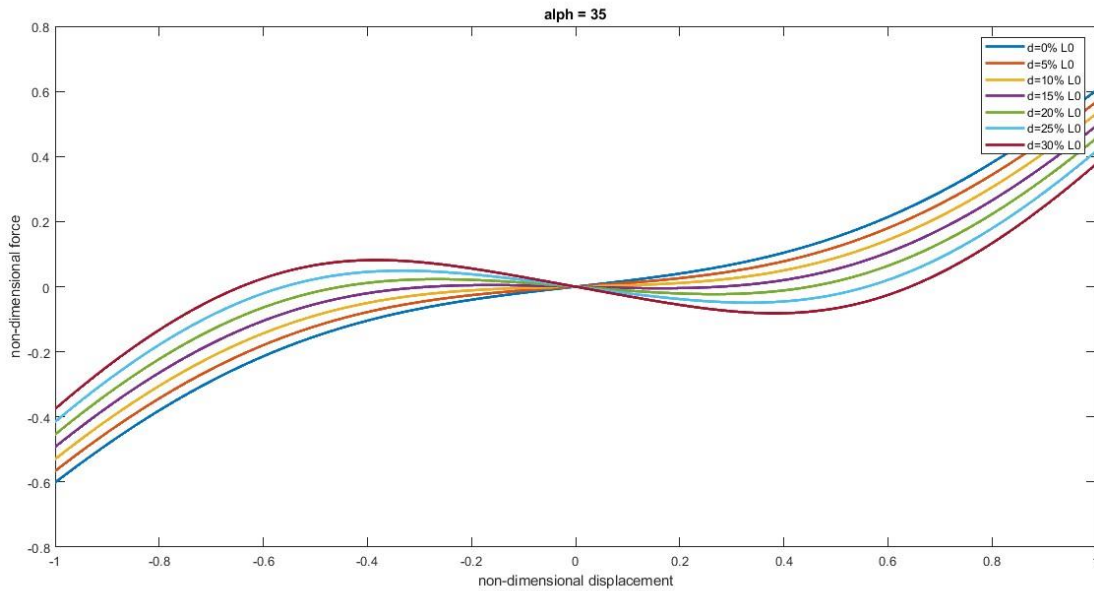


Fig 3.1.2b non-dimensional force along the displacement of V-shape beam

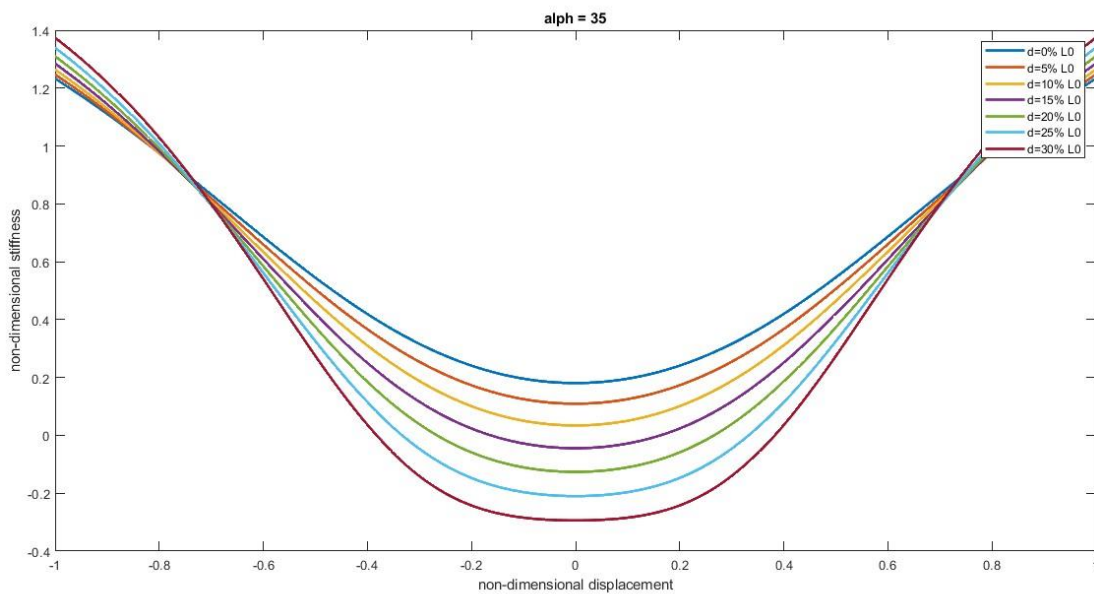


Fig 3.1.2c non-dimensional stiffness along the displacement of V-shape beam

Fig 3.1.2a shows that the structure changes from a single stable state to a bistable state. Correspondingly, in the bistable region, structure reaction force decreases as the displacement increases which is the

negative stiffness region (Fig 3.1.2b). According to the oblique spring model, spring stiffness has no relationship with the negative stiffness appears, which only manifests when the preloading distance ( $d$ ) exceeds 10% of  $L_0$ .

Although the oblique spring model can display negative stiffness as shown in Fig 3.1.2c, this only happens when a constant material property is present, therefore the spring and beam always behave linearly. Consequently, it is hard to determine the spring stiffness.

## 3.2 V-shape beam force analysis

### 3.2.1 Force analysis

This section presents a simplified analytical model to directly analyze the force of the V-shape beam. Compared with the oblique spring model, it can show the stress and displacement of each element in more detail.

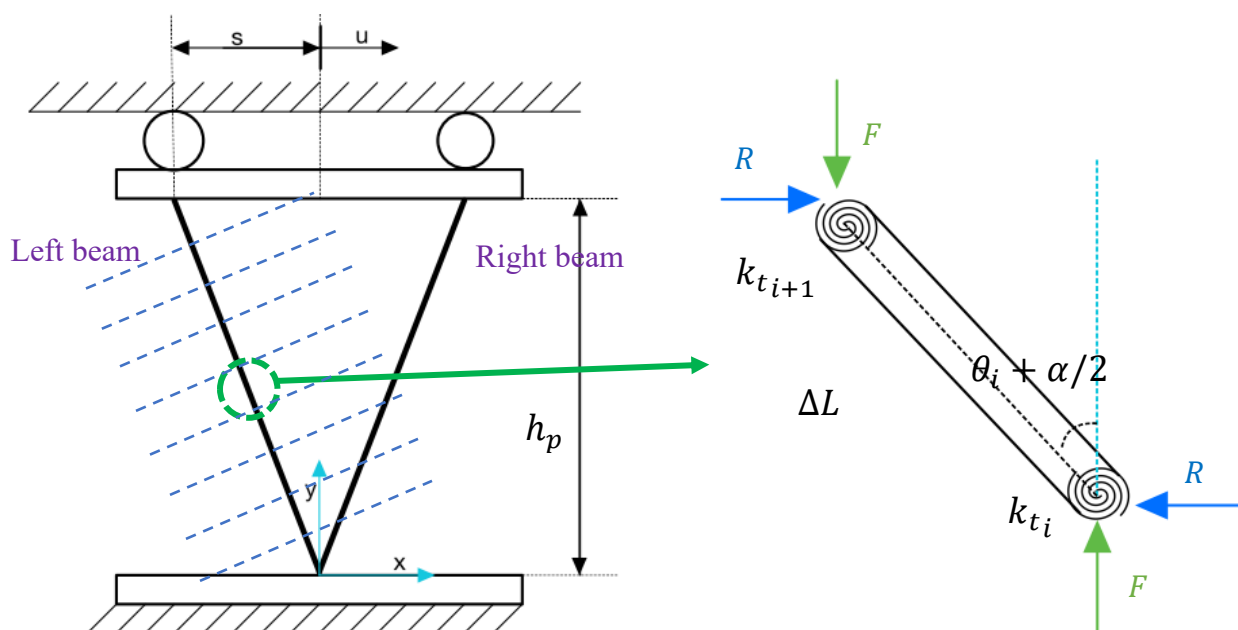


Fig 3.2.1.1 Force analysis of V-shap beam

Let us consider the deformed beam structure. Since the entire structure is symmetrical about the y-axis, only the beam on one side needs to be analyzed. Let us divide the beam into  $N$  parts and take one part for analysis ( $\Delta L = L_0/N$ ). It is always under the forces  $F$  (along Y) and  $R$  (along X) during the preloading and the displacement process. For  $N$  equal beams, the force analysis can be obtained as:

$$k_{t_{i+1}} \times (\theta_{i+1} - \theta_i) + k_{t_i} \times (\theta_i - \theta_{i-1}) + F \times \Delta L \times \sin\left(\theta_i + \frac{\alpha}{2}\right) - R \times \Delta L \times \cos\left(\theta_i + \frac{\alpha}{2}\right) = 0 \quad (\text{Eq } 3.2.1.1)$$

Where  $k_{t_i}$  is  $i_{th}$  beam element torsional stiffness. Since the beam are equally divided, the element torsional stiffness is considered the same for all the beam elements in this following. The angles  $\theta_0$  and  $\theta_{N+1}$  correspond to the upper and lower of the beam, thus they are set to  $0^\circ$  to be compliant with the boundary conditions. It can be seen from Fig 3.2.1.1 that there are always two geometric relationships in the entire deformed V-shape beam, which is:

$$\sum_{i=1}^N \Delta L \times \cos\left(\theta_i + \frac{\alpha}{2}\right) = h_p \quad (\text{Eq } 3.2.1.2)$$

$$\sum_{i=1}^N \Delta L \times \sin\left(\theta_i + \frac{\alpha}{2}\right) = s + u \quad (\text{Eq } 3.2.1.3)$$

By solving these  $N+2$  equations, we can find all unknowns including all  $\theta$ ,  $R$ ,  $F$ . It should be noted that if the preloading is 0, this model cannot work, because when the  $d = 0$ , the displacement will definitely lead a tension effect on the beam, violating the assumptions of the model.

Solving the  $N + 2$  non-linear equation is not easy, and it can be done by using MATLAB command “vpasolve” to solve equations numerically.

*Matlab Command:* `solution = vpasolve([Equations],(Variables),(Initial parameter)]`

**Equations** : the equation that explain in above,  $N$  equation of force relationship and 2 equation of geometric relationship. (Eq 3.2.1.1; Eq 3.2.1.2 and Eq 3.2.1.3).

**Variables** : there are  $N + 2$  variables, which is  $N$  angles ( $\theta_1, \theta_2, \theta_3 \dots \theta_N$ ),  $R$  and  $F$ .

**Initial parameter** : Initial guess or search range for solution. In fact, if only a single initial parameter is set for the entire loop, the direction of solution will be wrong in some steps of loop (Fig 3.2.1.3).

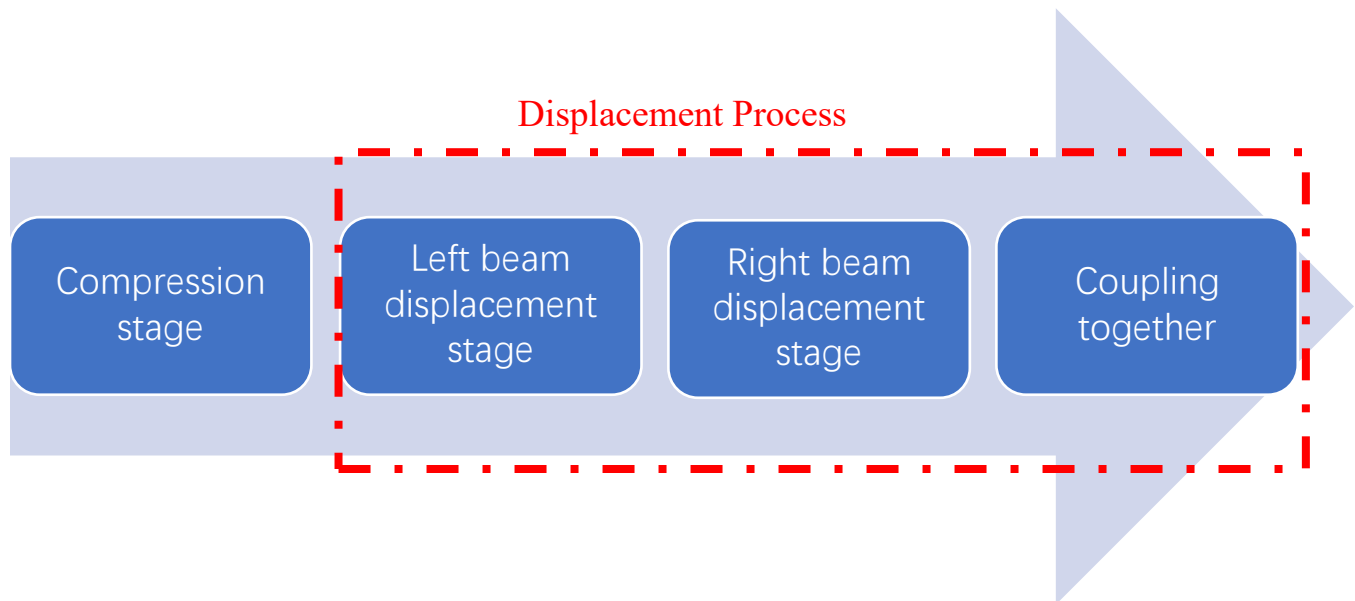


Fig 3.2.1.2 Solving process

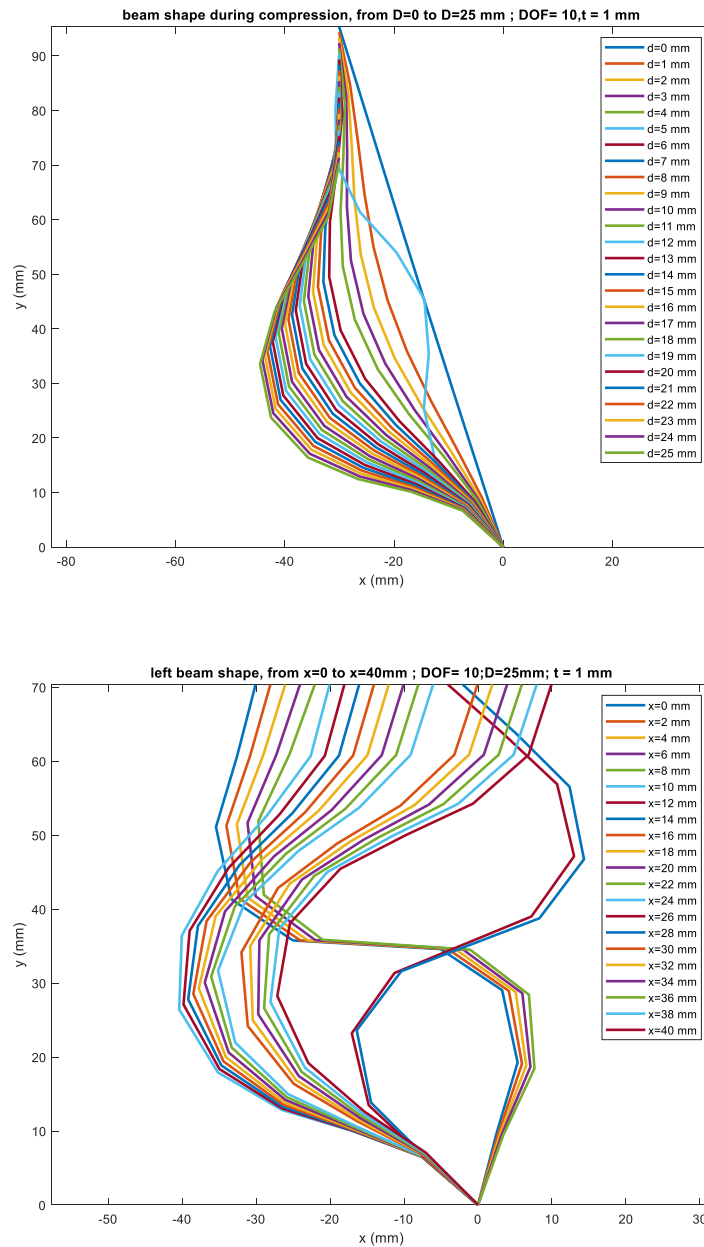


Fig 3.2.1.3 Wrong solution for displacement and compression process

Solving the entire behavior can be divide as four part (Fig 3.2.1.2):

1. Compression stage
2. Left beam displacement stage and Right beam displacement stage
3. Coupling left beam displacement and right beam displacement

### 3.2.2 Consideration on the torsional stiffness $K_t$ (Flexure Hinges)

As discussed before, a complete beam can be assumed as several rigid parts connected by flexure hinges (Fig 1.3.5). Finding the appropriate torsional stiffness directly determines whether the mechanical analysis model can fit the simulation results. In fact, it is the geometric parameter of the beam that determines the torsional stiffness. According to the simulation results of Ansys, use the Force Analysis model to find the appropriate torsional stiffness, so that the Force Analysis model can get better fitting to the Ansys simulation results.

In this thesis, the following values will be considered:

$$K_{t_{t=1\text{ mm}}} = 160\text{ Nmm/rad}$$

$$K_{t_{t=1.2\text{ mm}}} = 260\text{ Nm/rad}$$

### 3.2.3 Compression process simulation

The base procedure is:

First, define the step size of compression ( $\Delta d$ ), so the total step of compute compression process is:

$$N_{comp} = D/\Delta d + 1 \quad (\text{Eq 3.2.3.1})$$

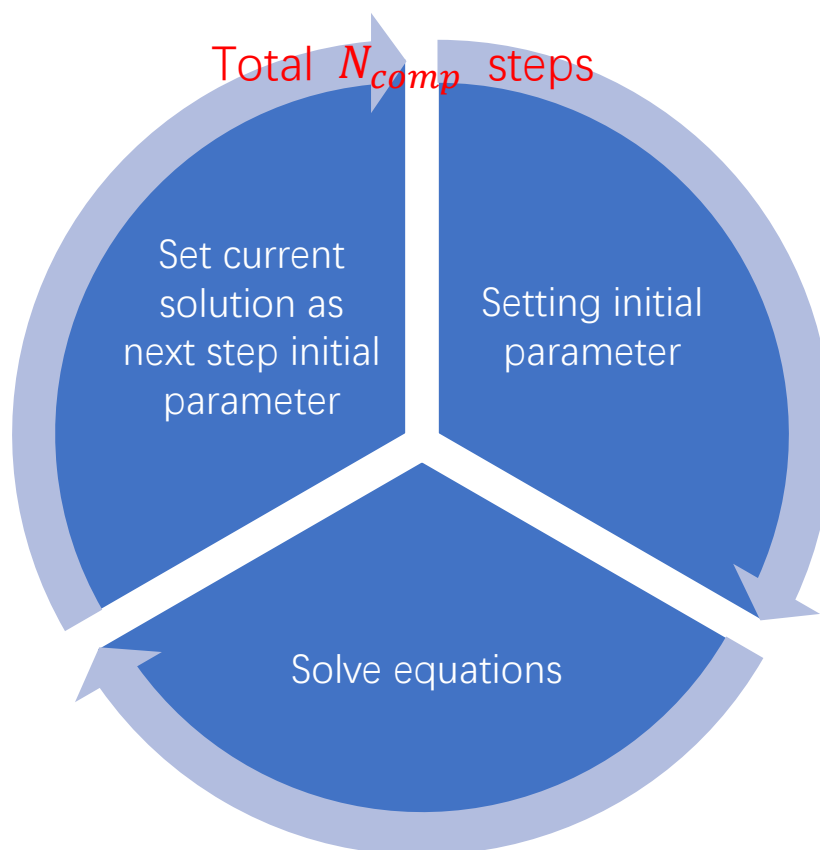


Fig 3.2.3.1 Procedure of solving compression process

Which means that for each step, there are  $N+2$  equations need to be solved. The ‘for’ loop can easy build the iterative procedure step by step. The solving procedure is shown in Fig 3.2.3.1.

For angle  $(\theta_1, \theta_2, \theta_3 \dots \theta_N)$ , as previous discussion (Chapter 3.2.1, Fig 1.3.5 and Fig 3.2.1), the whole beam can consider as  $N + 1$  flexure hinges connect with  $N$  rigid part. Each rigid part has angle with respect to Y axis. For divide one beam as multiple DOF, it must consider the  $N$  is odd number or even number.

If the  $N$  is even number, the  $N/2$  DOF can be oriented to positive direction, other  $N/2$  DOF can be oriented to negative direction (Fig 3.2.3.2  $N = 8$ ).

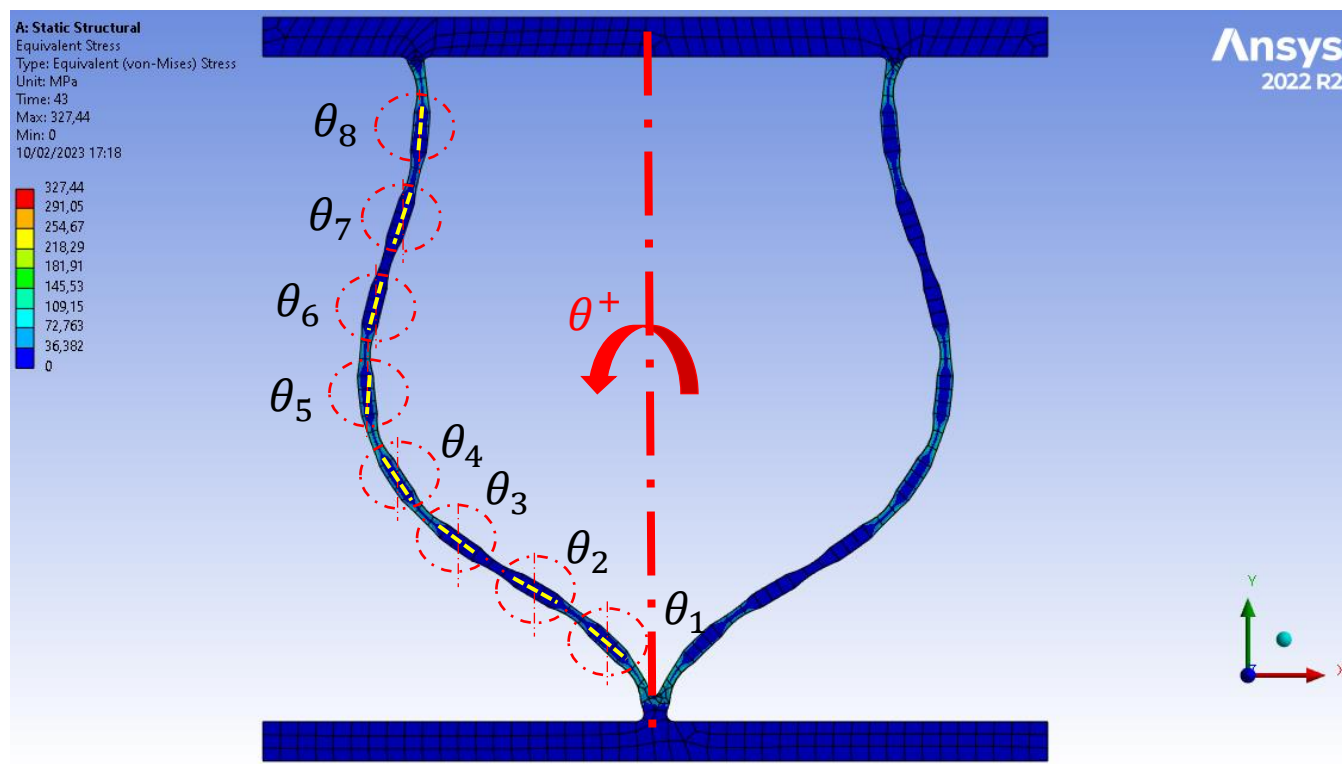


Fig 3.2.3.2 V-shape beam with 8 flexure hinges

So, define the first step initial value of angle is critical, but cannot exceed the proper value, only define the trend. An initial angle of 0.0001 seems to be a suitable value.

If the  $N$  is odd number, the  $(N - 1)/2$  DOFs can be oriented to positive direction, and the others  $(N - 1)/2$  DOFs can be oriented to negative direction, the DOF which in the center of beam remain at original position which means the angle of DOF in the center of beam is  $\alpha/2$  with respect to Y axis (Fig 3.2.3.3  $N = 9$ ).

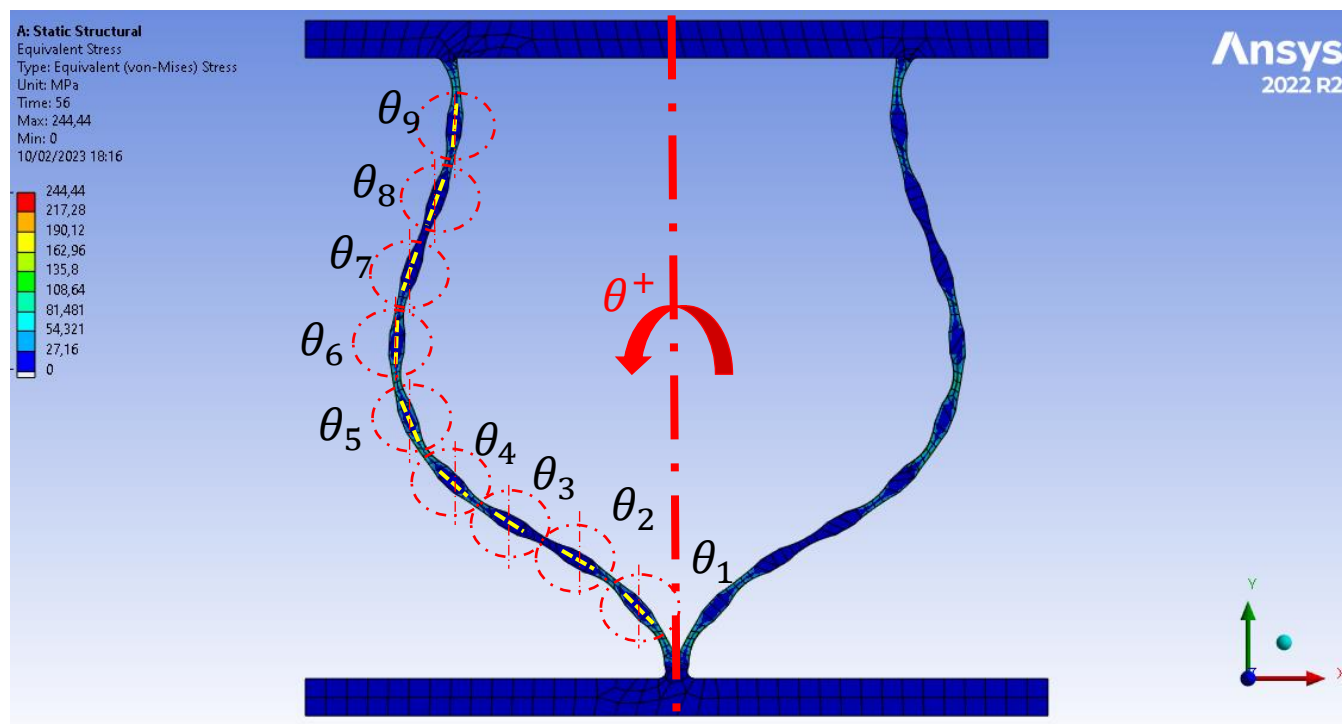


Fig 3.2.3.3 V-shape beam with 9 flexure hinges

For the first step, the following summary can be seen:

$$\text{for } N \text{ is even number, if } i < \frac{N}{2}, \theta_i = 0.0001; \text{ if } i > \frac{N}{2}, \theta_i = -0.0001$$

$$\text{for } N \text{ is odd number, if } i < \frac{N+1}{2}, \theta_i = 0.0001; \text{ if } i = \frac{N+1}{2}, \theta_i = 0; \text{ if } i > \frac{N+1}{2}, \theta_i = -0.0001$$

In fact, the whole compression process starts from  $d = 0 \text{ mm}$ , but in the first step, the MATLAB solver recognize the trivial solution as non-solution, so the computation will end at first step. So, one may consider  $d = 0.0001 \text{ mm}$ , just to avoid the trivial solution. For the initial parameter of force  $R_c$  and  $F_c$  can setting to be  $0.0001 \text{ N}$  in the first step.

As for next step, using the solution of first step as the initial parameter, the whole process will be successful completion.

beam shape during compression, from  $D=0$  to  $D=25$  mm ;  $DOF= 10, t = 1$  mm

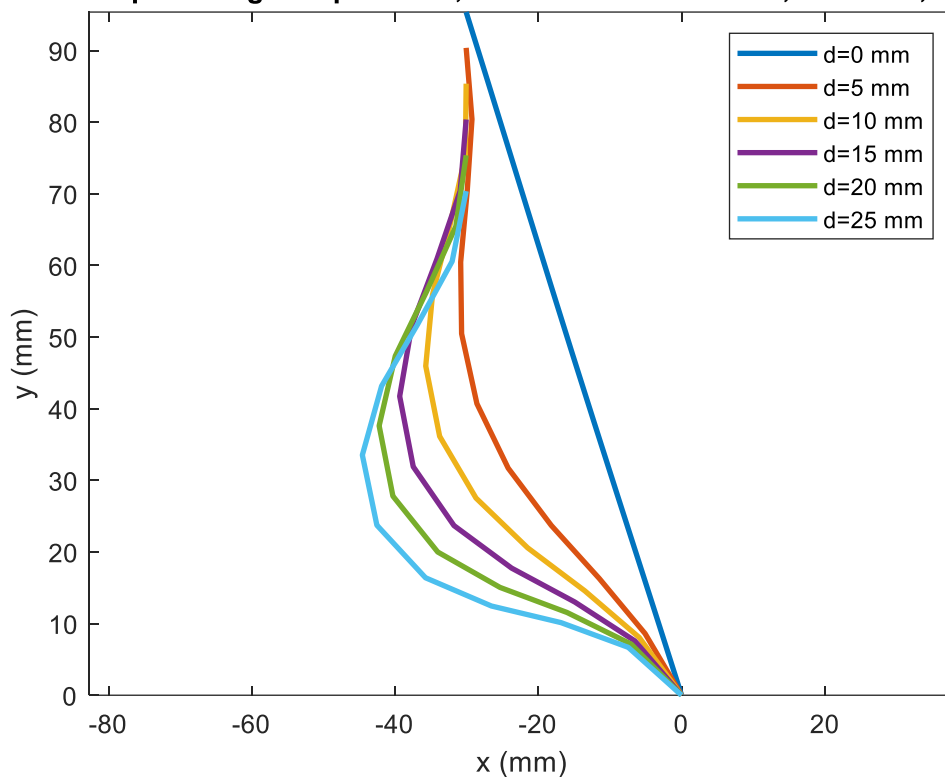


Fig 3.2.3.4 beam shape during compression process ( $t = 1mm$ )

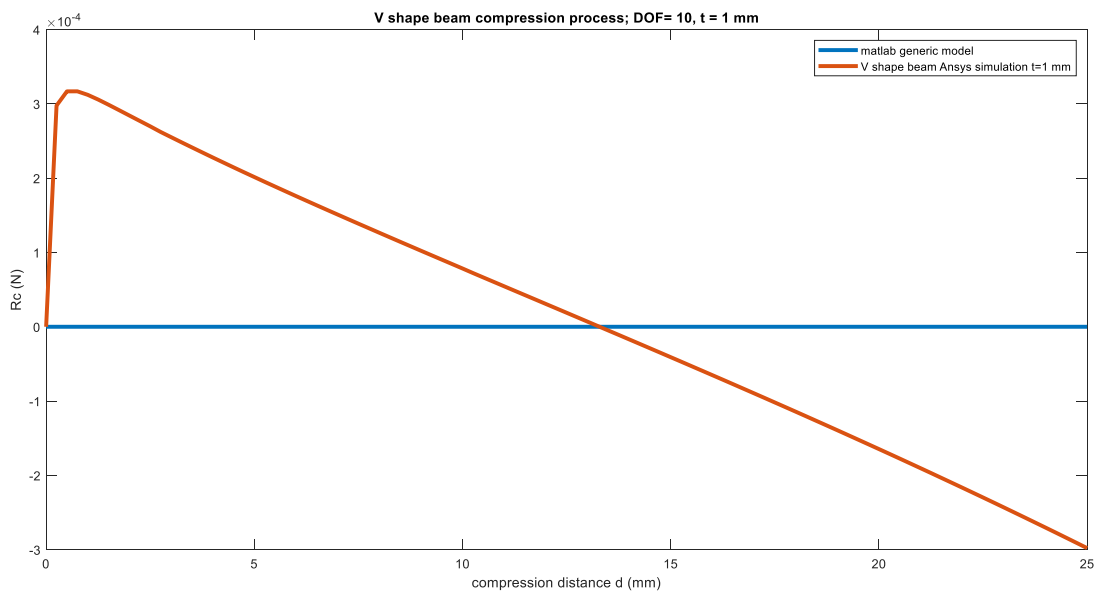


Fig 3.2.3.5  $R_c$  result comparison ( $t = 1mm, N = 10$ )

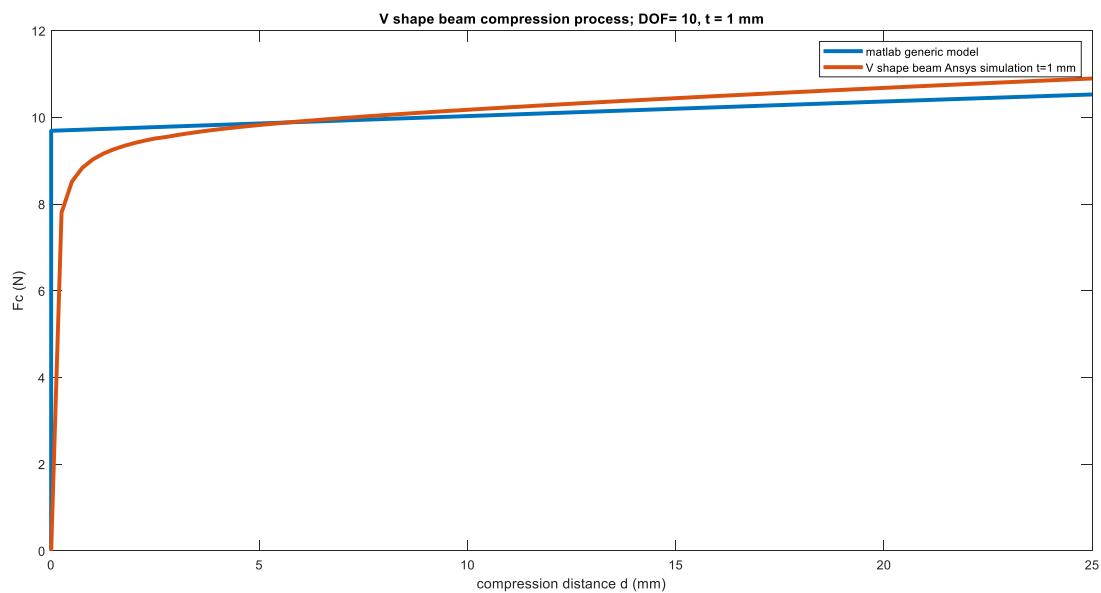


Fig 3.2.3.6  $F_c$  result comparison ( $t = 1\text{mm}$ ,  $N = 10$ )

**beam shape during compression, from  $D=0$  to  $D=25$  mm ; DOF= 10,  $t = 1.2$  mm**

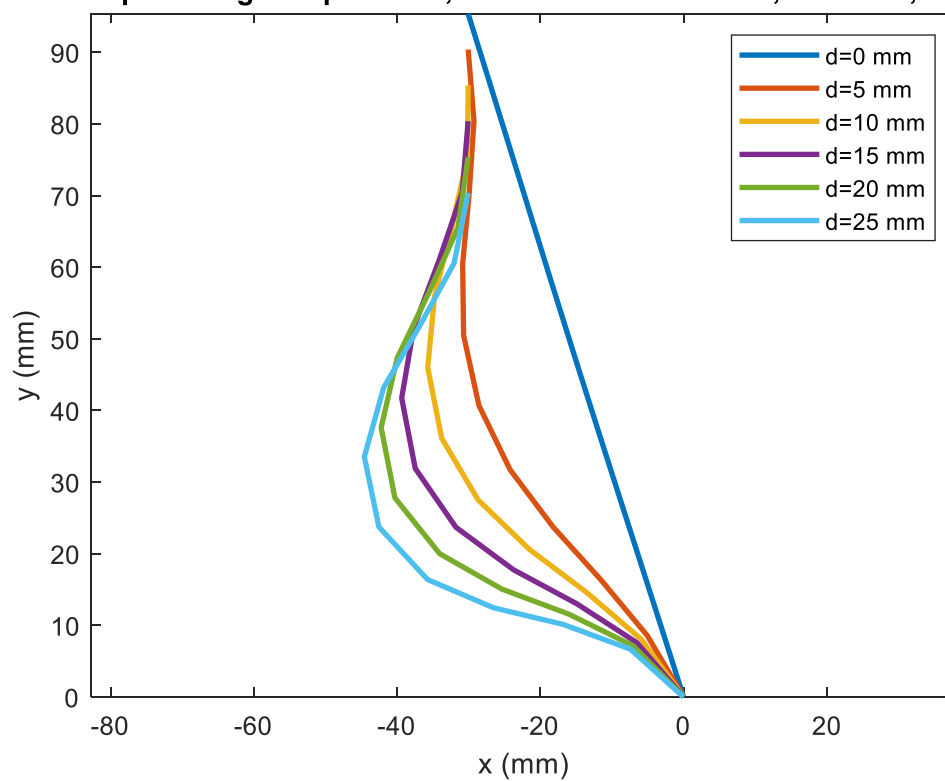


Fig 3.2.3.7 beam shape during compression process ( $t = 1.2\text{mm}$ ,  $N = 10$ )

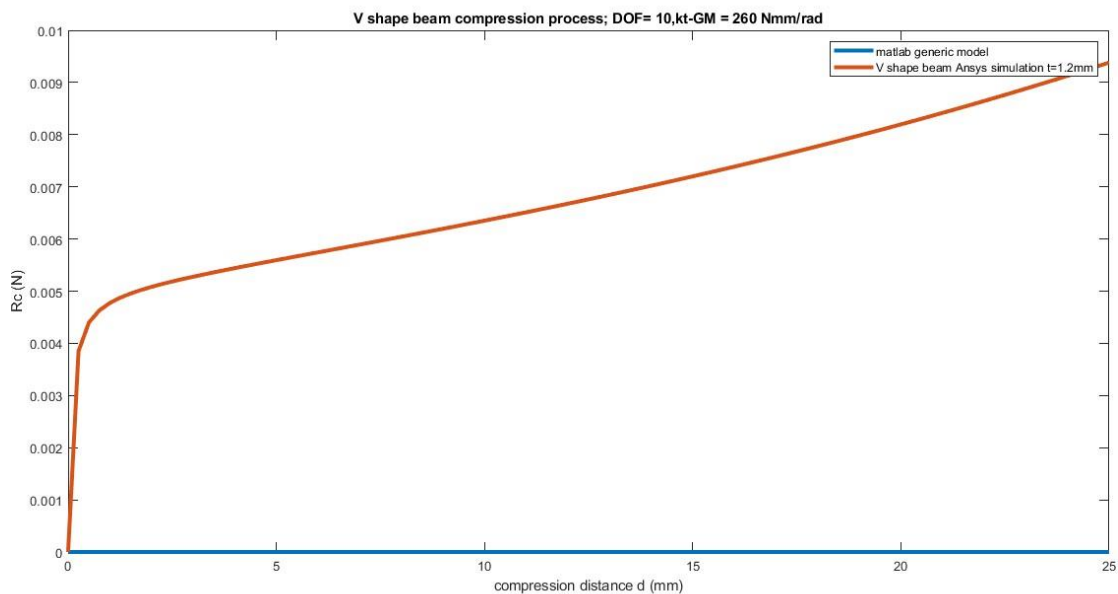


Fig 3.2.3.8  $R_c$  result comparison ( $t = 1.2mm$ ,  $N = 10$ )

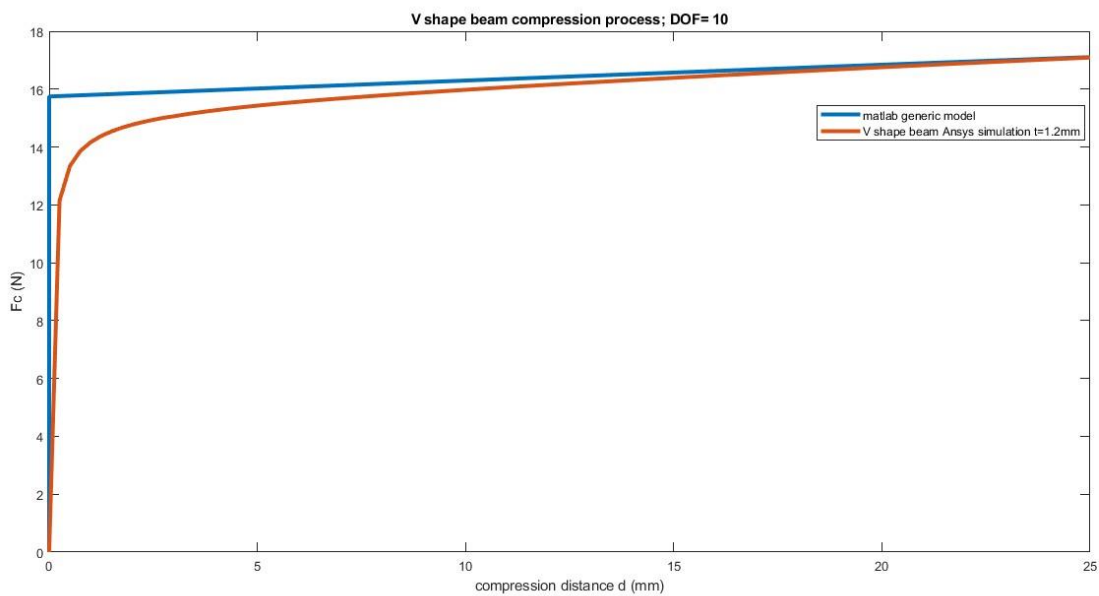


Fig 3.2.3.9  $F_c$  result comparison ( $t = 1.2mm$ ,  $N = 10$ )

By solving the whole process, the comparison with Ansys simulation result shows a good fitting both for  $t = 1mm$  and  $t = 1.2mm$ . As for the shape of beam during compression, the result shows each DOF rotation angle ( $\theta_i$ ) for each preloading distance (Fig 3.2.3.4; Fig 3.2.3.7).

As for the vertical force  $F_c$ , MATLAB model shows a good fitting when the beam thickness is  $1mm$ , and a small overestimation when the beam thickness is  $1.2mm$  (Fig 3.2.3.6; Fig 3.2.3.9).

As for the horizontal force  $R_c$ , MATLAB model shows a quite similar result to the Ansys simulation both for  $t = 1mm$  and  $t = 1.2mm$  (Fig 3.2.3.5; Fig 3.2.3.8).

### 3.2.4 Displacement process simulation

After solving the compression stage, it is possible to extract the  $\theta_i$  ( $i = 1,2,3, \dots, N$ ),  $F_c$  and  $R_c$  results corresponding to  $D$ , and to use the value from the compression process result as the initial parameter for first step of displacement stage.

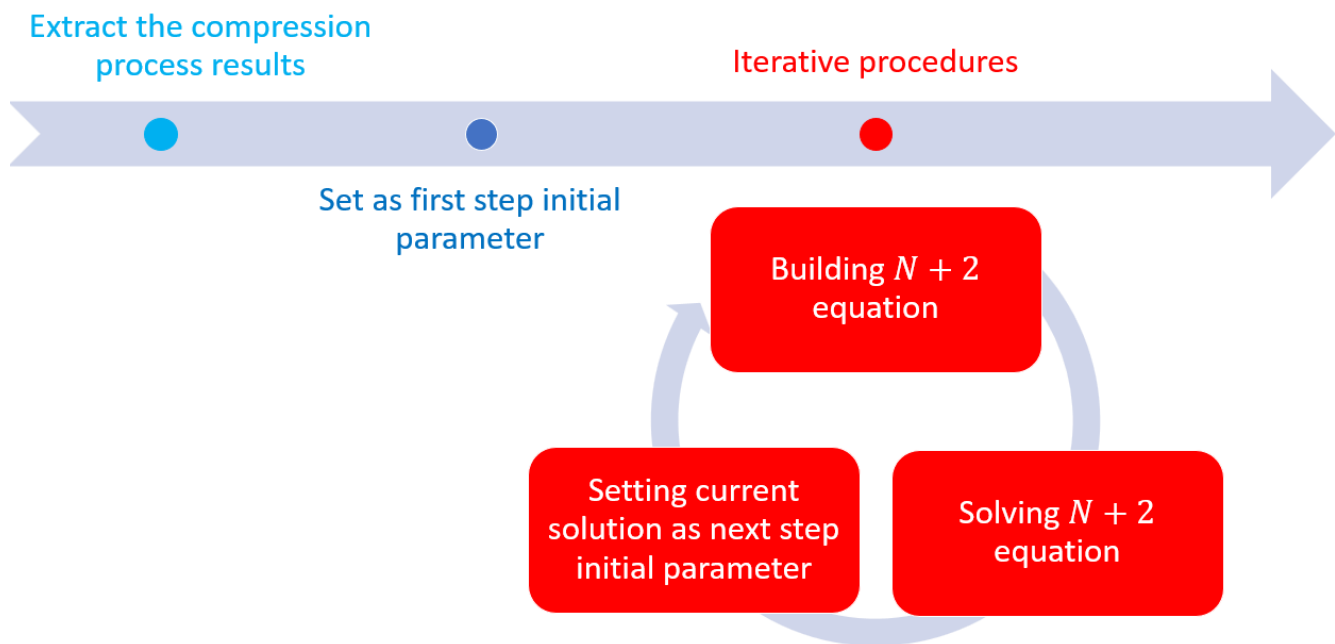


Fig 3.2.4.1 Procedure of solving displacement process

The whole procedure is shown in Fig 3.2.4.1, and it can be repeated two times (one for  $u = 0 \sim u_{lim}$ , other

for  $u = -u_{lim} \sim 0$ ).

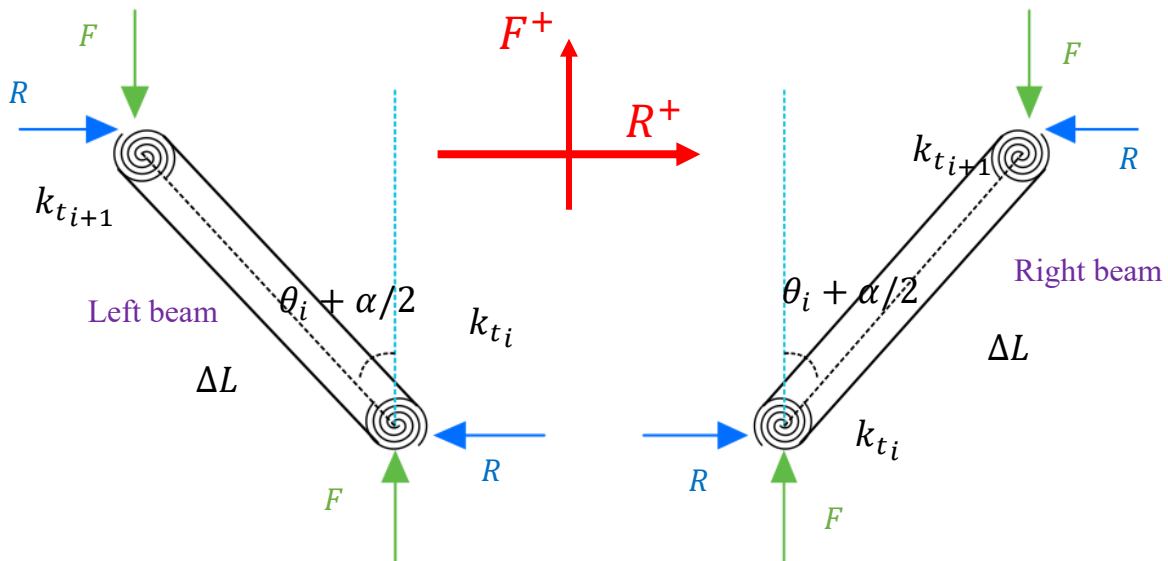


Fig 3.2.4.1 Left and right beam force analysis

The simulation will be divided as two parts:

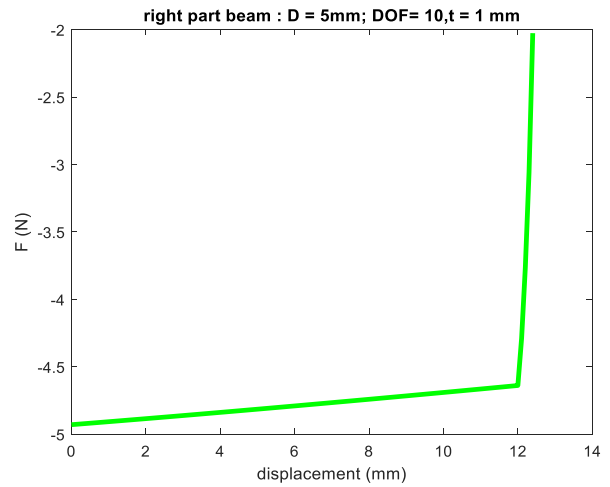
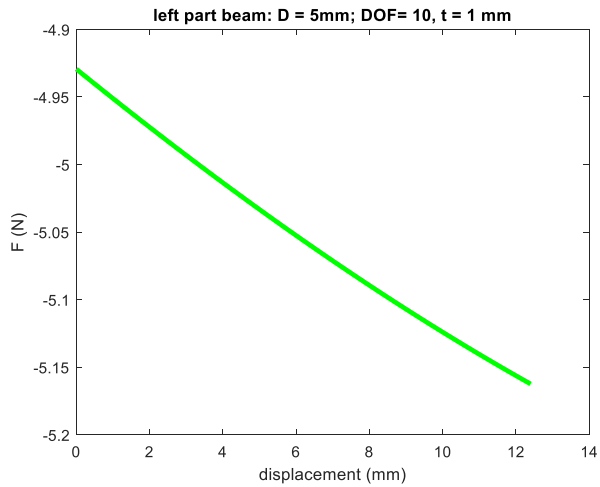
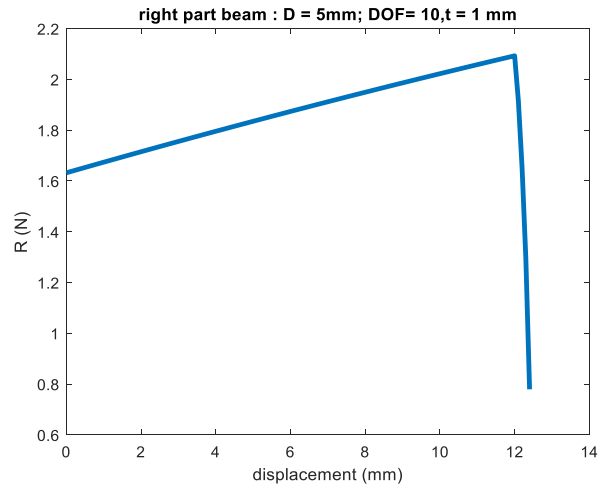
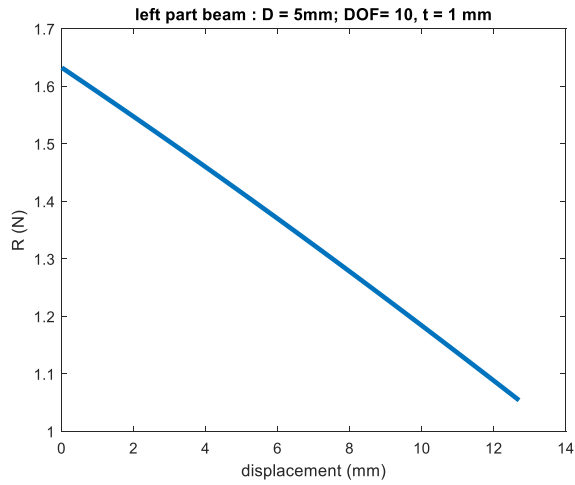
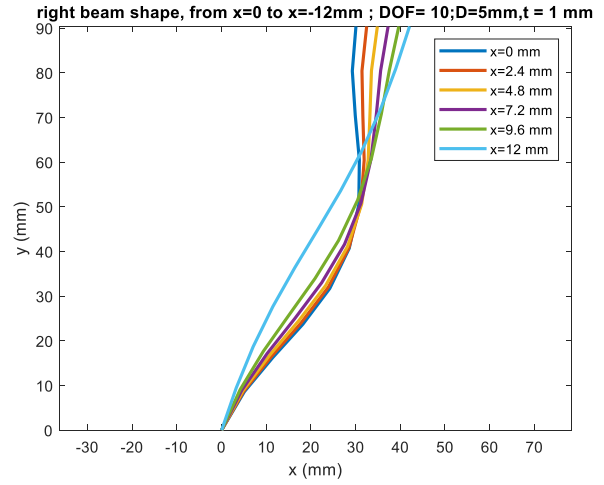
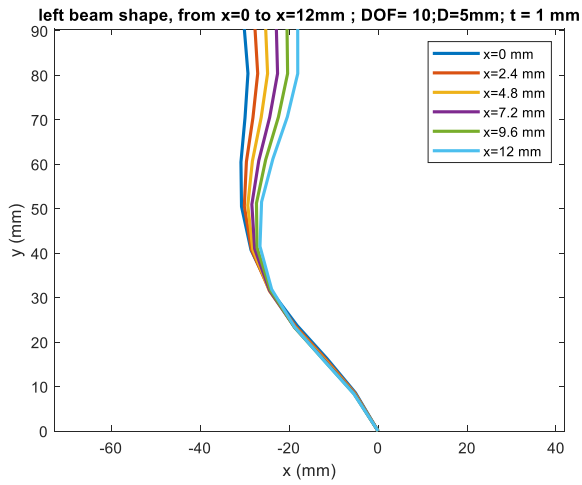
1. Set  $u = 0 \sim -u_{lim}$  in order to compute left part of the beam during the displacement.
2. Set  $u = 0 \sim u_{lim}$  in order to compute right part of the beam during the displacement.
3. Couple left beam and right beam results.

The coupling can be written as:

$$R_{tot} = R_{left\ beam} - R_{right\ beam} \quad (\text{Eq 3.2.4.1})$$

$$F_{tot} = F_{left\ beam} + F_{right\ beam} \quad (\text{Eq 3.2.4.2})$$

For  $D = 5\text{mm}$ :



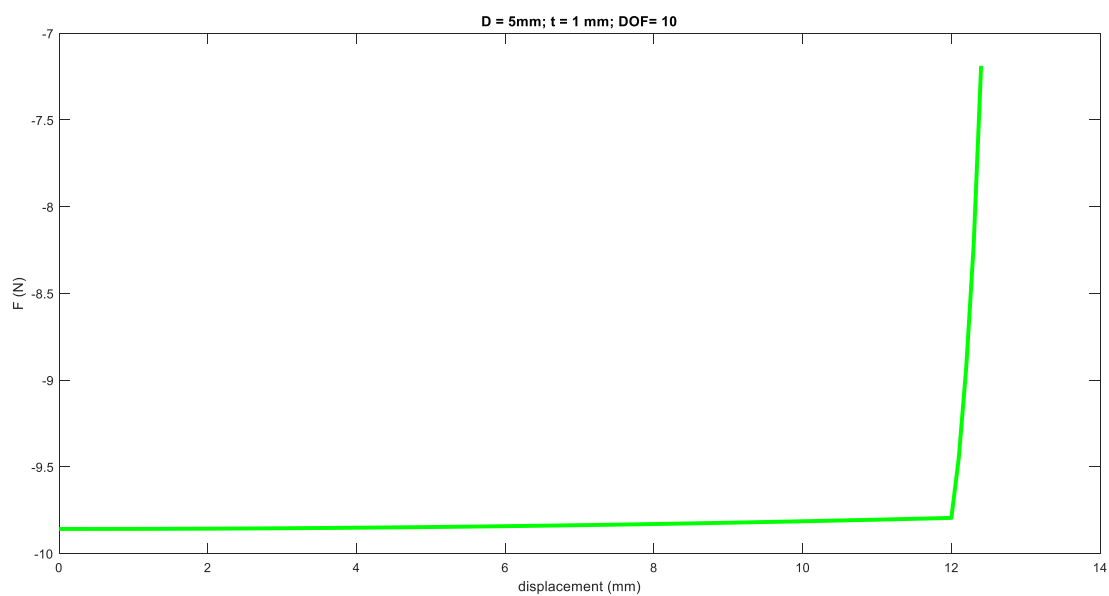
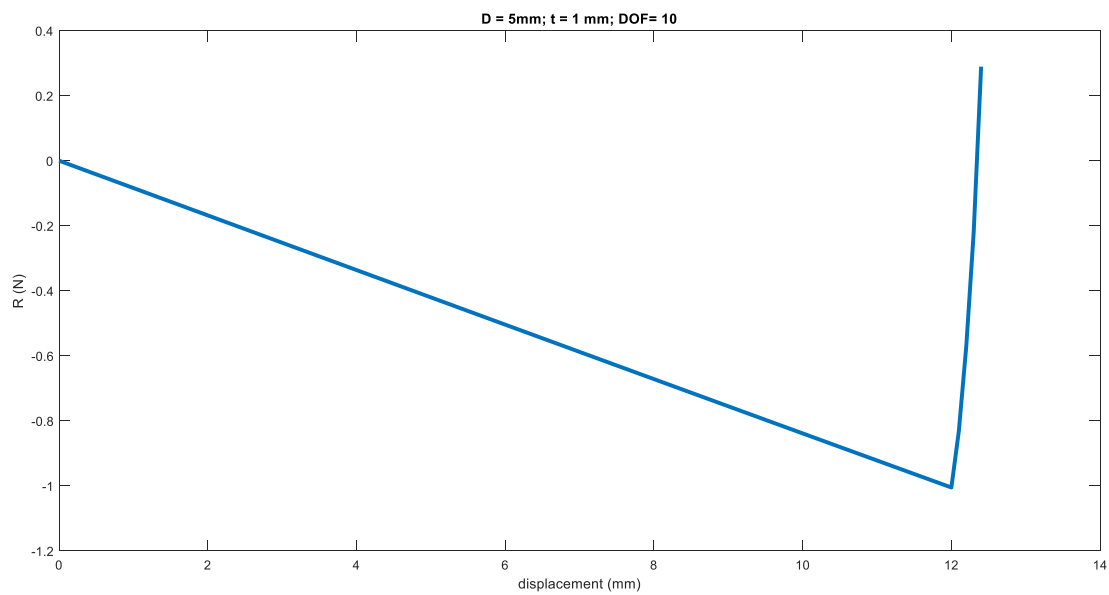
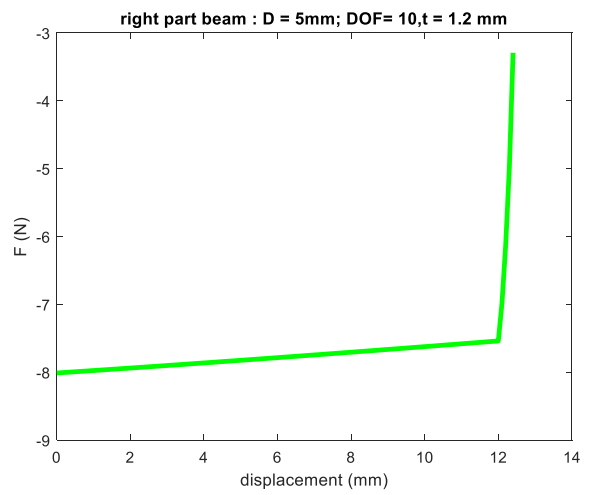
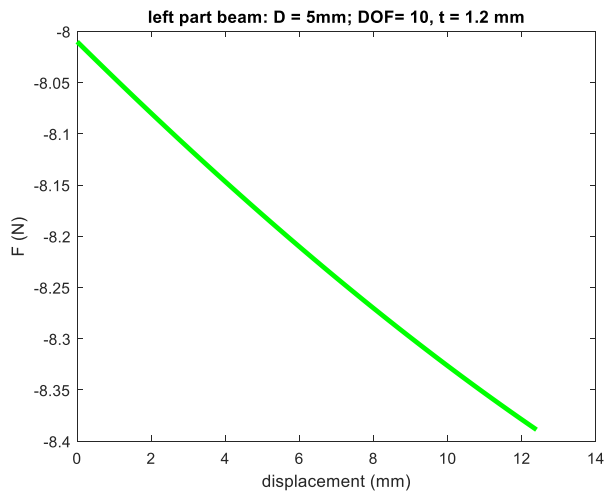
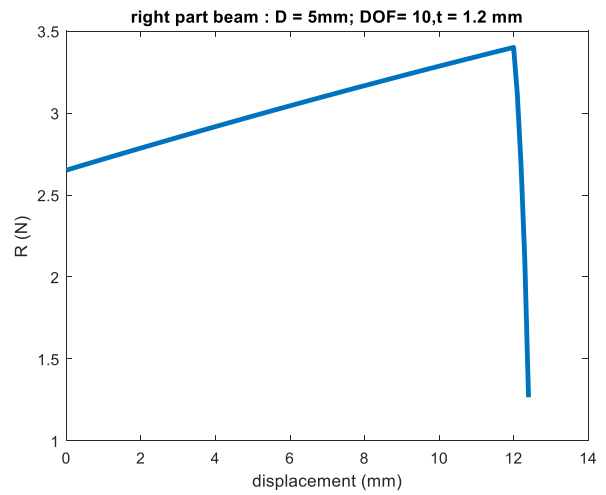
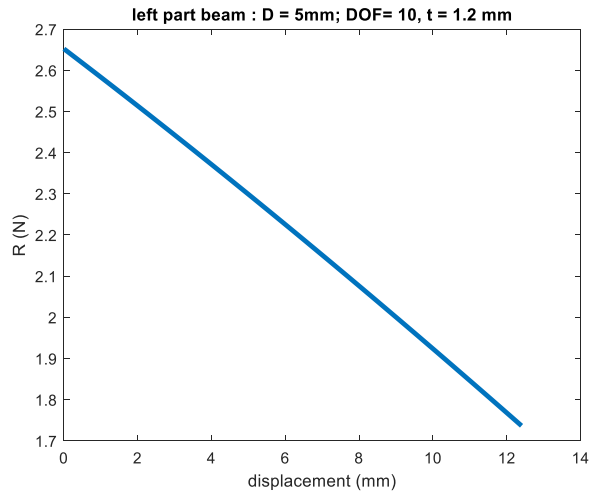
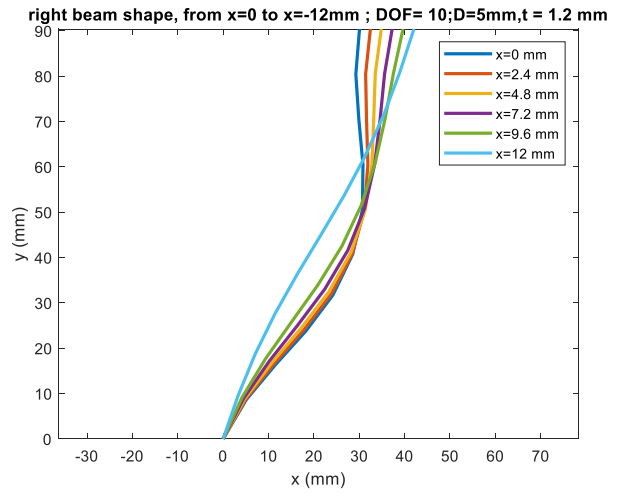
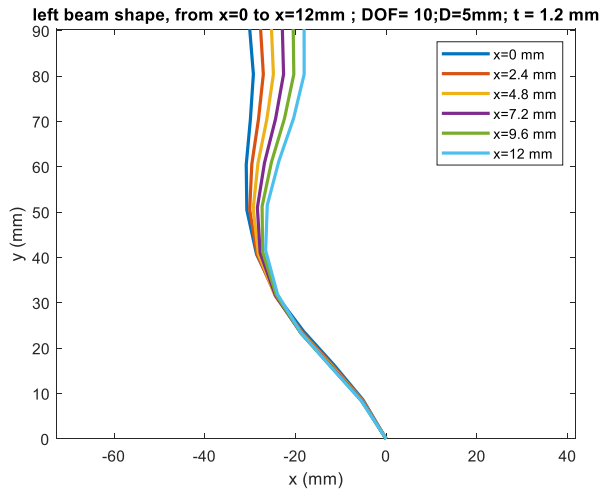


Fig 3.2.4.2  $t = 1mm$ ,  $D = 5mm$



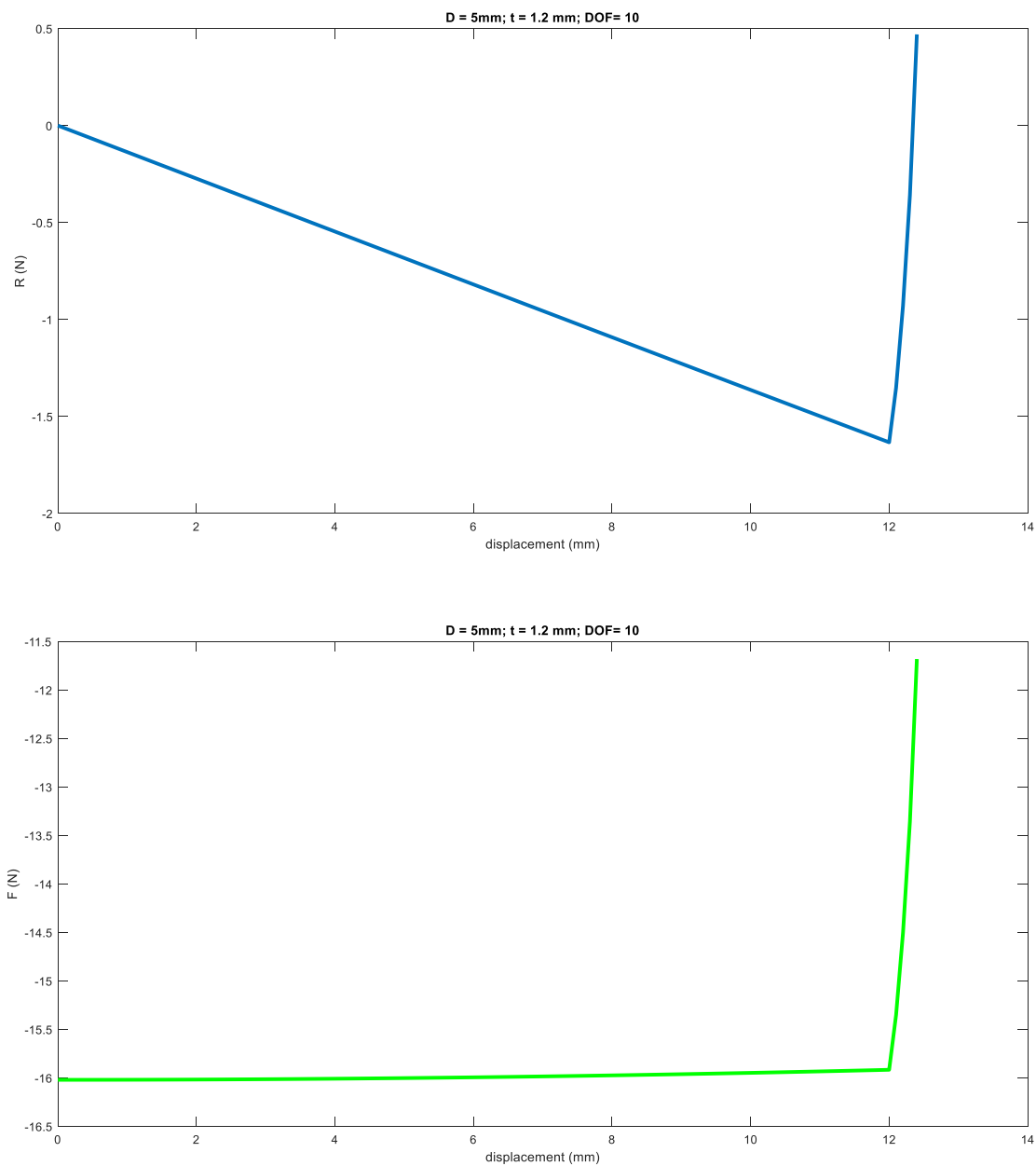
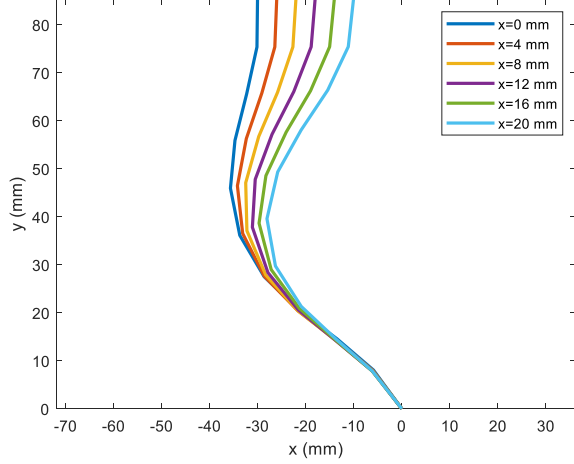


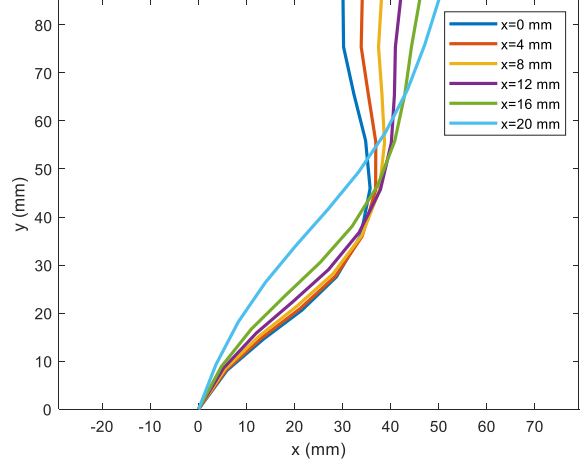
Fig 3.2.4.3  $t = 1.2\text{mm}$ ,  $D = 5\text{mm}$

For  $D = 10\text{mm}$ :

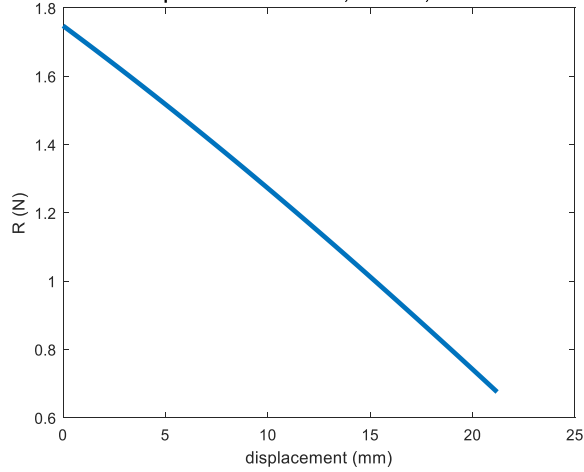
left beam shape, from  $x=0$  to  $x=20$  mm ; DOF= 10;  $D=10$ mm;  $t = 1$  mm



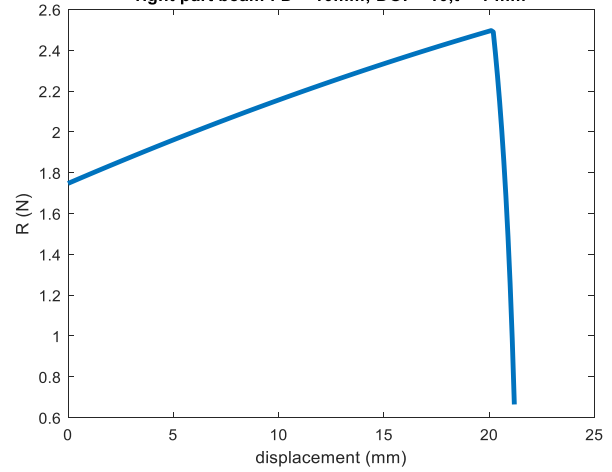
right beam shape, from  $x=0$  to  $x=-20$  mm ; DOF= 10;  $D=10$ mm;  $t = 1$  mm



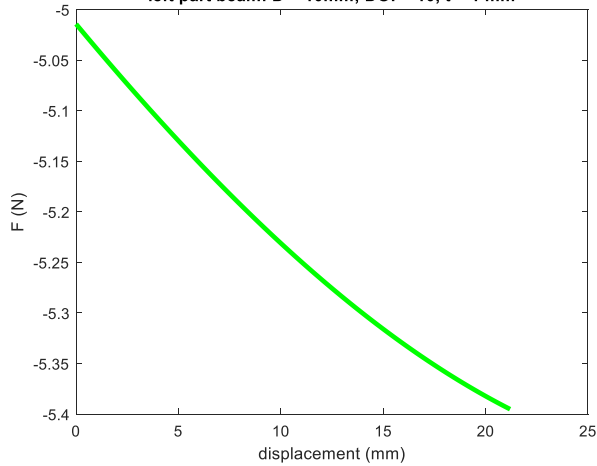
left part beam :  $D = 10$ mm; DOF= 10,  $t = 1$  mm



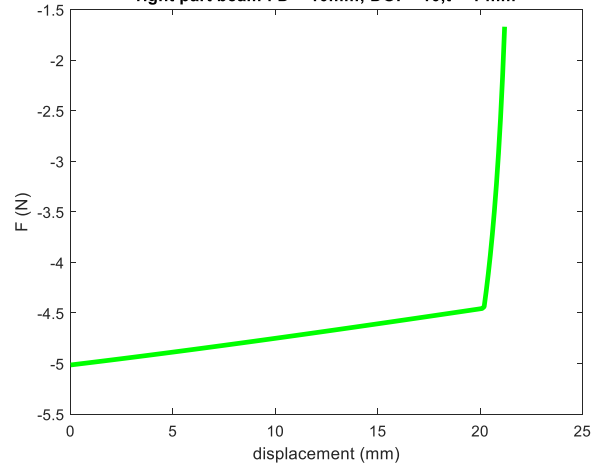
right part beam :  $D = 10$ mm; DOF= 10,  $t = 1$  mm



left part beam:  $D = 10$ mm; DOF= 10,  $t = 1$  mm



right part beam :  $D = 10$ mm; DOF= 10,  $t = 1$  mm



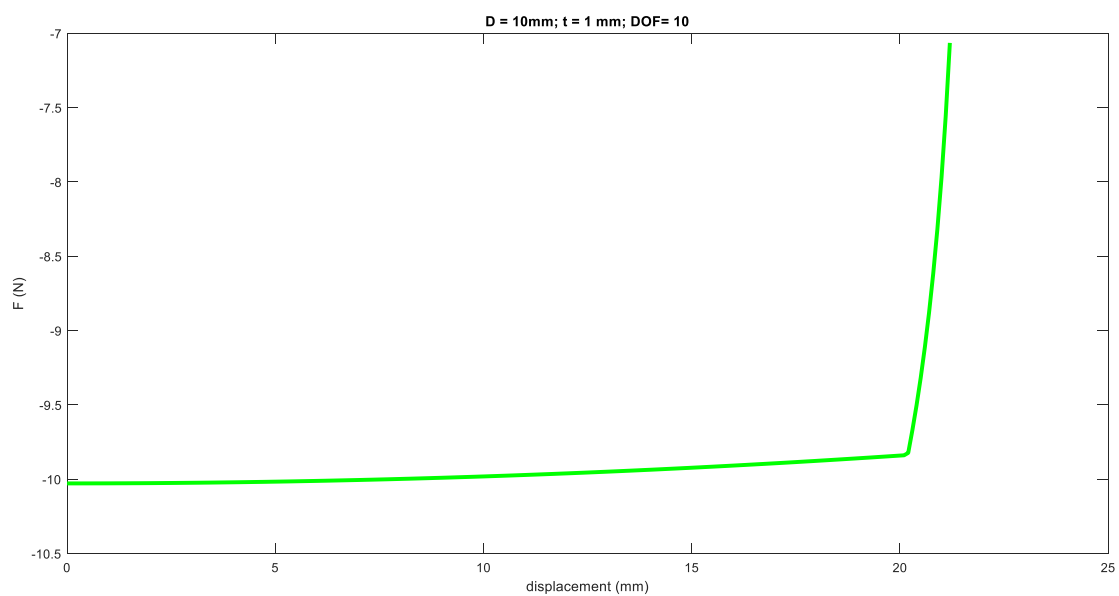
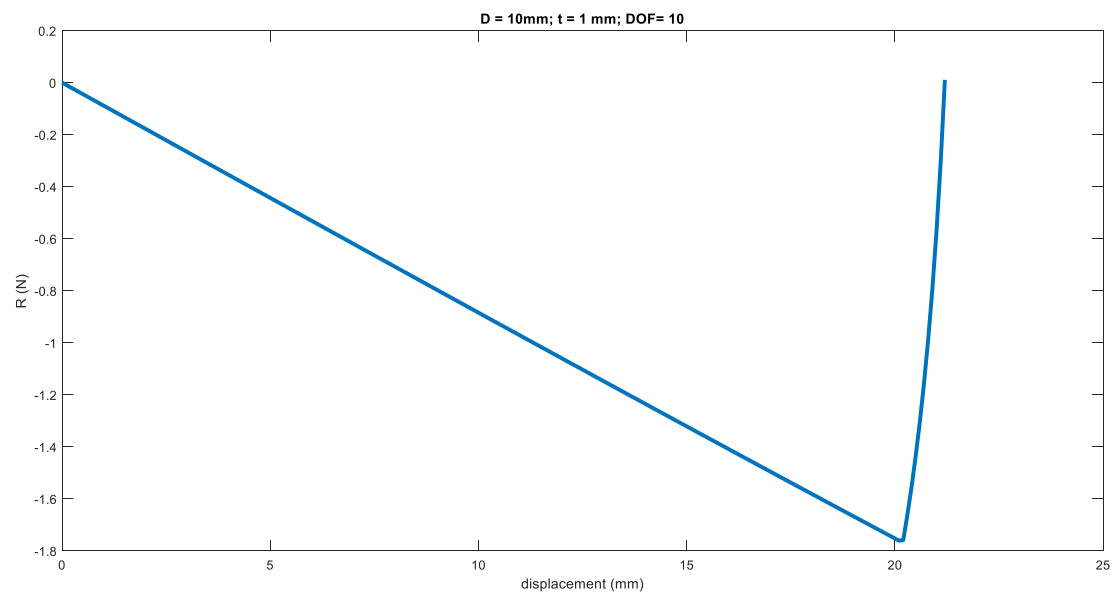
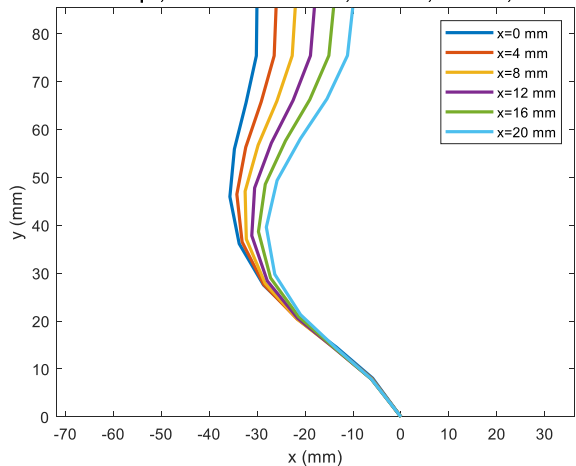
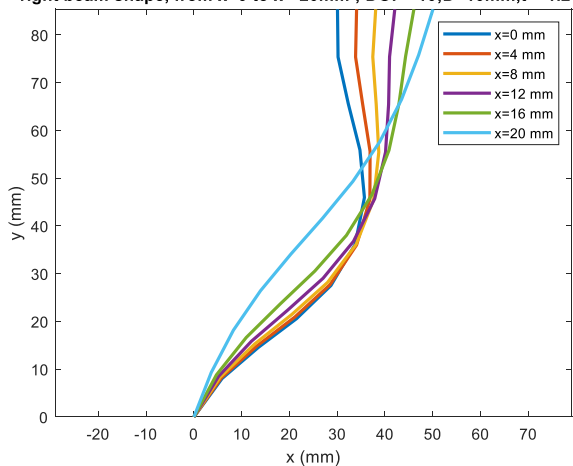


Fig 3.2.4.4  $t = 1\text{mm}$ ,  $D = 10\text{mm}$

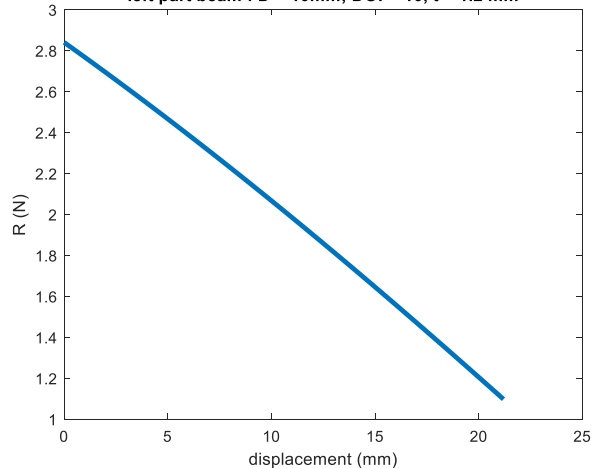
left beam shape, from x=0 to x=20mm ; DOF= 10;D=10mm; t = 1.2 mm



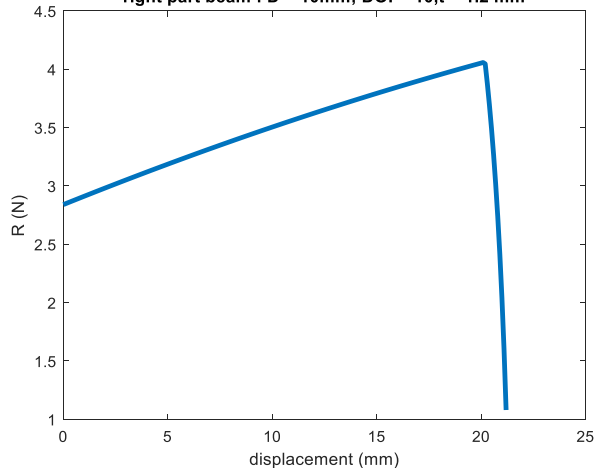
right beam shape, from x=0 to x=-20mm ; DOF= 10;D=10mm,t = 1.2 mm



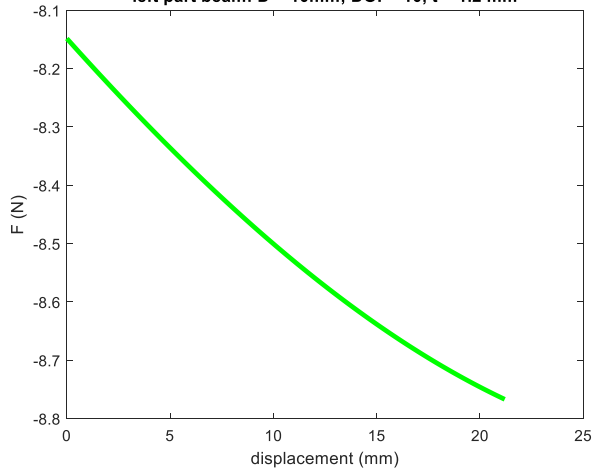
left part beam : D = 10mm; DOF= 10, t = 1.2 mm



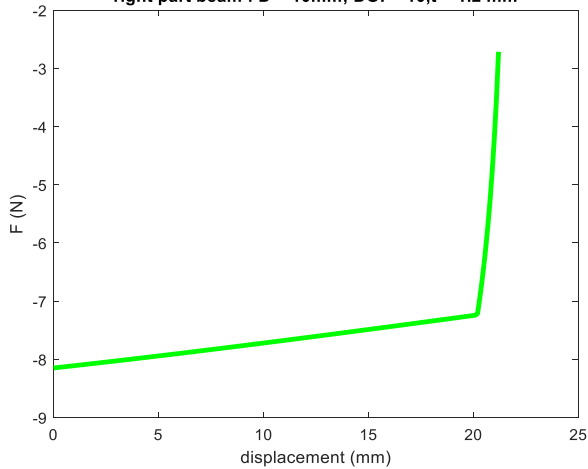
right part beam : D = 10mm; DOF= 10, t = 1.2 mm



left part beam: D = 10mm; DOF= 10, t = 1.2 mm



right part beam : D = 10mm; DOF= 10, t = 1.2 mm



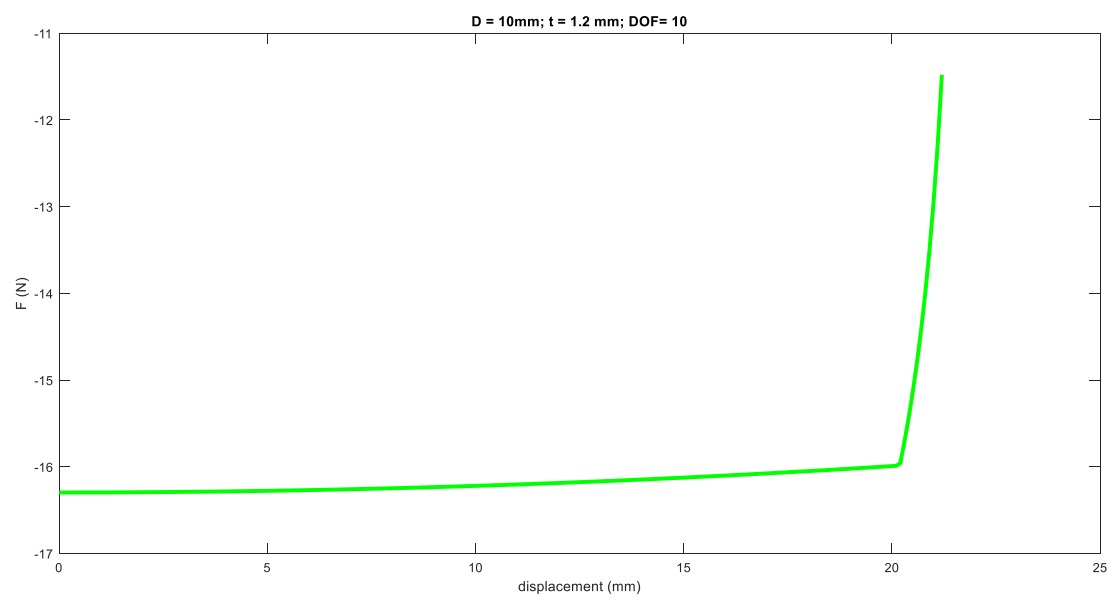
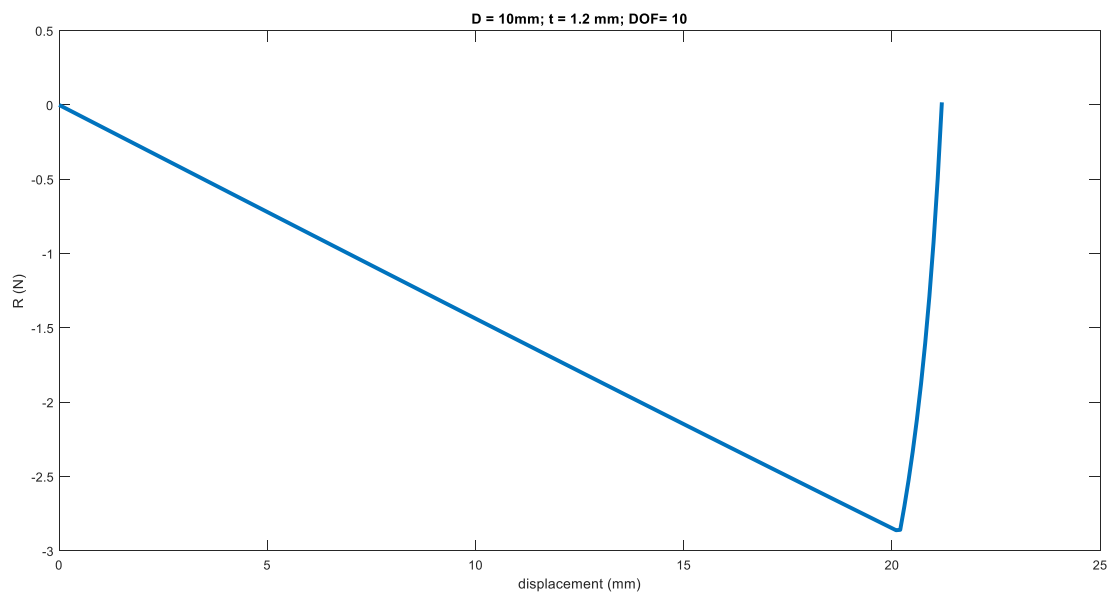
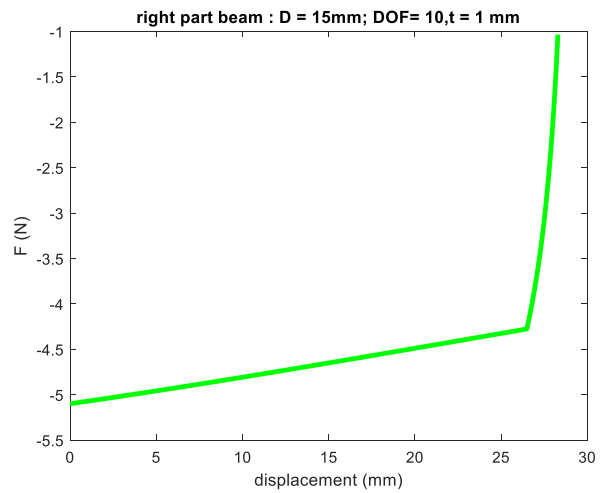
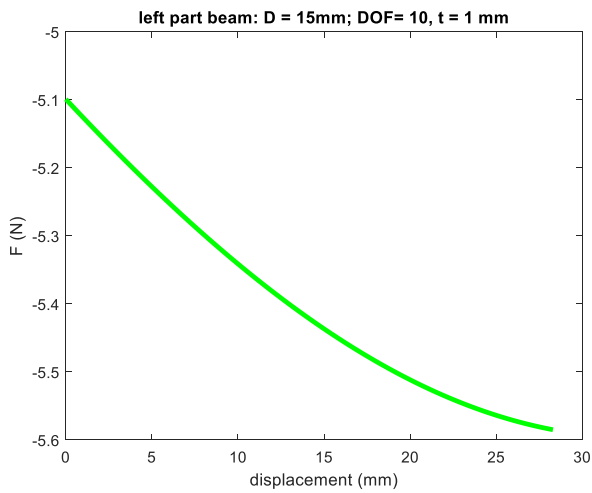
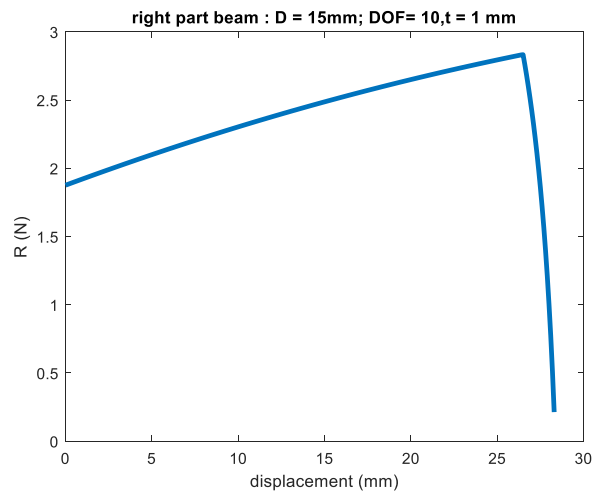
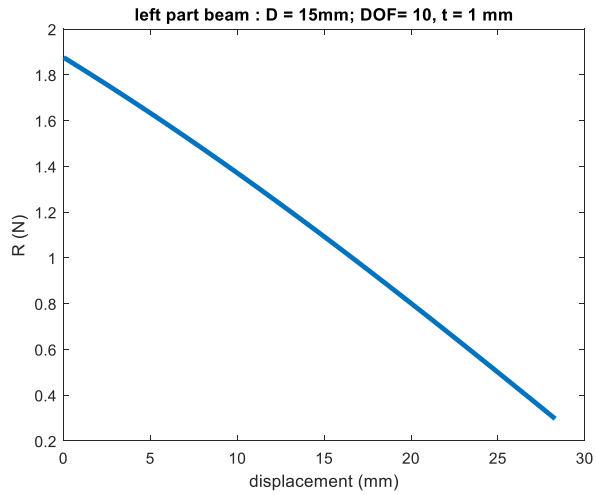
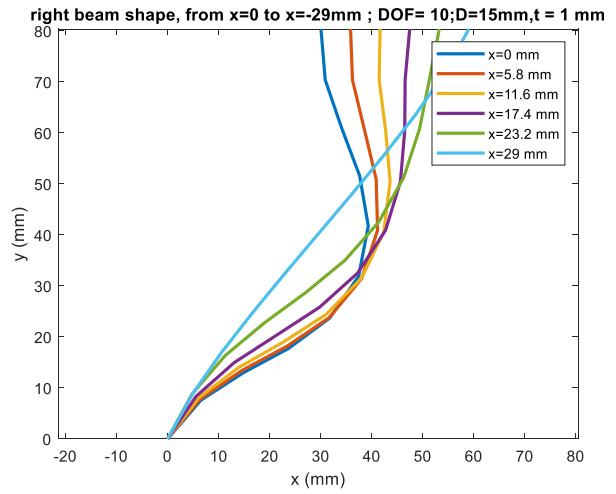
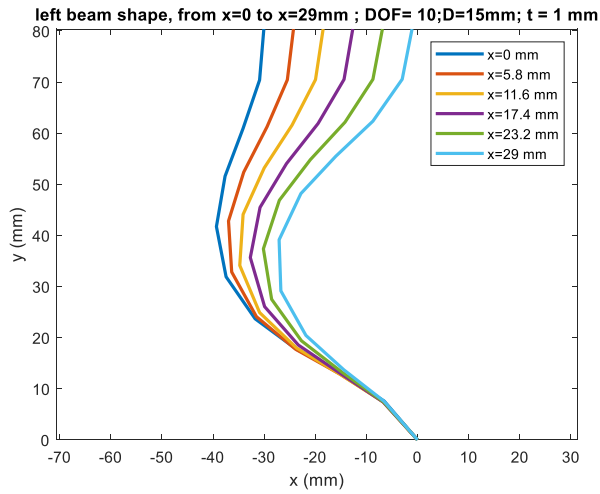


Fig 3.2.4.5  $t = 1.2\text{mm}$ ,  $D = 10\text{mm}$

For  $D = 15\text{mm}$ :



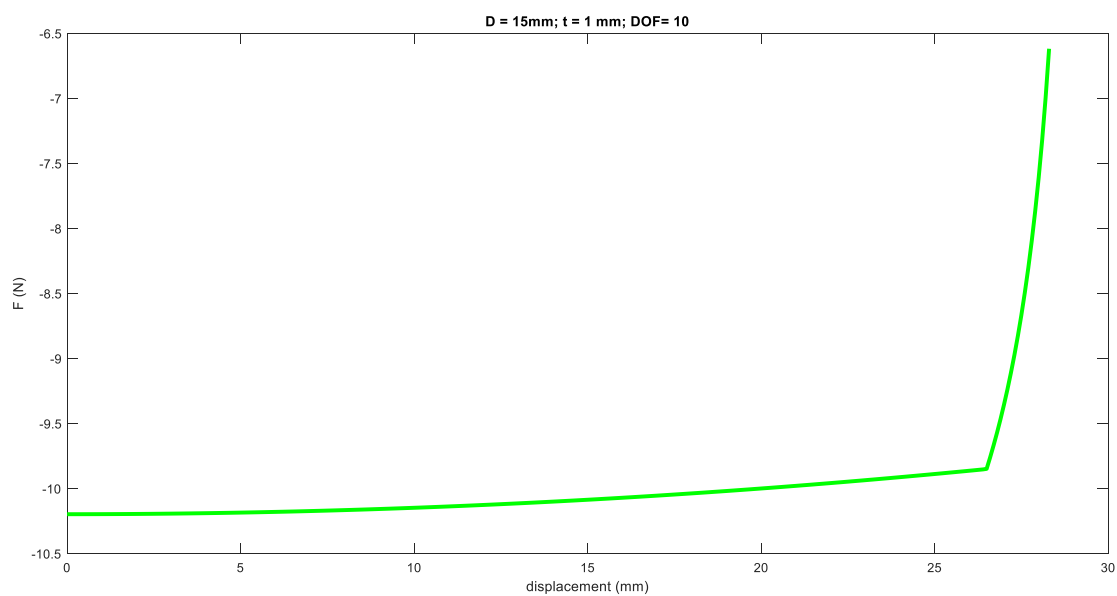
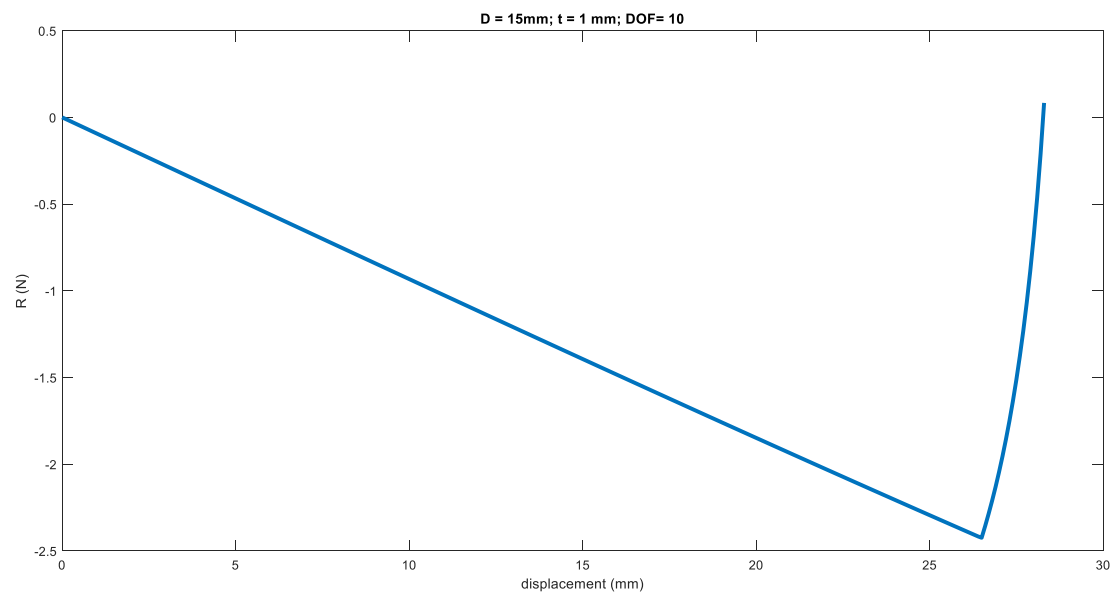
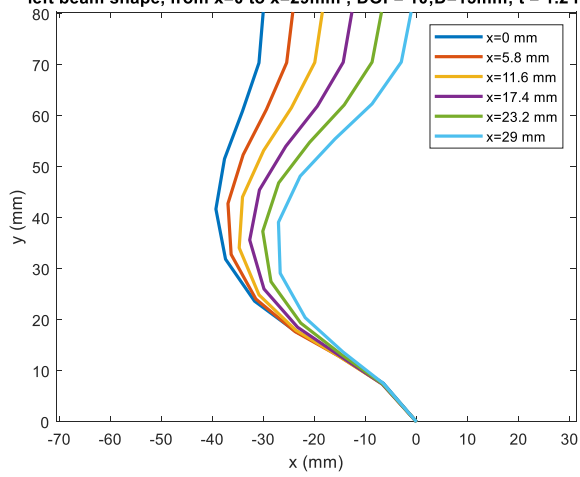
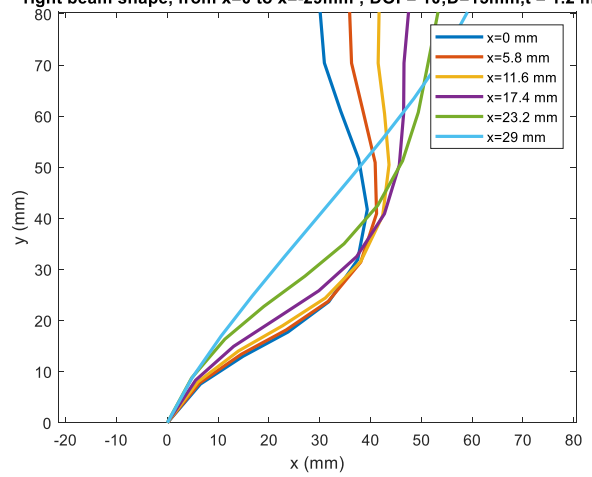


Fig 3.2.4.6  $t = 1mm$ ,  $D = 15mm$

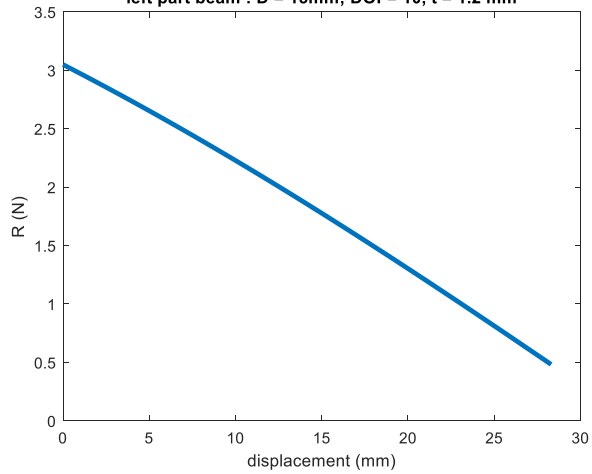
left beam shape, from  $x=0$  to  $x=29$  mm ; DOF= 10;D=15mm; t = 1.2 mm



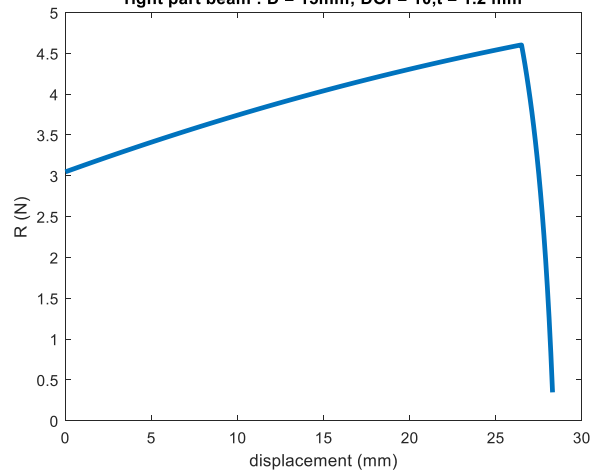
right beam shape, from  $x=0$  to  $x=-29$  mm ; DOF= 10;D=15mm,t = 1.2 mm



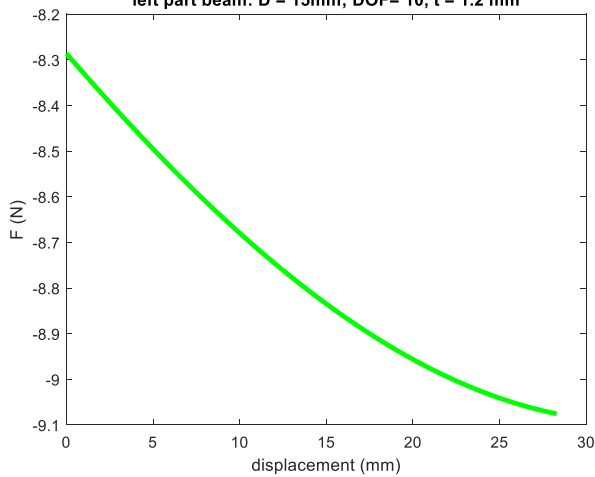
left part beam : D = 15mm; DOF= 10, t = 1.2 mm



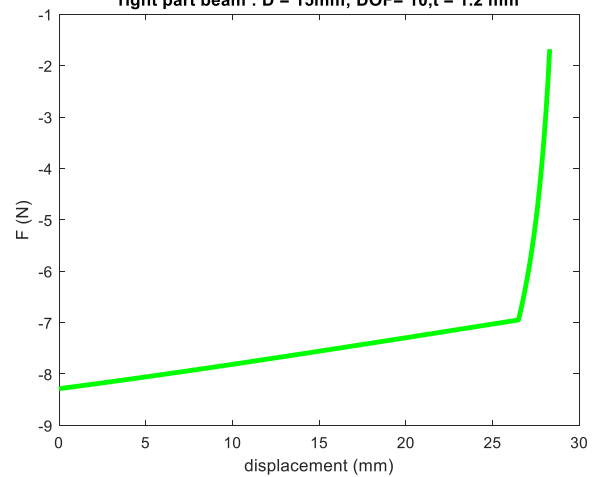
right part beam : D = 15mm; DOF= 10, t = 1.2 mm



left part beam: D = 15mm; DOF= 10, t = 1.2 mm



right part beam : D = 15mm; DOF= 10, t = 1.2 mm



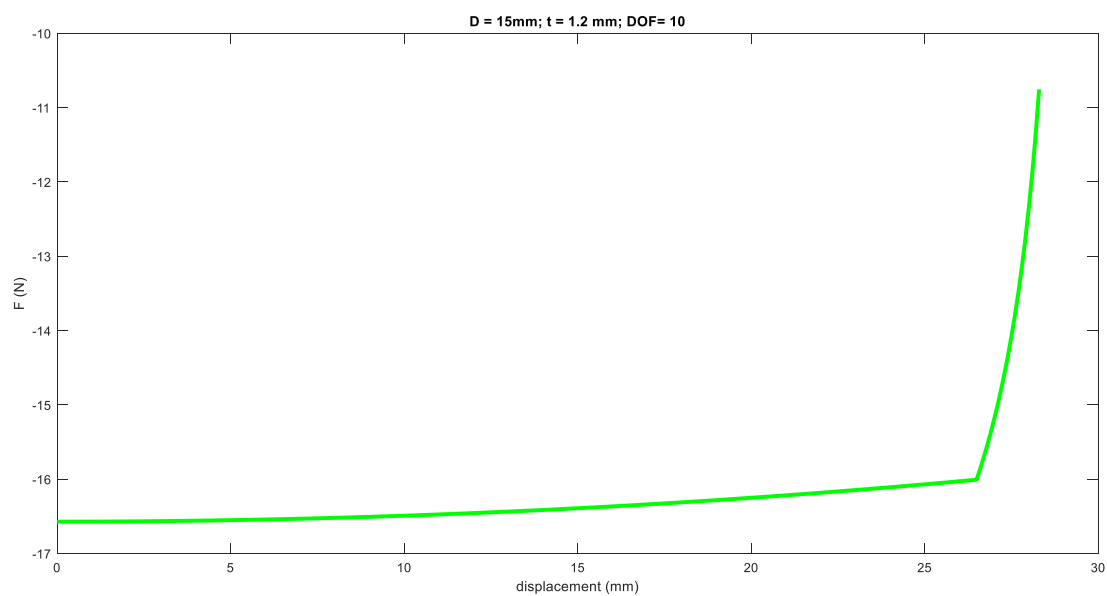
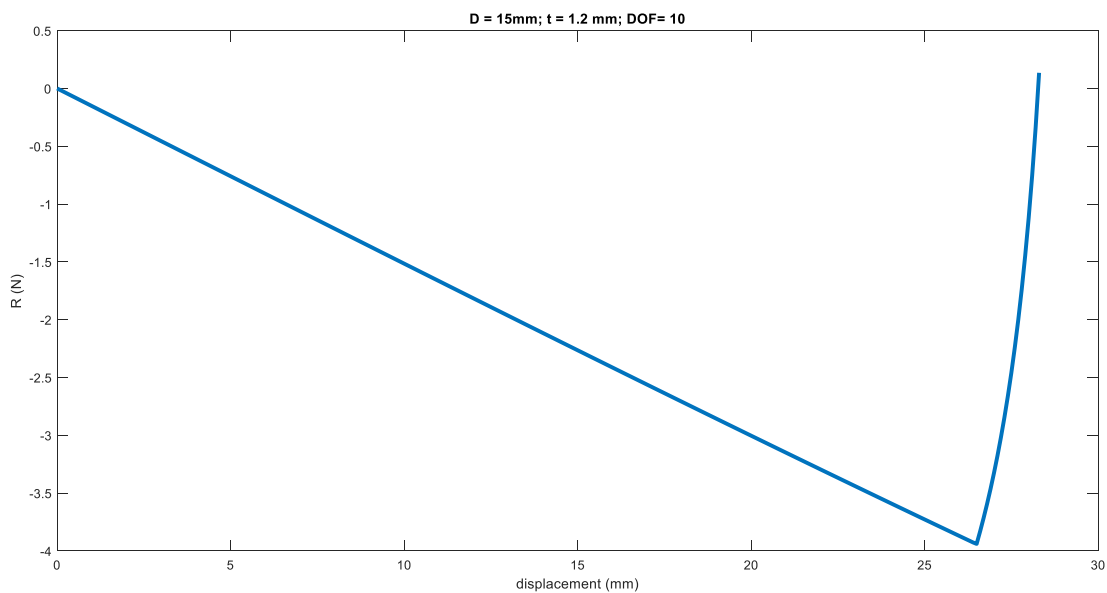
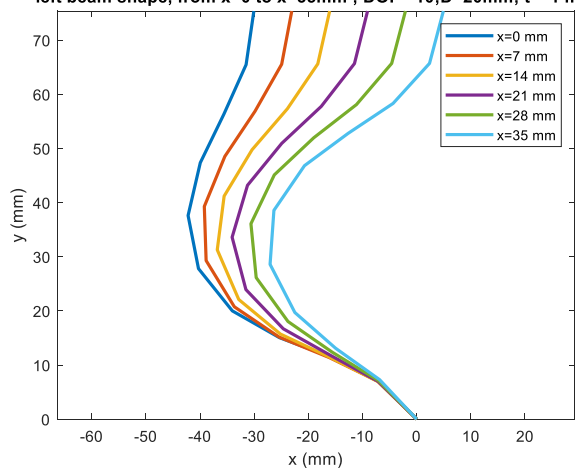


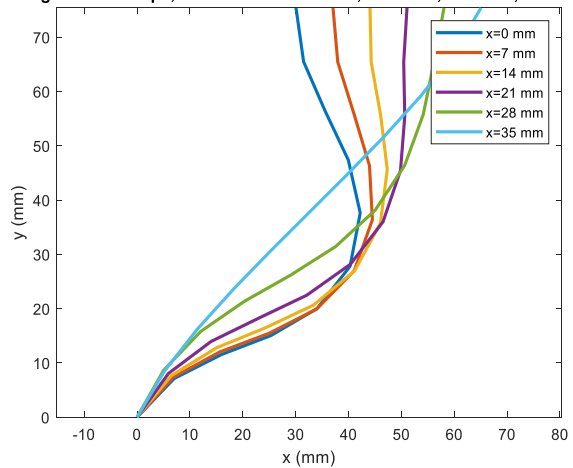
Fig 3.2.4.7  $t = 1.2mm$ ,  $D = 15mm$

For  $D = 20mm$ :

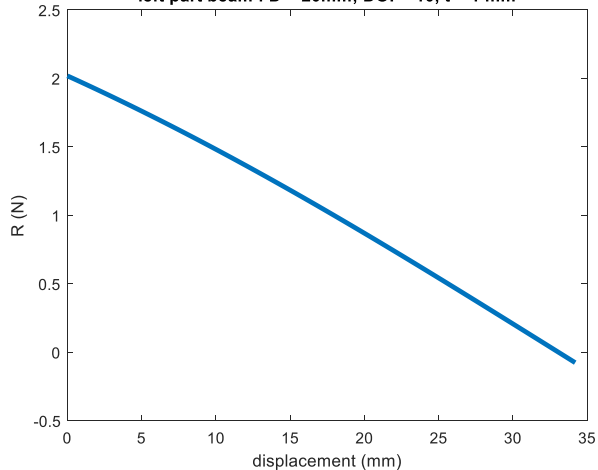
left beam shape, from  $x=0$  to  $x=35$  mm ; DOF= 10;D=20mm; t = 1 mm



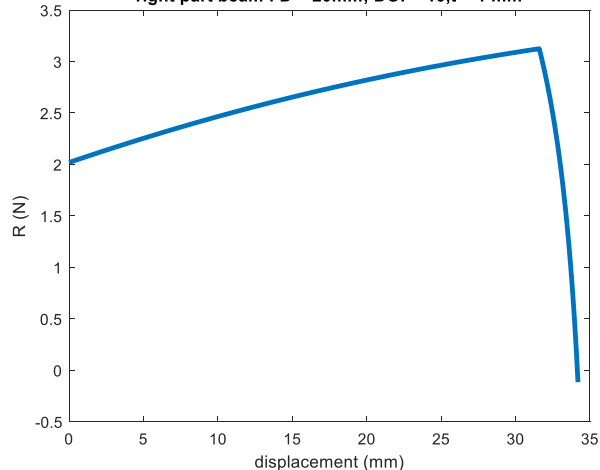
right beam shape, from  $x=0$  to  $x=35$  mm ; DOF= 10;D=20mm,t = 1 mm



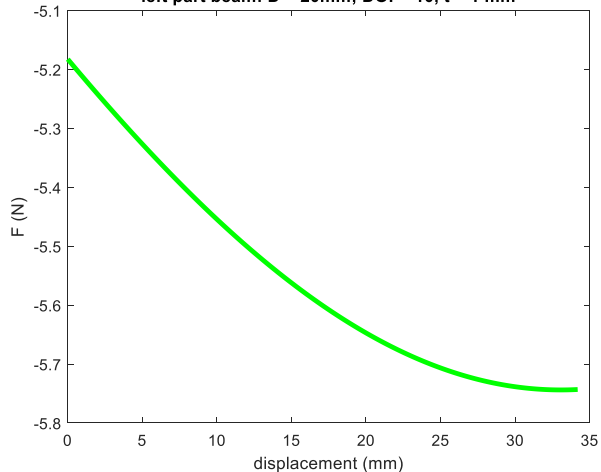
left part beam : D = 20mm; DOF= 10, t = 1 mm



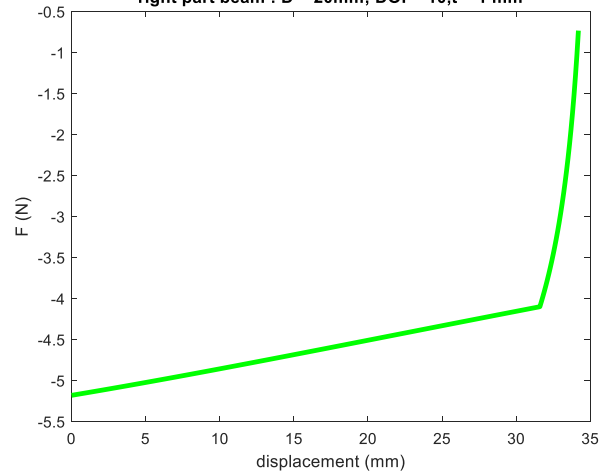
right part beam : D = 20mm; DOF= 10,t = 1 mm



left part beam : D = 20mm; DOF= 10, t = 1 mm



right part beam : D = 20mm; DOF= 10,t = 1 mm



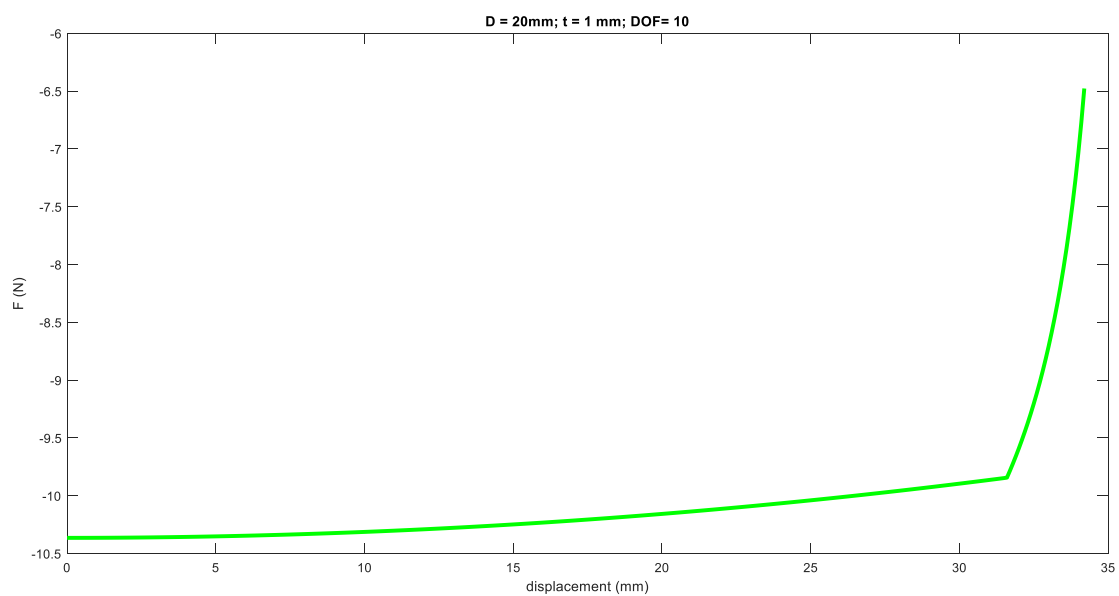
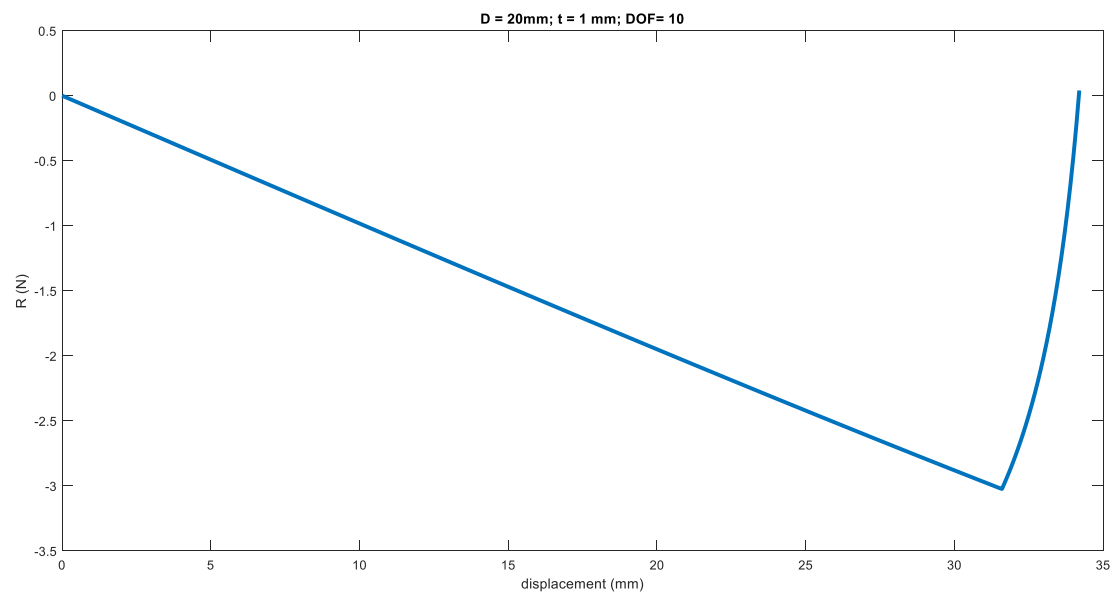
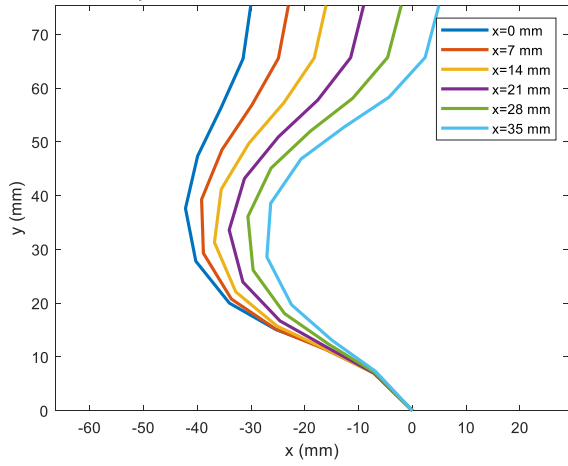
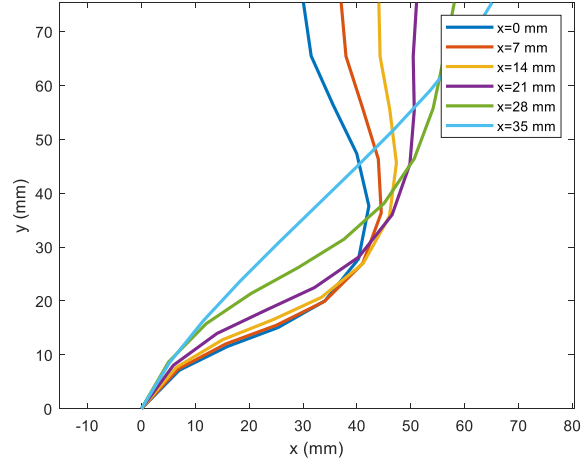


Fig 3.2.4.8  $t = 1mm$ ,  $D = 20mm$

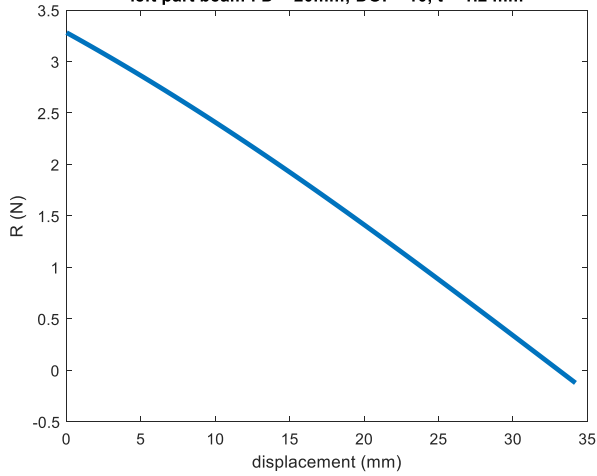
left beam shape, from x=0 to x=35mm ; DOF= 10;D=20mm; t = 1.2 mm



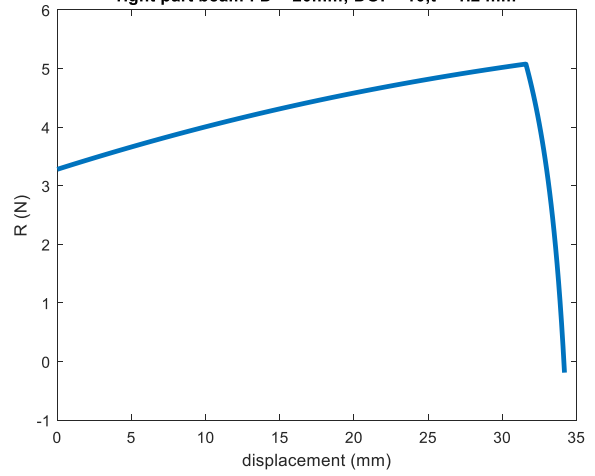
right beam shape, from x=0 to x=-35mm ; DOF= 10;D=20mm,t = 1.2 mm



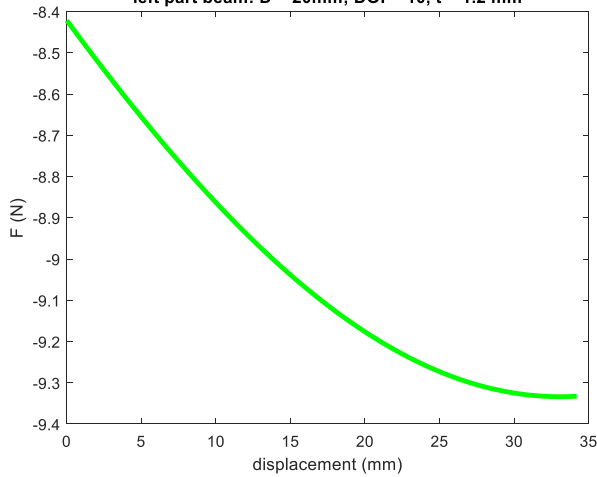
left part beam : D = 20mm; DOF= 10, t = 1.2 mm



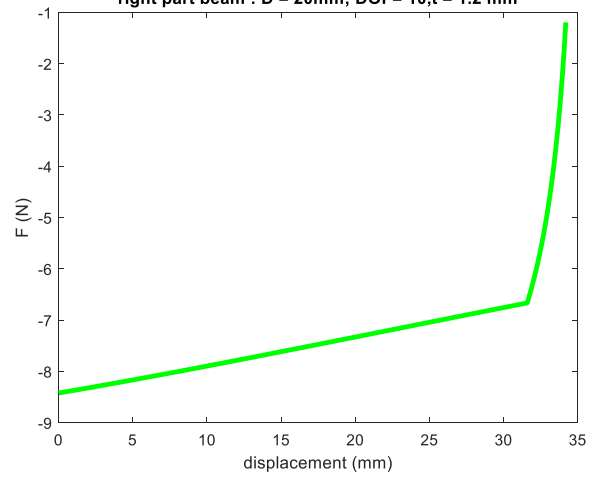
right part beam : D = 20mm; DOF= 10,t = 1.2 mm



left part beam : D = 20mm; DOF= 10, t = 1.2 mm



right part beam : D = 20mm; DOF= 10,t = 1.2 mm



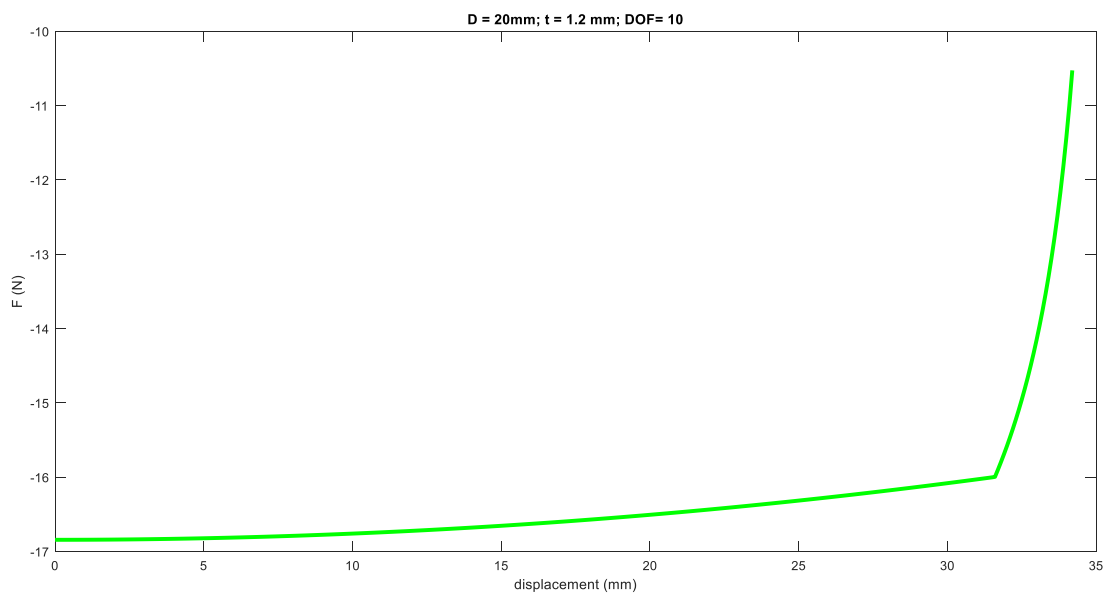
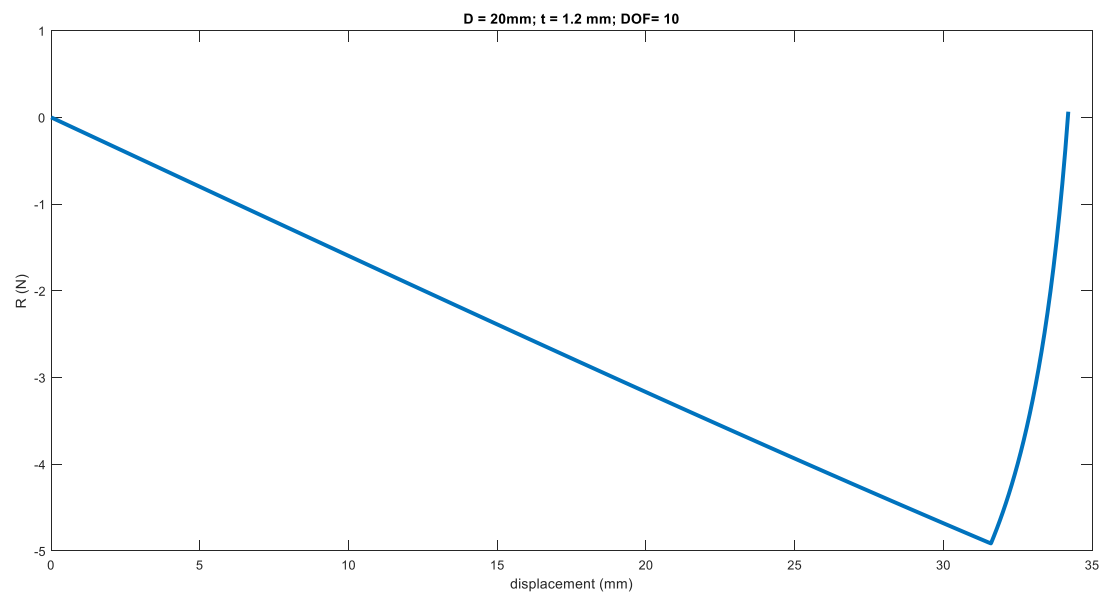
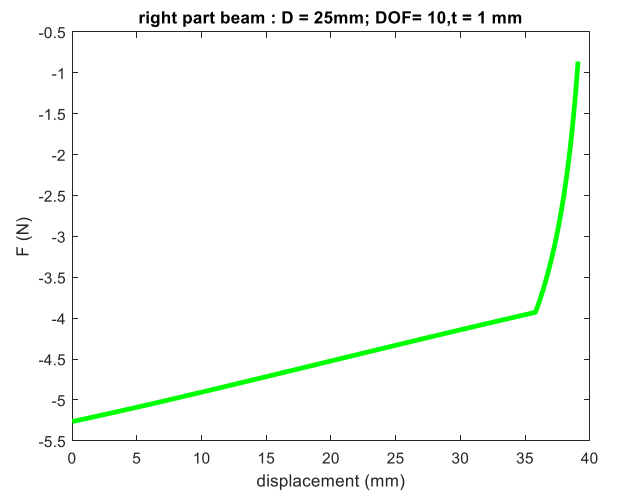
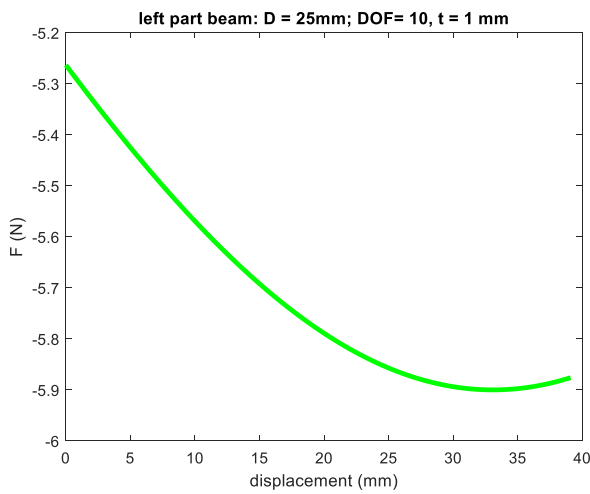
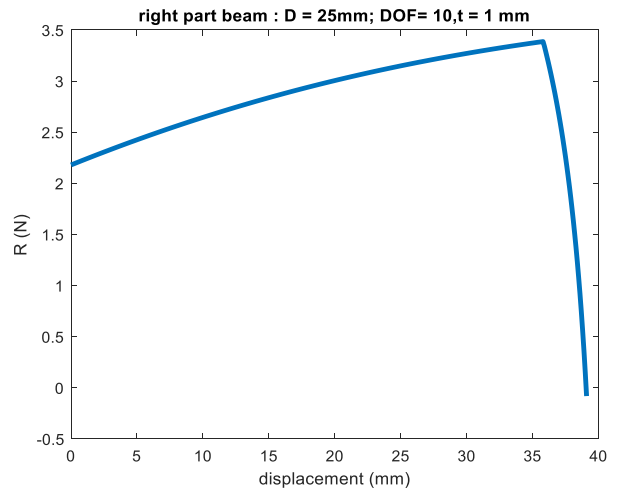
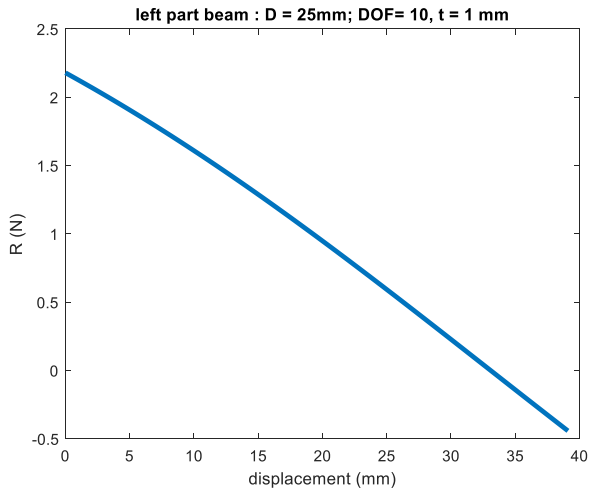
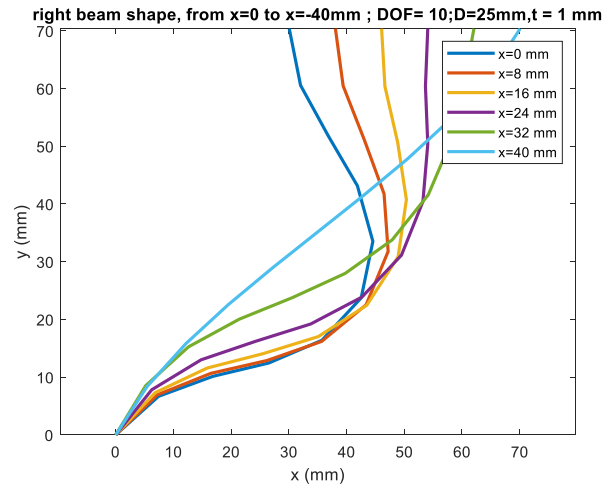
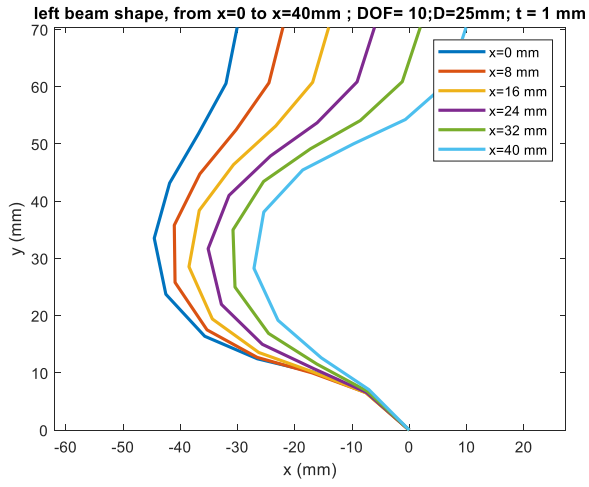


Fig 3.2.4.9  $t = 1.2\text{mm}$ ,  $D = 20\text{mm}$

$D = 25\text{mm}$ :



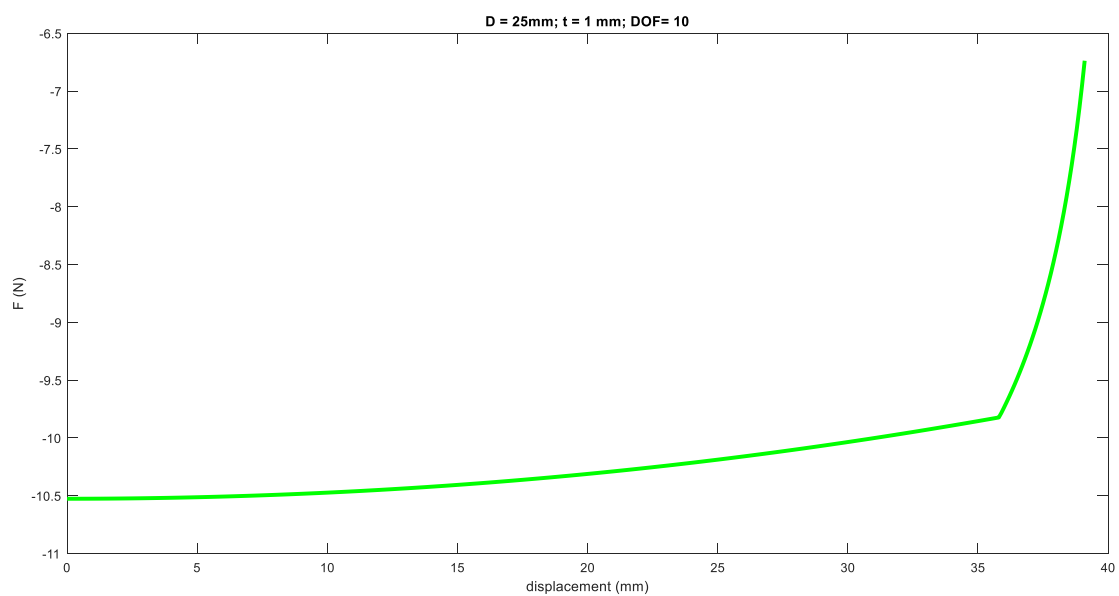
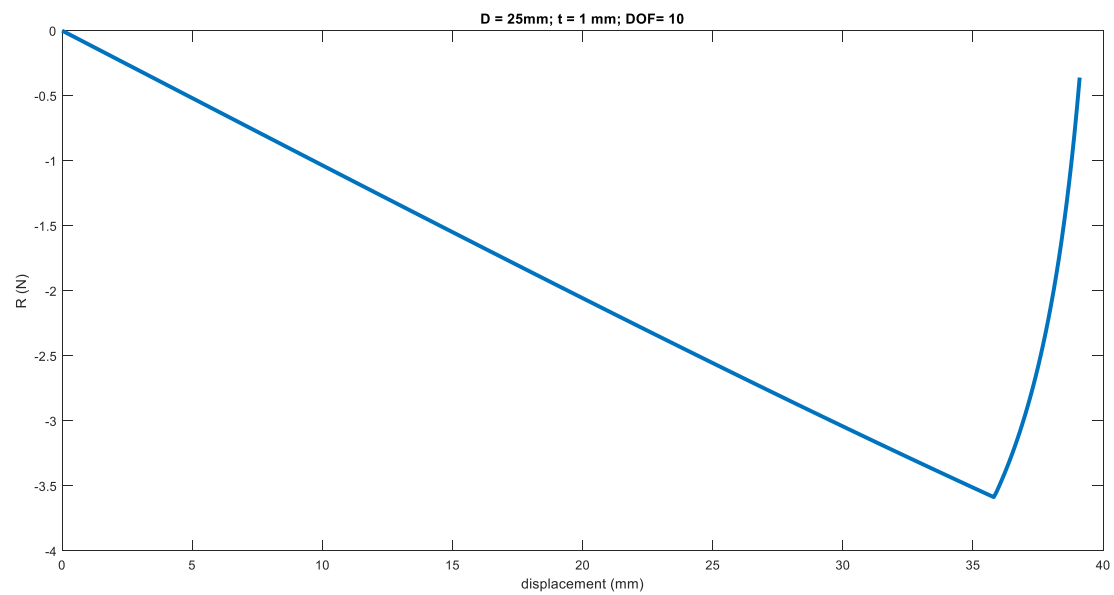
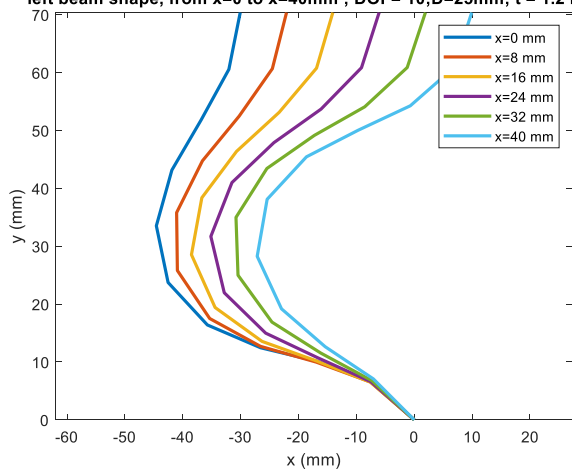
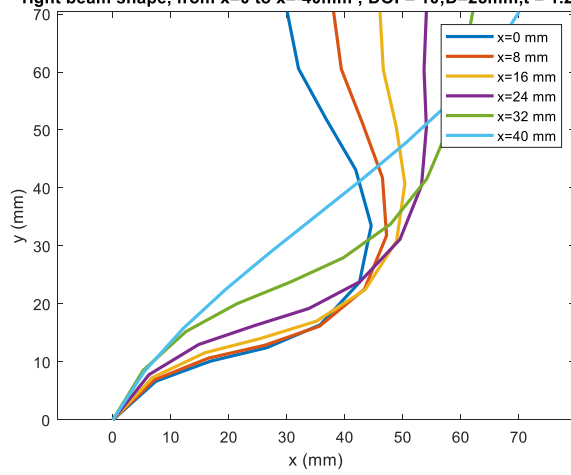


Fig 3.2.4.10  $t = 1\text{mm}$ ,  $D = 25\text{mm}$

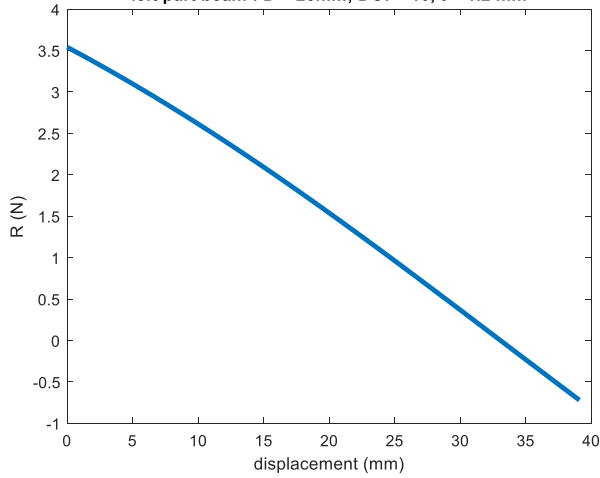
left beam shape, from x=0 to x=40mm ; DOF= 10;D=25mm; t = 1.2 mm



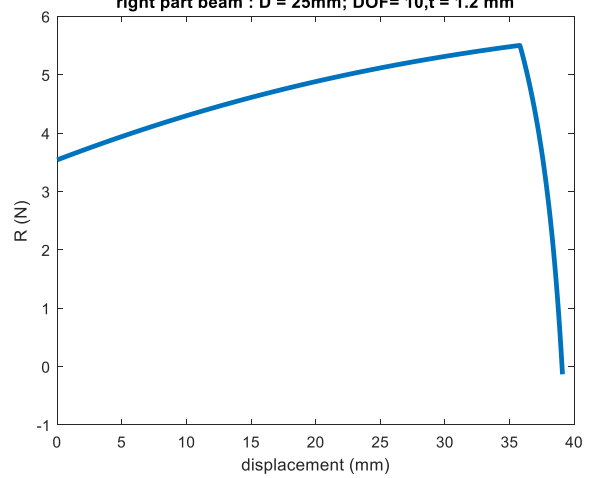
right beam shape, from x=0 to x=-40mm ; DOF= 10;D=25mm,t = 1.2 mm



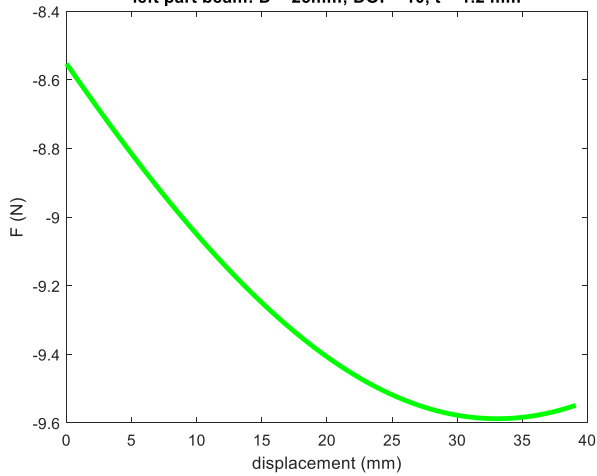
left part beam : D = 25mm; DOF= 10, t = 1.2 mm



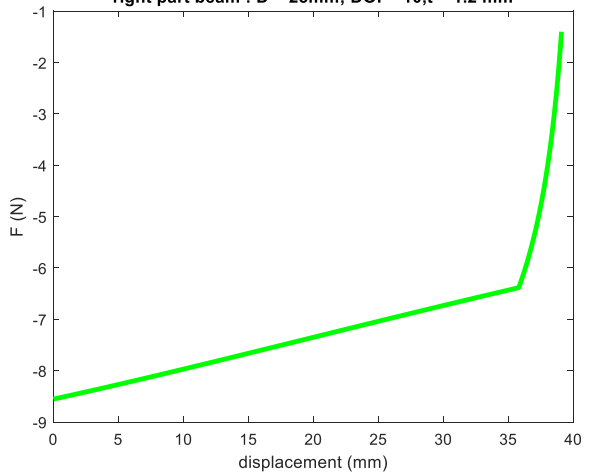
right part beam : D = 25mm; DOF= 10,t = 1.2 mm



left part beam: D = 25mm; DOF= 10, t = 1.2 mm



right part beam : D = 25mm; DOF= 10, t = 1.2 mm



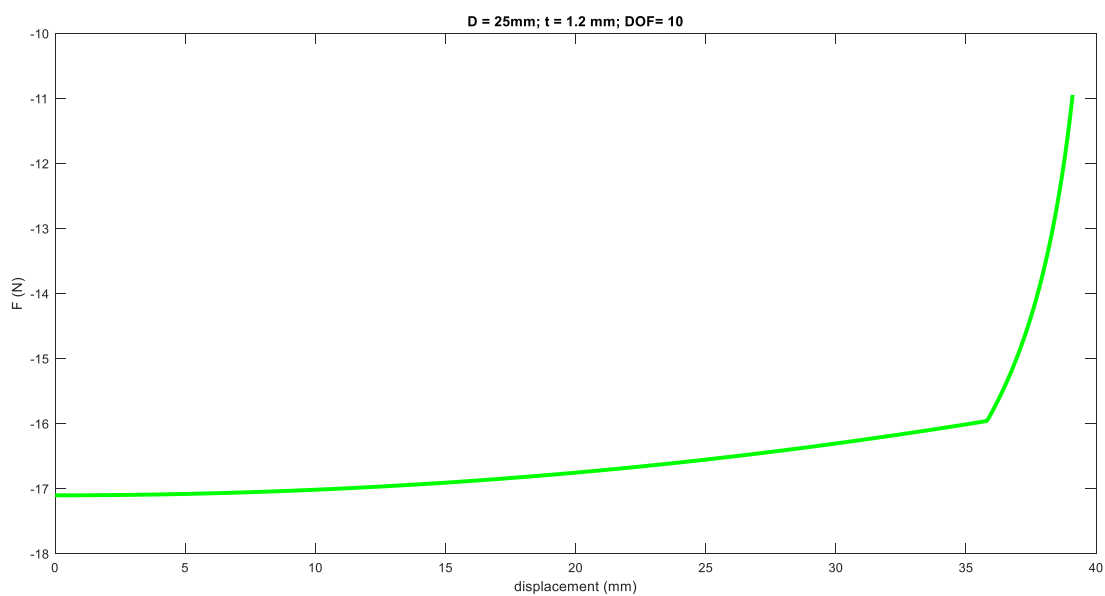
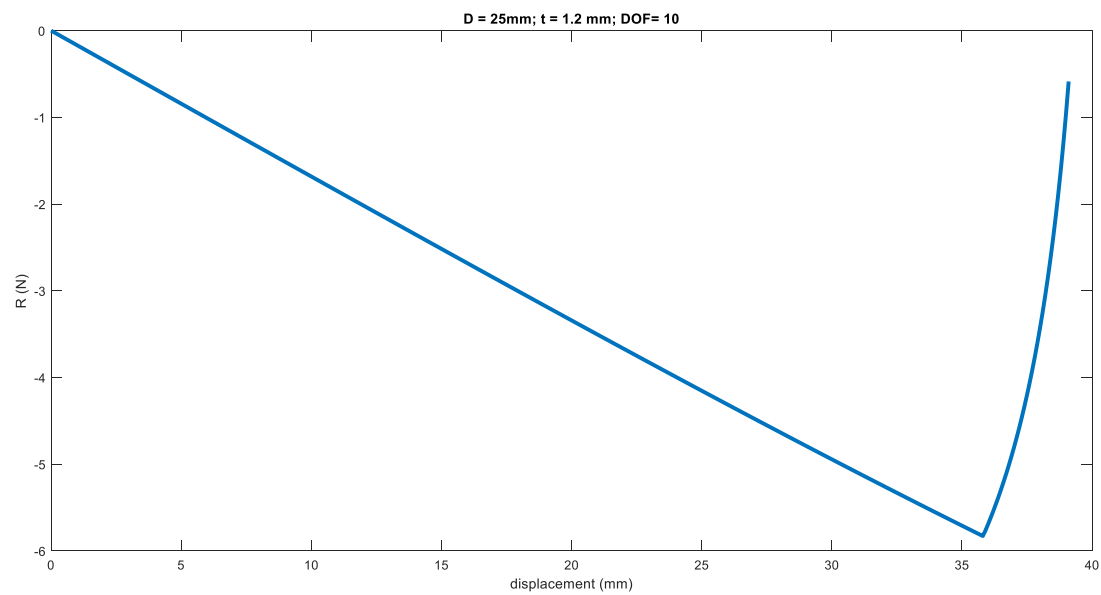


Fig 3.2.4.11  $t = 1.2\text{mm}$ ,  $D = 25\text{mm}$

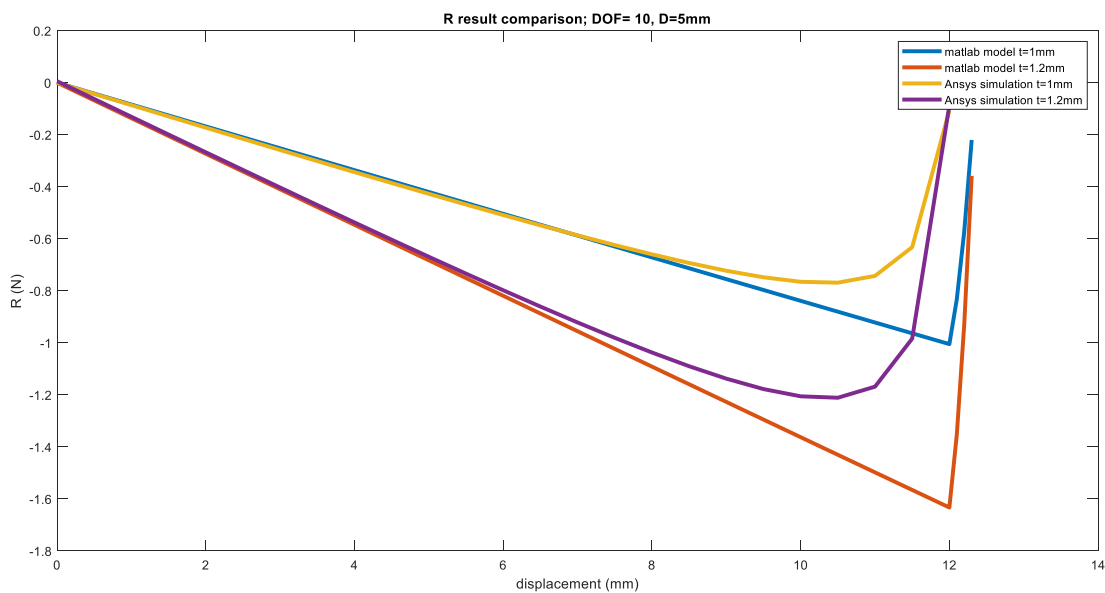


Fig 3.2.4.12 R result comparison,  $D = 5 \text{ mm}$

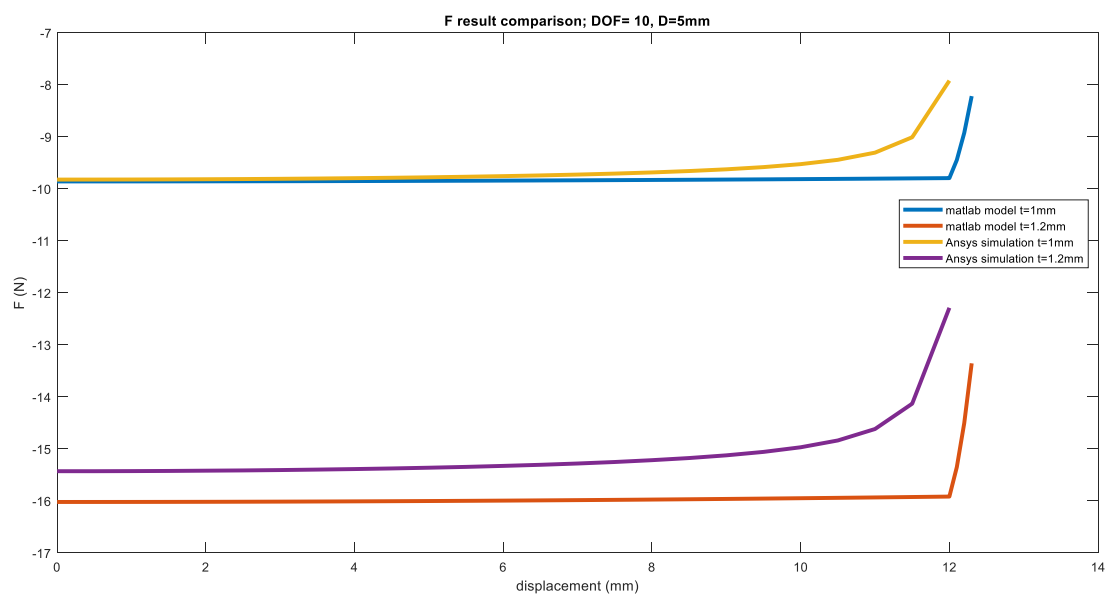


Fig 3.2.4.13 F result comparison,  $D = 5 \text{ mm}$

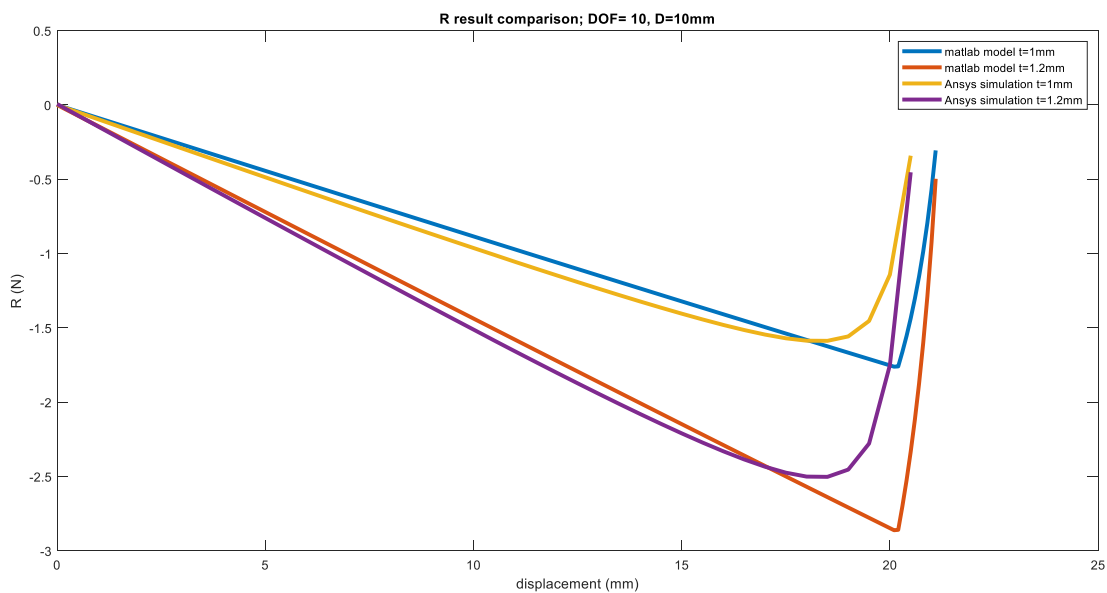


Fig 3.2.4.14 R result comparison,  $D = 10 \text{ mm}$

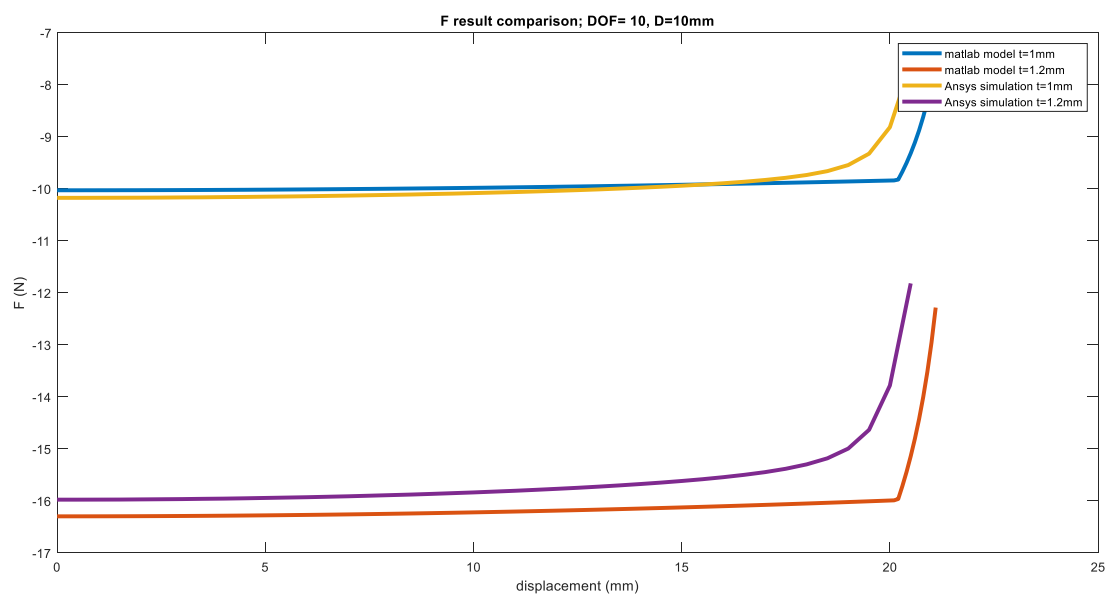


Fig 3.2.4.15 F result comparison,  $D = 10 \text{ mm}$

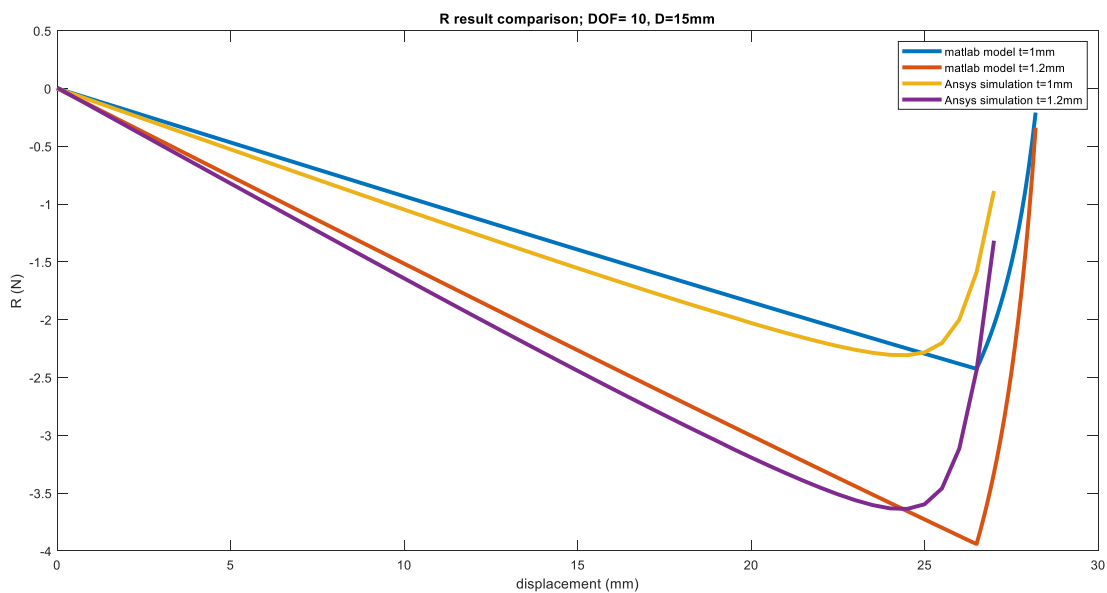


Fig 3.2.4.16 R result comparison,  $D = 15 \text{ mm}$

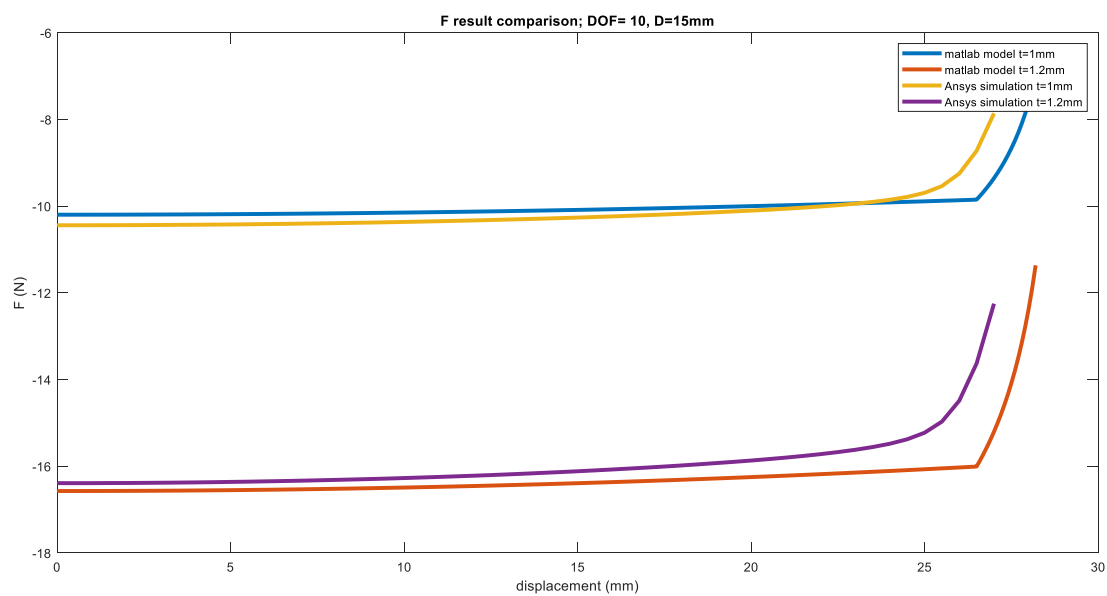


Fig 3.2.4.17 F result comparison,  $D = 15 \text{ mm}$

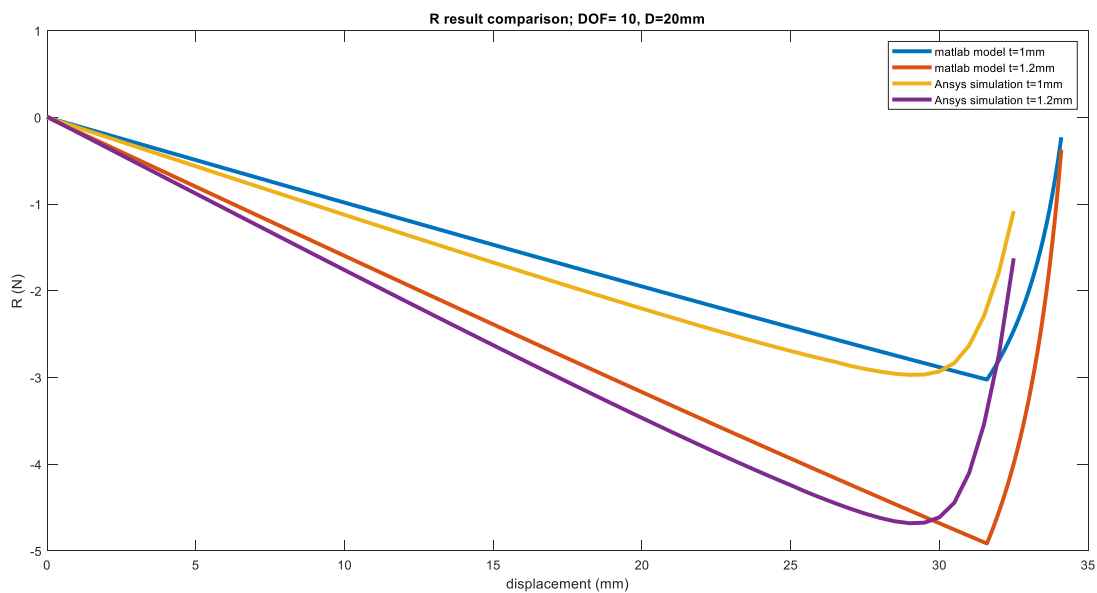


Fig 3.2.4.18 R result comparison,  $D = 20 \text{ mm}$

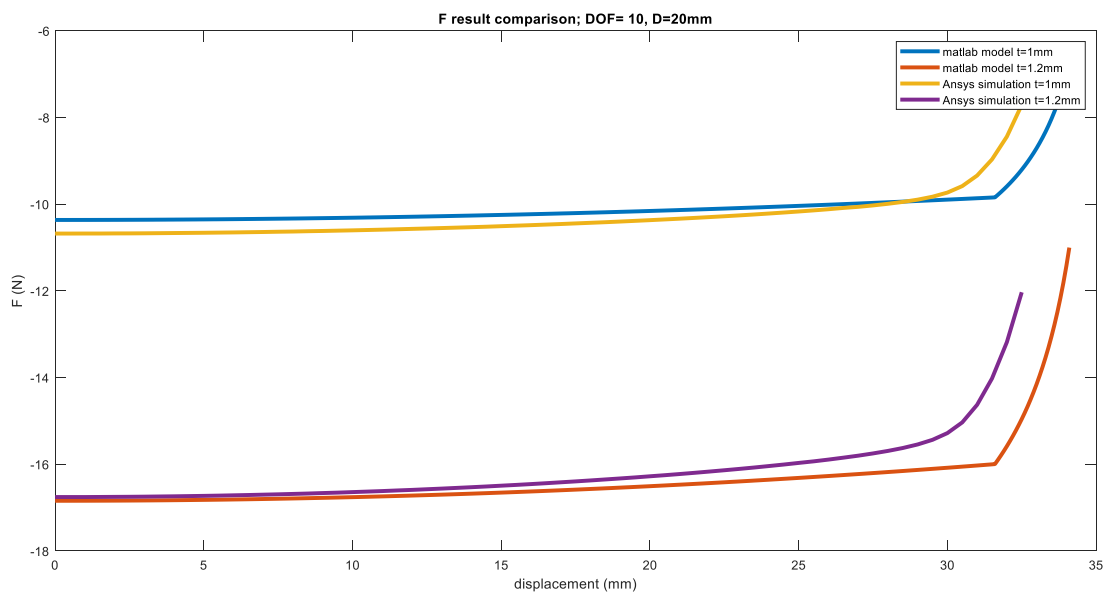


Fig 3.2.4.19 F result comparison,  $D = 20 \text{ mm}$

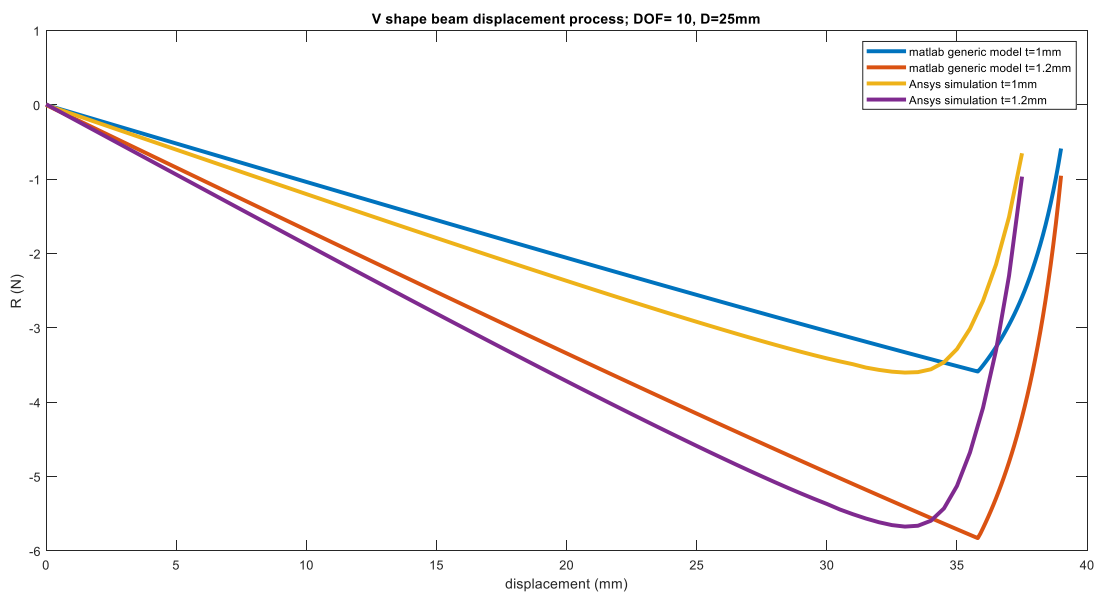


Fig 3.2.4.20 R result comparison,  $D = 25 \text{ mm}$

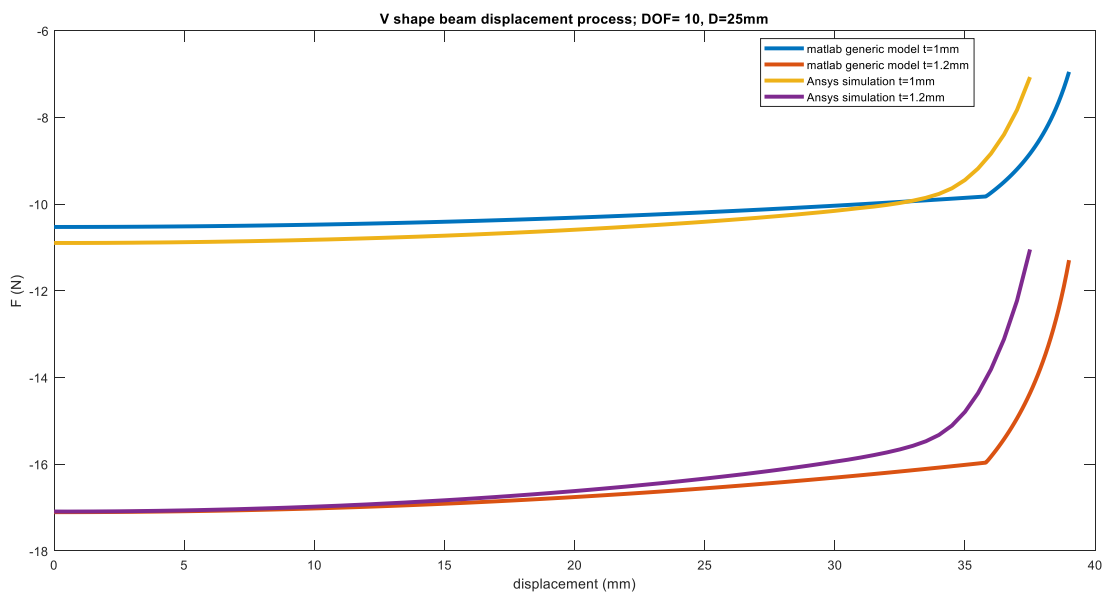


Fig 3.2.4.21 F result comparison,  $D = 25 \text{ mm}$

Comparing the MATLAB model result with Ansys simulation result under different preloading, it can

---

clearly be seen that the MATLAB model shows a very good fit in negative stiffness region for  $R$  and  $F$ . Moreover, in the negative stiffness region,  $R$  and  $F$  have a linear relationship with the displacement meaning that the stiffness of the V-shape beam structure remains constant in the negative stiffness region. Instead, when the displacement reaches the geometry limitation, some large differences appears. The reason for these differences is that in the MATLAB model, it is assumed that the upper and lower parts are connected by torsional springs, but there are fillets in reality, so the torsional springs cannot well represent the connection between the fillet and the beam.

## 4 Experiment

### 4.1 Design the experiment model

The V-shape beam needs a series of supports to be mounted on the test bench. First, the V-shape beam upper surface must be in contact with a fixed boundary that also allows the V-shape beam upper surface to slide along the displacement direction. A series of rolling bearings is therefore adopted to accomplish this purpose. As for the V-shape beam lower surface instead, there is the need of generating the preloading and fixing the lower surface while the upper surface is moving. So, based on these demands, the chosen design is depicted in Fig 4.1.1 and Fig 4.1.2.

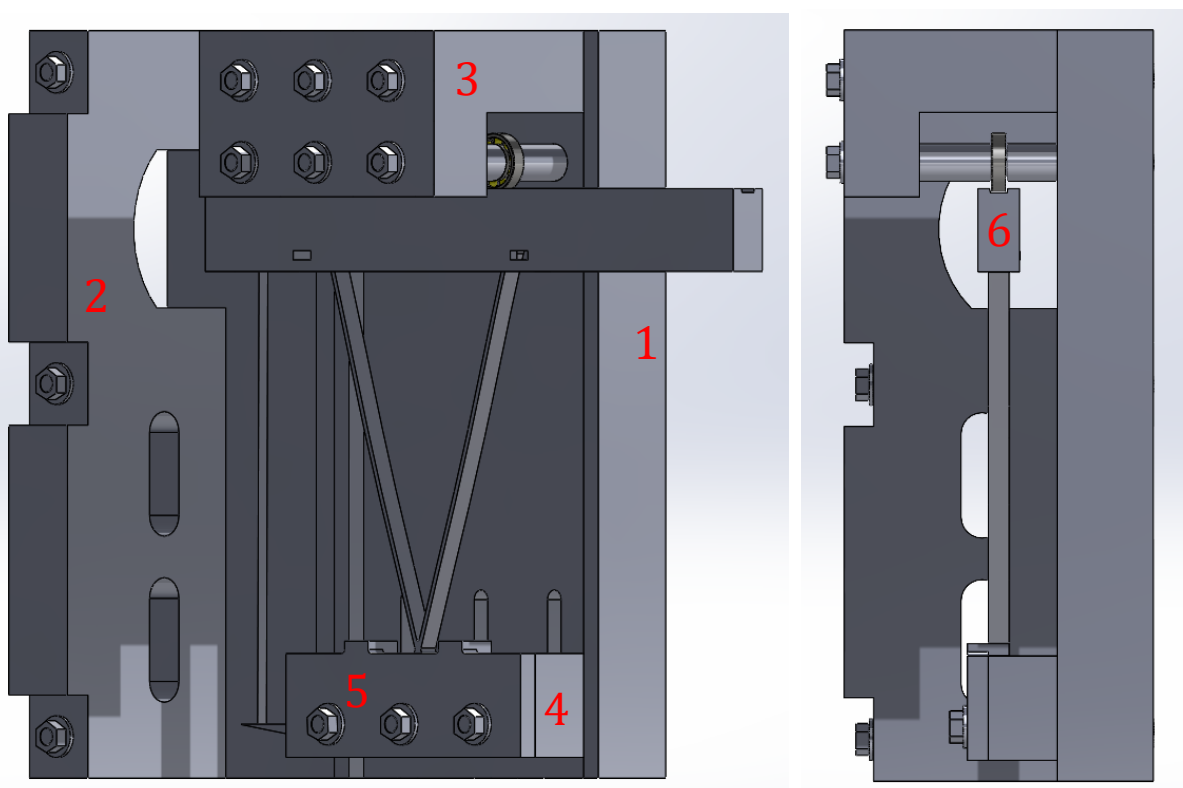


Fig 4.1.1 Experimental assembly (CAD model)

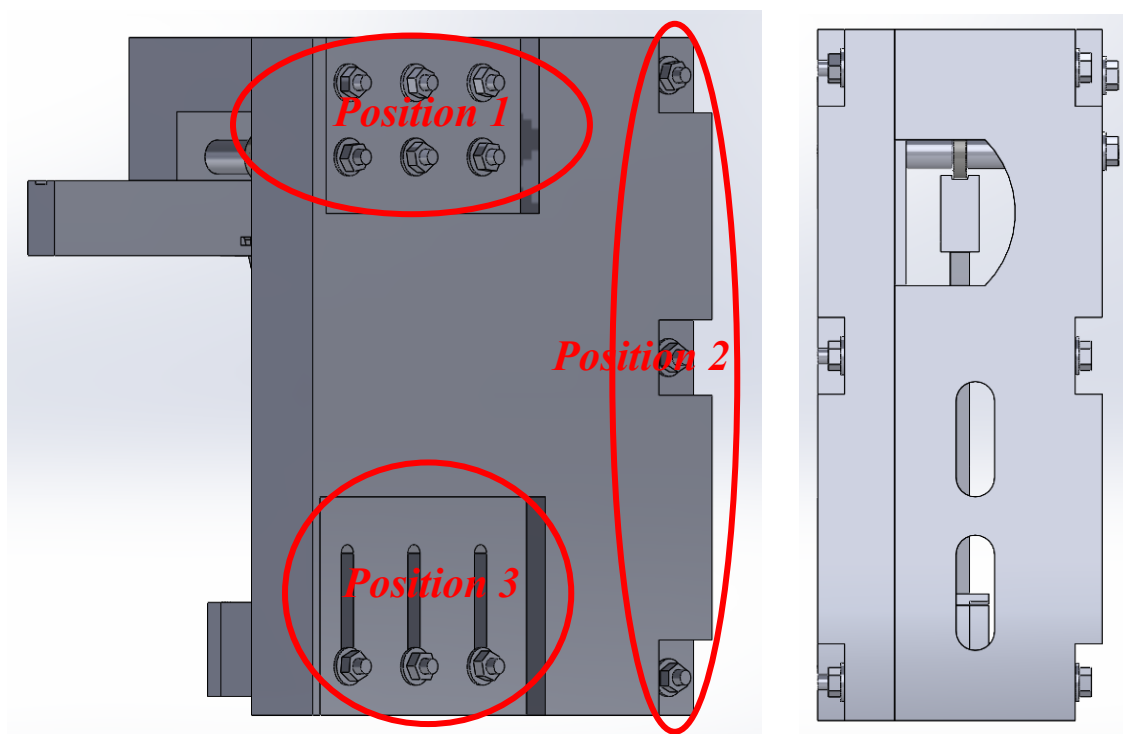


Fig 4.1.2 Experimental assembly (CAD model)

The main support part can be assembled with *component 1*, *component 2* and *component 3*. These three parts can be easily connected using M4 studs. The geometry requirement of the studs for each position is shown in Table 4.1.1. The nuts and washers are standard ones.

Position	Number of M4 studs	Length of stud (mm)
<b>1</b>	6	85
<b>2</b>	3	72
<b>3</b>	3	50

Table 4.1.1

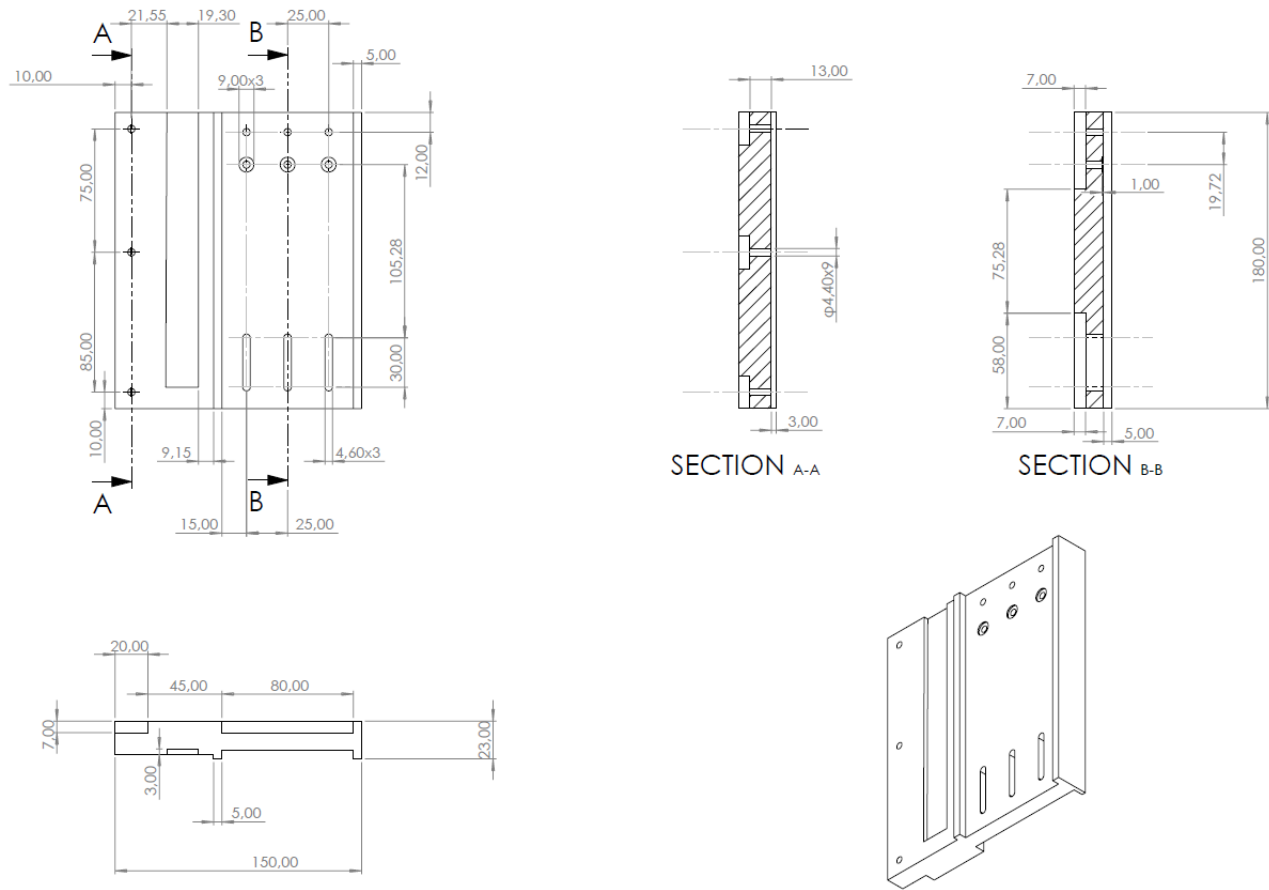


Fig 4.1.3 component 1 drawing

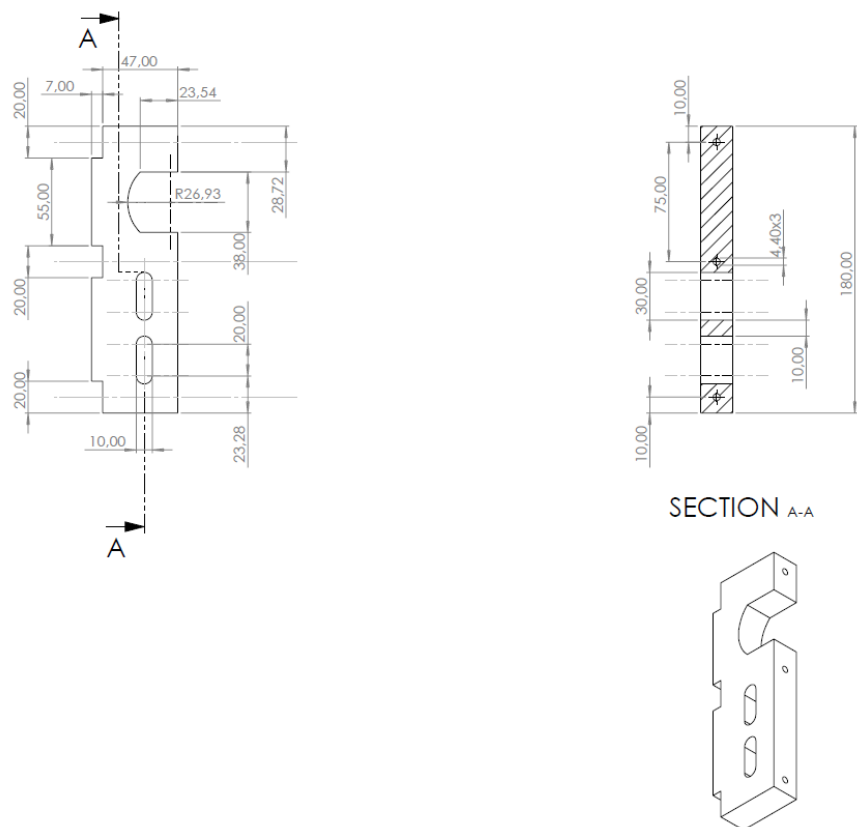


Fig 4.1.4 component 2 drawing

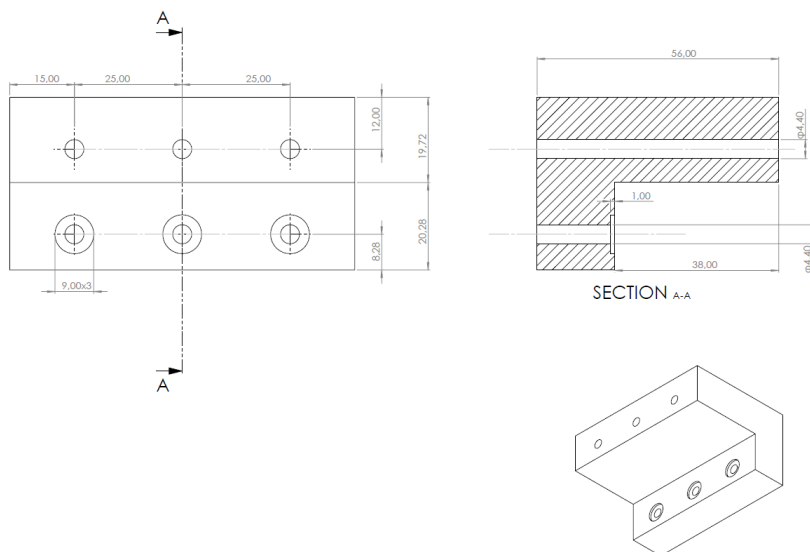


Fig 4.1.5 component 3 drawing

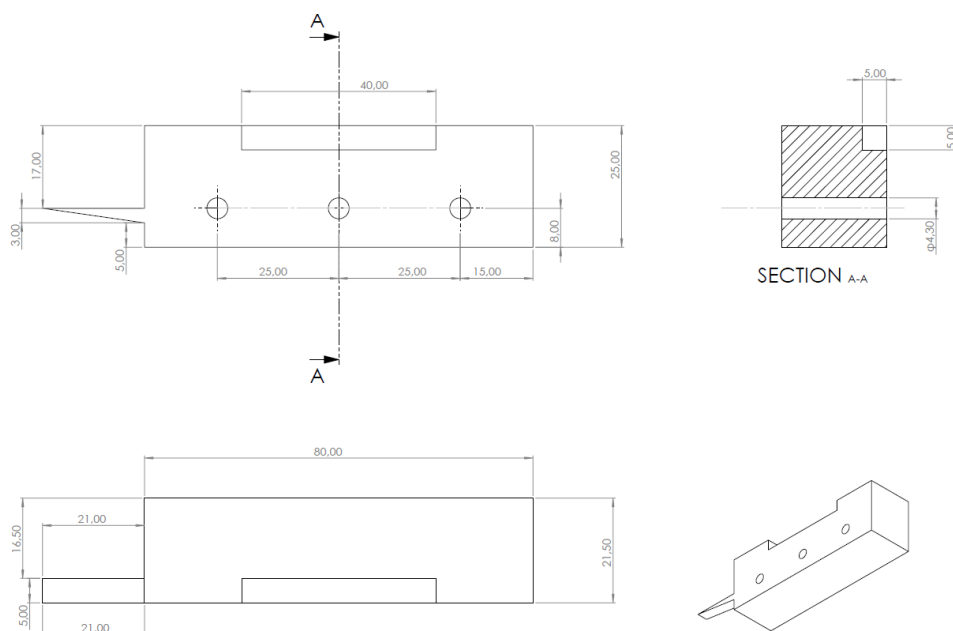


Fig 4.1.6 *component 4* drawing

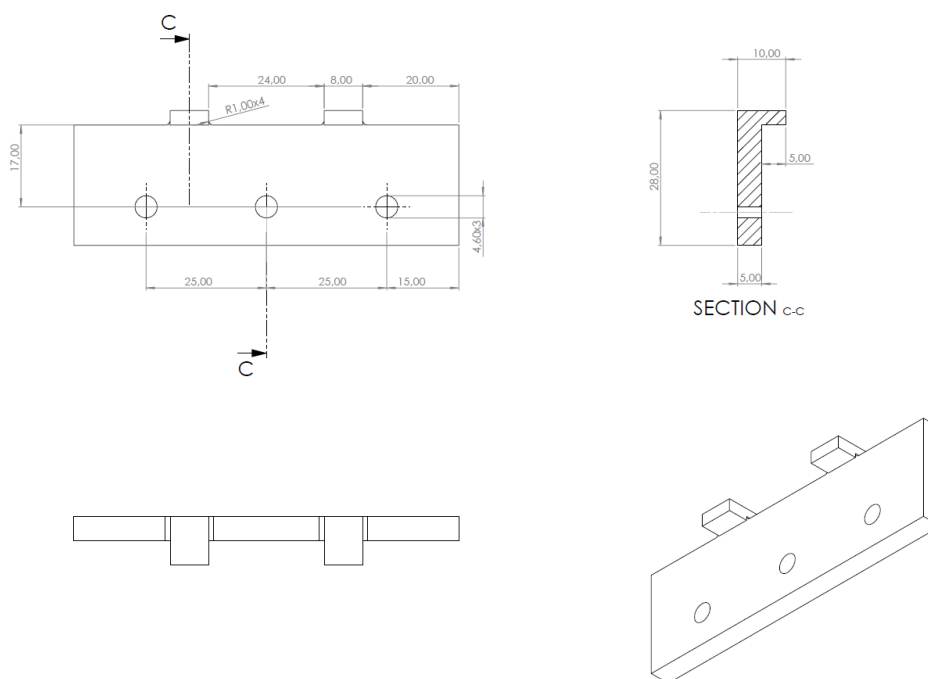


Fig 4.1.7 *component 5* drawing

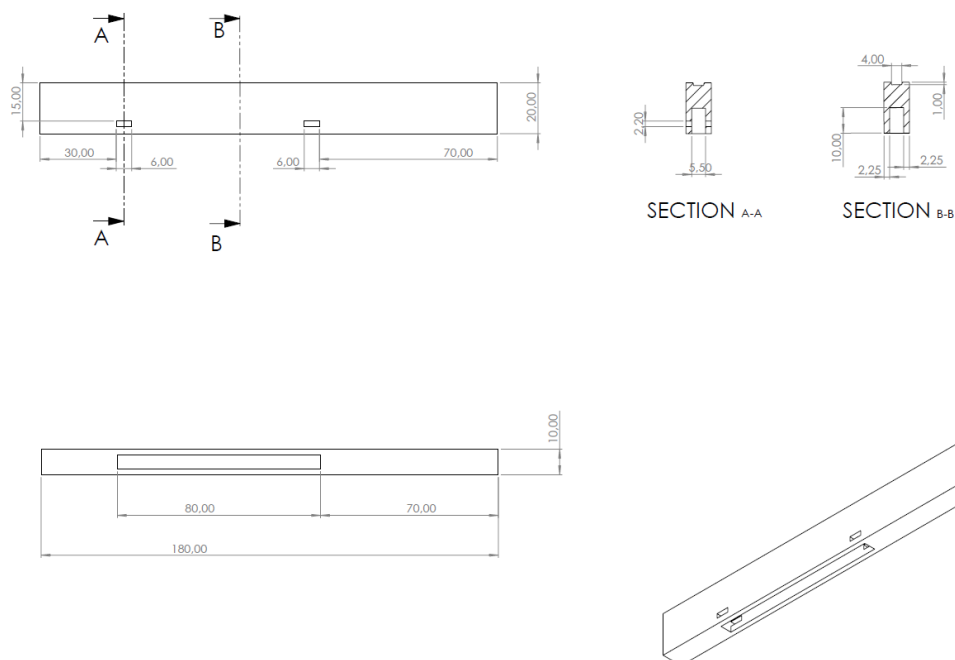


Fig 4.1.8 *component 6* drawing

By combining *component 5* and *component 4*, the V-shape beam lower surface can be fixed to the desired preloading position. *Component 6* will then be coupled with the V-shape beam. Asset of keyways ensure that the two components remain bounded together. It can be noted that the upper surface presents a groove running for all its length, so that *component 6* can only move along the desired motion direction (X direction).

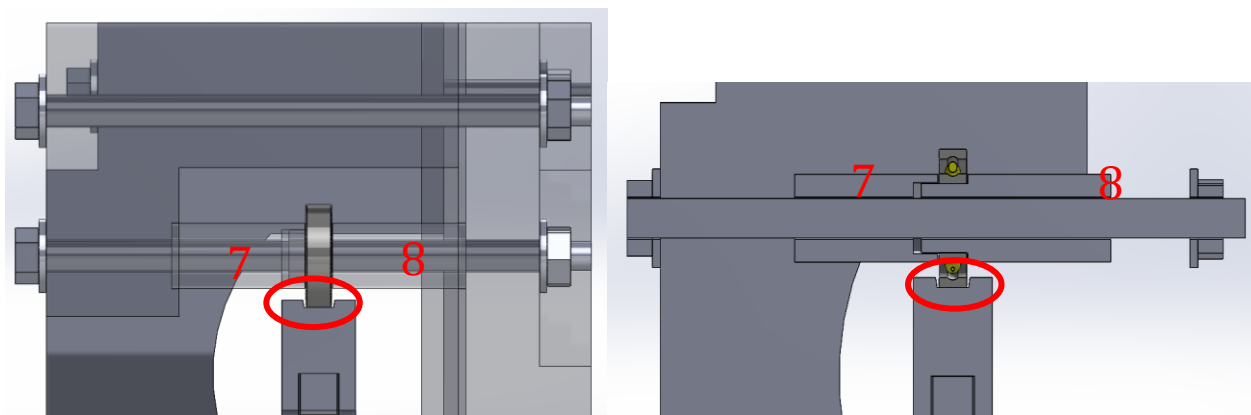


Fig 4.1.9 Section of bearing support

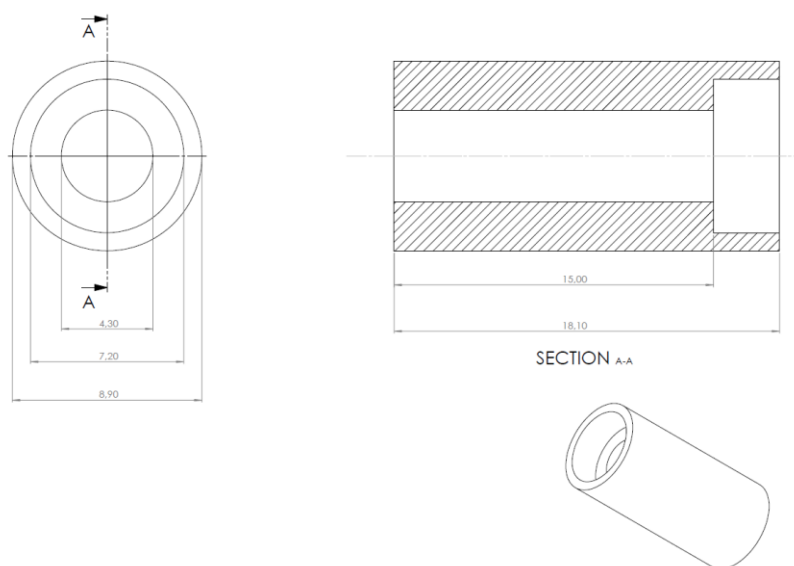


Fig 4.1.10 *component 7* drawing

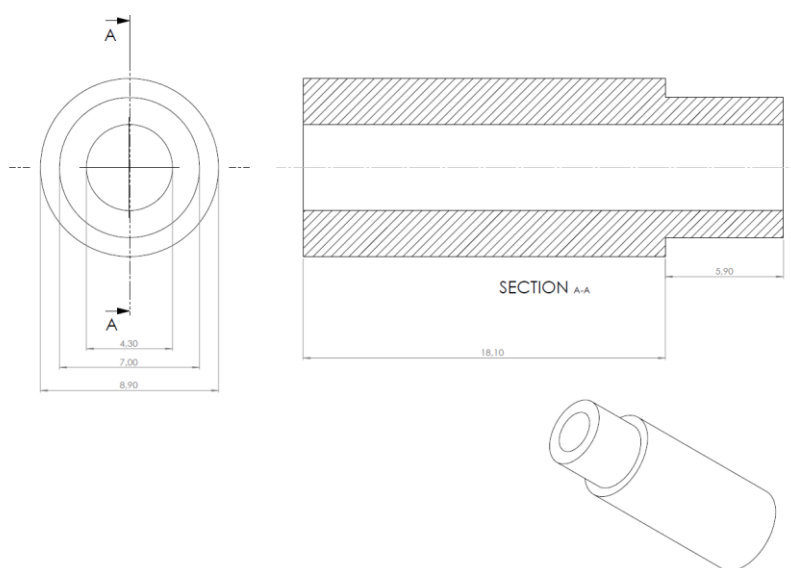


Fig 4.1.11 *component 8* drawing

The *component 7* and *component 8* will be coupled with M4 studs and act as shafts connected with the bearings. In experiments, the influence of friction force cannot be avoided. An ingenious design is to use the rolling of the bearing to reduce friction. The bearing is fixed on the base, and after preloading is

applied to the V-shape beam, the upper surface of *component 6* will contact the outer ring of the bearing due to compression. In this way, during the displacement process of the V-shape beam, the outer ring of the bearing will roll as the *component 6* moves. In this way, the rolling friction between the outer ring and the upper surface of the *component 6* will be converted into the internal friction of the bearing. The type of bearing is *ADR ALCEN X7*.

## 4.2 3d-printing process

### 4.2.1 3d-printing for V-shape beam

Due to all components are Non-standard component. Using 3d-printing technique can be represent a valid alternative for prototyping the system, ensuring with low cost at the same time. Thanks to the 3d-printer provided by the Politecnico di Torino, all the components can be easily printed.

The 3d-printer is UltiMaker 3 Extended and the filament is generic Polylactic acid (generic PLA). The slicing software is UltiMaker Cura 5.2.1 (Fig 4.2.1.1).

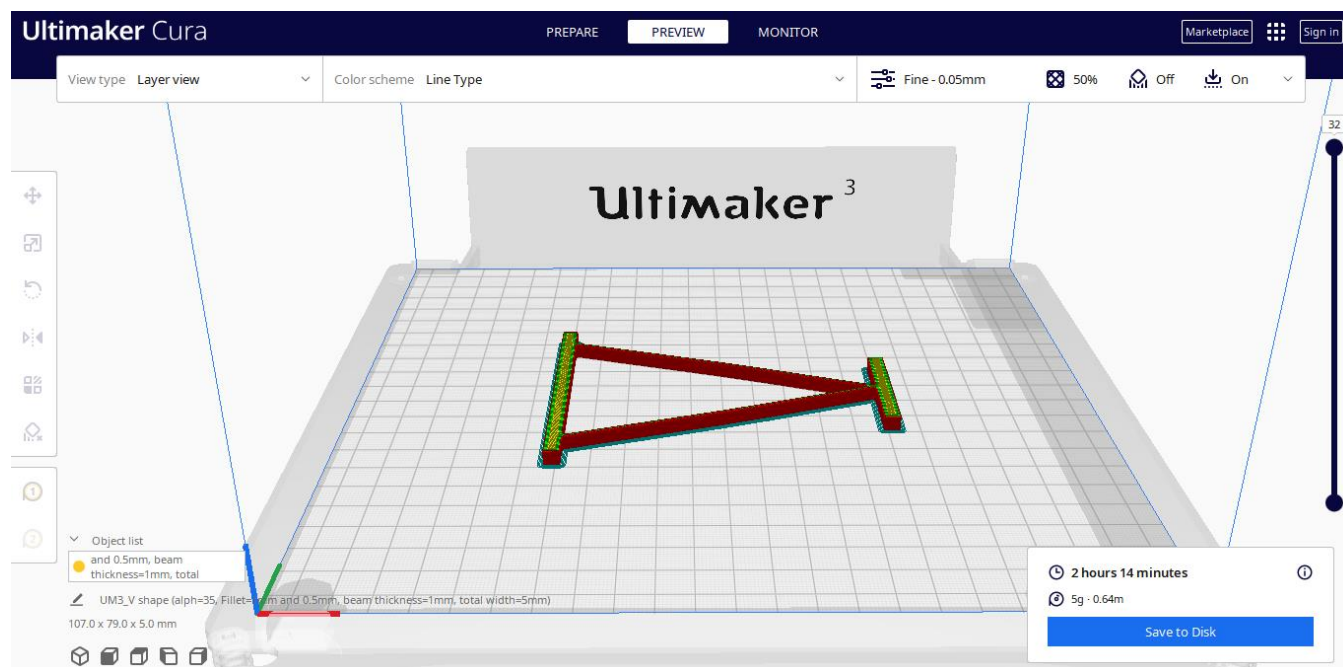


Fig 4.2.1.1 Cura interface

Setting the printing parameter is not an easy task, especially if a high accuracy is demanded. Just using default setting either does not get the samples with good quality, or in some cases it does not succeeds at all.

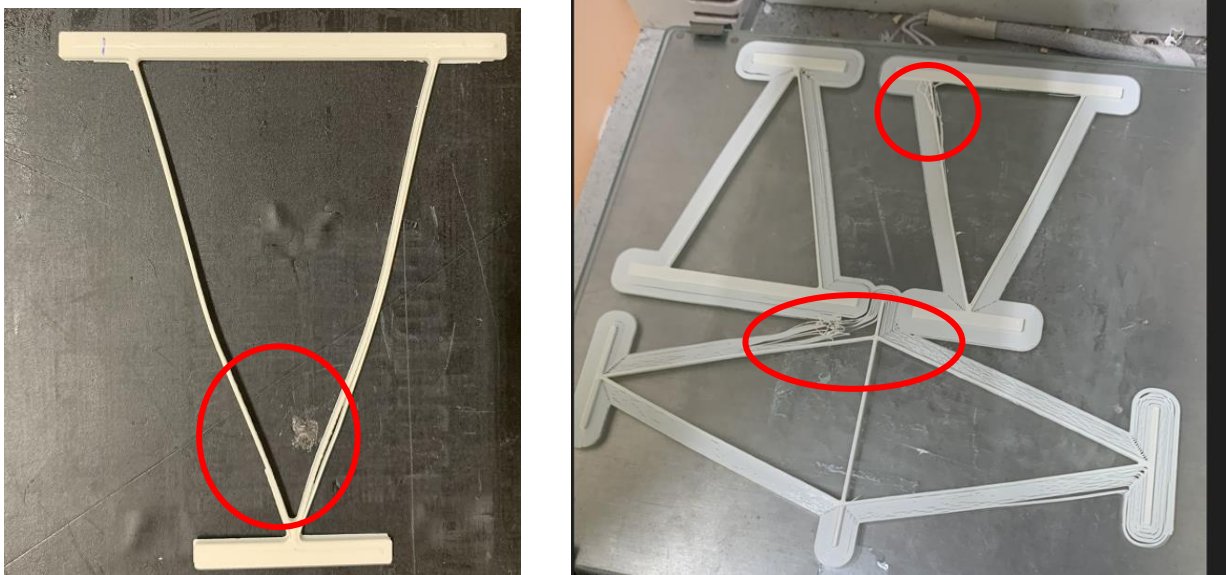


Fig 4.2.1.2 The defect of printed sample

Fig 4.2.1.2 shows the printed sample using default setting. It can clearly seen that the beam filaments did not blend well together. After long time of testing (one month), the optimal printing setting were finally determined.

**Quality**

Layer Height: 0.05 mm

Initial Layer Height: 0.27 mm

Line Width: 0.3 mm

**Material**

Printing Temperature: 215.0 °C

Printing Temperature Initial Layer: 220.0 °C

Initial Printing Temperature: 205.0 °C

Final Printing Temperature: 200.0 °C

Build Plate Temperature: 75.0 °C

Flow Rate Compensation Max Extrusion Offset: 0.0 mm

Flow Rate Compensation Factor: 100.0 %

Wire Printing:

Use Adaptive Layers:

Adaptive Layers Maximum Variation: 0.1 mm

Adaptive Layers Variation Step Size: 0.01 mm

Adaptive Layers Topography Size: 0.2 mm

Overhanging Wall Angle: 3.0 °

Overhanging Wall Speed: 50.0 %

Enable Bridge Settings:

Minimum Bridge Wall Length: 2.4 mm

**Speed**

Print Speed: 30.0 mm/s

Infill Speed: 30.0 mm/s

Wall Speed: 13.0 mm/s

Outer Wall Speed: 9.0 mm/s

Inner Wall Speed: 13.0 mm/s

Top Surface Skin Speed: 13.0 mm/s

Top/Bottom Speed: 13.0 mm/s

Travel Speed: 250.0 mm/s

Fig 4.2.1.3 Optimized print set

Using the printing parameters shown in Fig 4.2.1.3 good quality samples can be obtained with a certain probability.

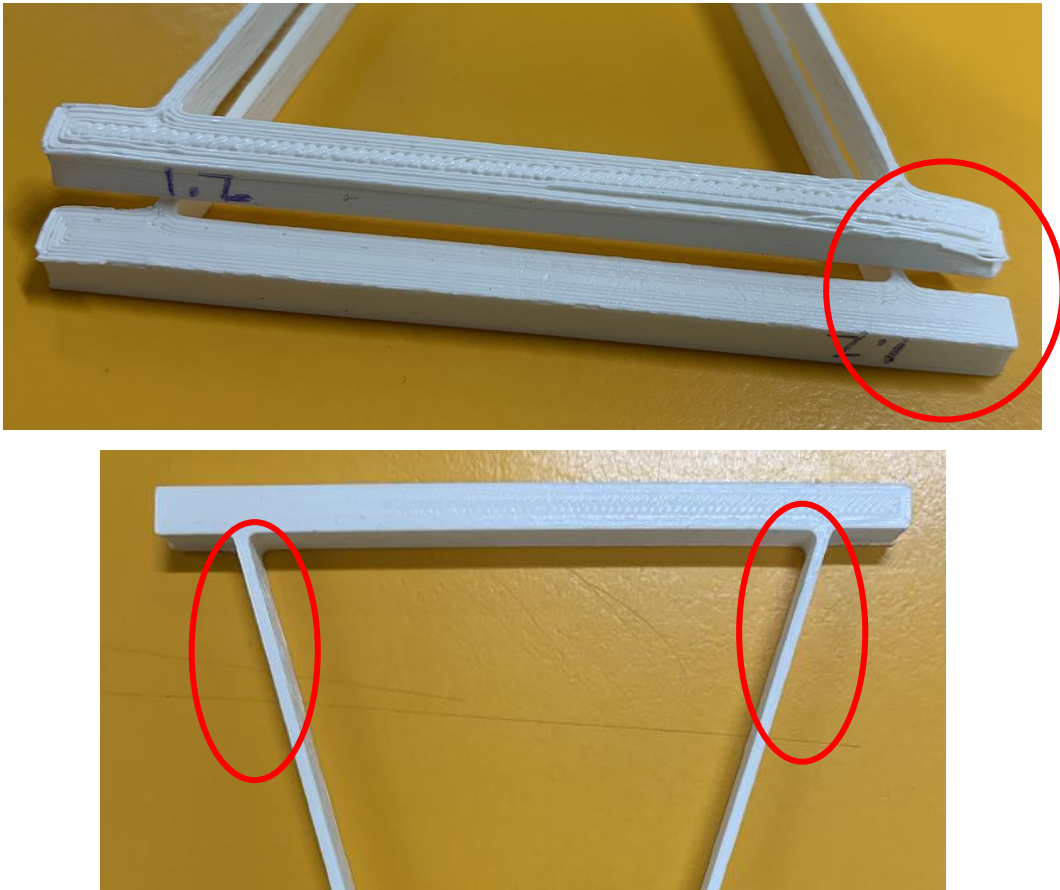


Fig 4.2.1.4 Printed sample by using optimized setting

As mentioned before, using optimized print setting only increases the probability of obtaining good quality samples. Even in the case of using the same printing setting, the obtained samples can be significantly differ one from the other. Fig 4.2.1.4 shows how even when using same print setting, one sample upper part is bent, the other one is not. Also, the two beams show slightly different thickness.

Due to the uncertainty of 3d-printer performance, the best way is to print a large number of samples, and select acceptable ones as experimental samples (Fig 4.2.1.5). Although there are geometric differences between the two beams in the same sample, the difference is very small and within an acceptable range.



Fig 4.2.1.5 Printed sample

#### *4.2.2 3d-printing for support part*

When designing the experimental model, the building volume of the 3D printer has to be taken into consideration, but despite this, it is still challenging to print a complete sample using a 3D printer with uncertain performance. After several attempts, the print settings were finally confirmed (Fig 4.2.2.1). Even if the infill density is 15%, it is strong enough to bear the load during compression and displacement processes. Once printed all the parts, the prototype can be assembled together as previously discussed (Fig 4.2.2.2).

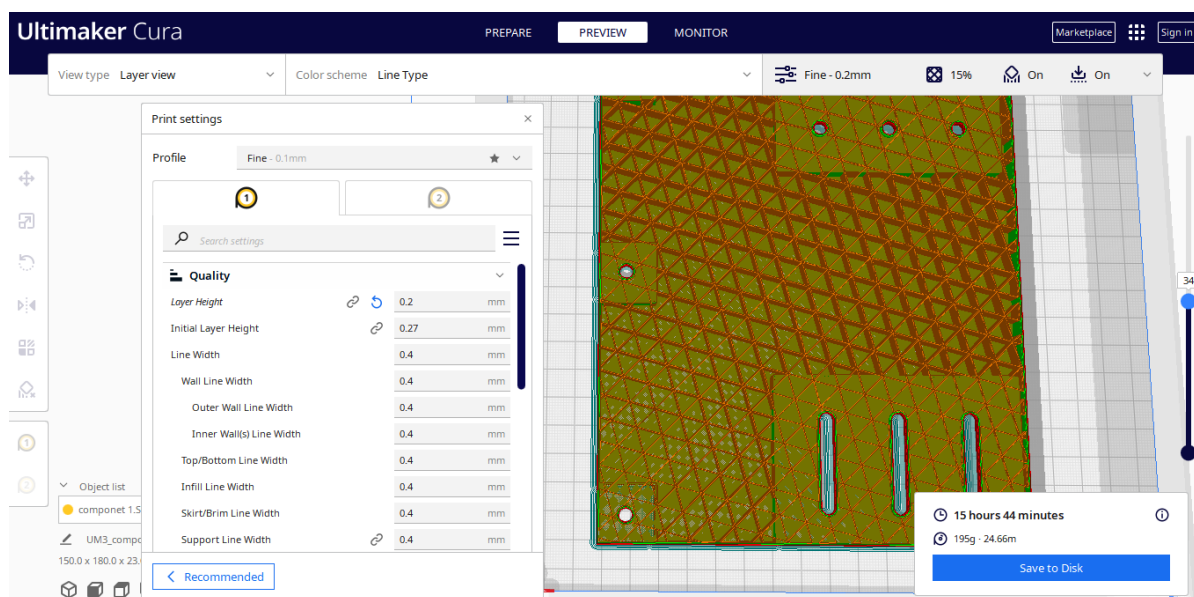


Fig 4.2.2.1 Cura interface of support part

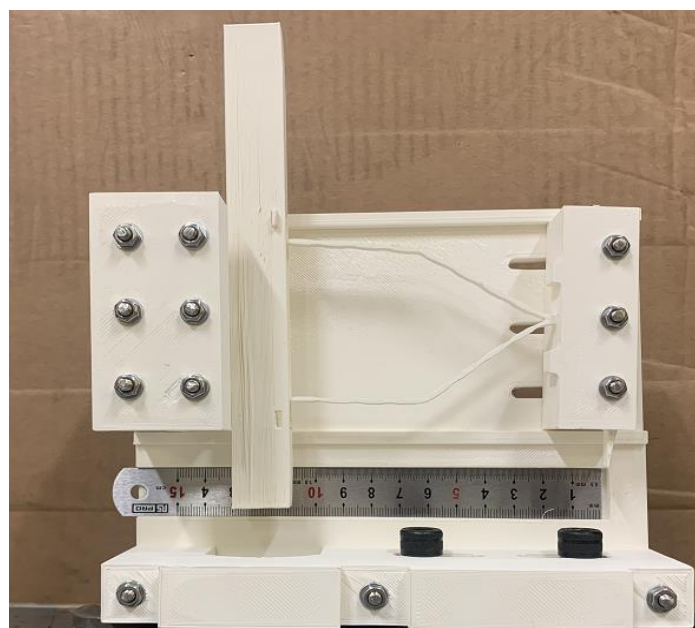


Fig 4.2.2.2 Experimental assemble

## 4.3 Measurement



Fig 4.3.1 MTS test bench

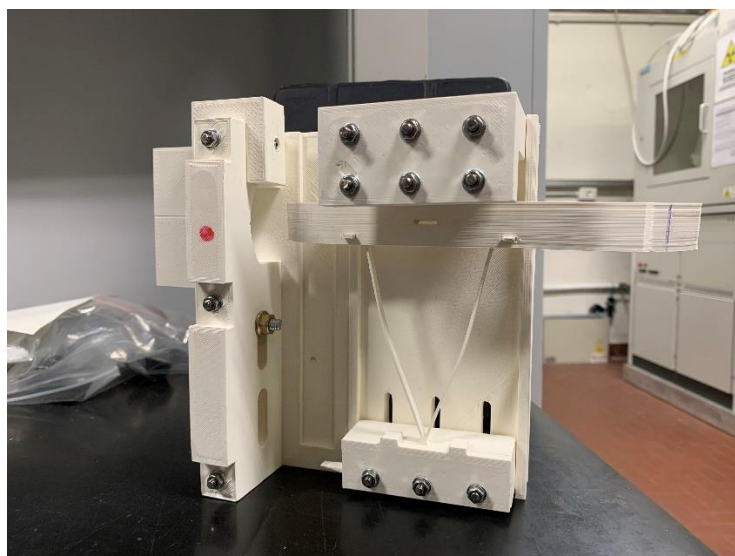


Fig 4.3.2 Experimental assemble

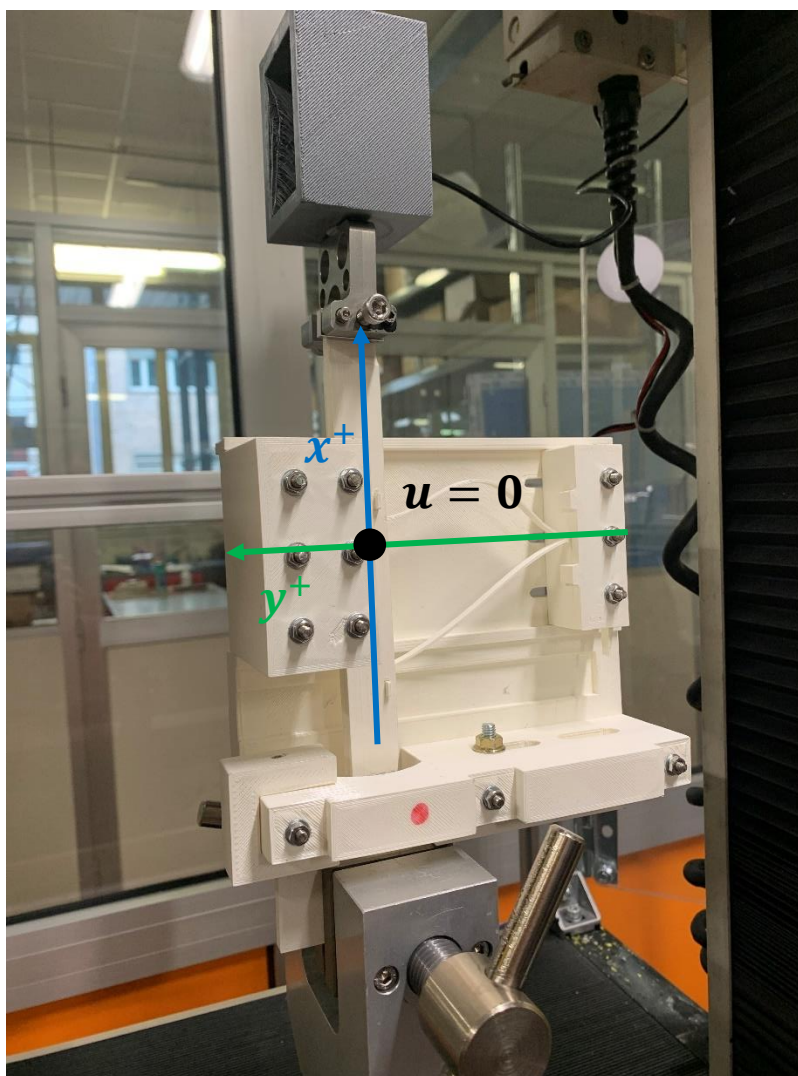


Fig 4.3.3 V-shape initial position

Force-deflection quasi-static measurements are done with an MTS test bench. The instrumentation uses a lower clip to fix the support and an upper clip to pull up or push down the sample. The V-shape beam structure is therefore mounted on the support, with the initial position (stable position) set to at lower side. During the process, the force and displacement are recorded. Transition from high to low stiffness is measured by actuating the linear stage bounded by a force of  $10\text{ N}$  at strain rate of  $10, 15\text{ mm}/\text{min}$ . Gravity is not accounted for.

There is a certain error for measuring the preloading distance due to geometry tolerance and manual error.

This error can be considered as  $\pm 1 \text{ mm}$ .

The experimental procedure is as follow:

1. Setting  $t = 1.2 \text{ mm}$ ,  $D = 5 \pm 1 \text{ mm}$  and strain rate  $10 \text{ mm}/\text{min}$ , measure the force-deflection curve (Experiment 1, Table 4.3.4).
2. Using same sample and preloading, measure the force deflection curve under  $15 \text{ mm}/\text{min}$  strain rate (Experiment 2, Table 4.3.4).
3. Change the preloading to  $D = 10 \pm 1 \text{ mm}$ , the strain rate remains at  $15 \text{ mm}/\text{min}$ . Measure the force deflection (Experiment 3, Table 4.3.4).
4. Use the  $t = 1 \text{ mm}$  V-shape beam, set the preloading to  $D = 10 \pm 1 \text{ mm}$ , measure the force deflection curve under same strain rate (Experiment 4, Table 4.3.4).

The purpose of the experiment is to compare the mathematical model (MATLAB model) and Ansys simulation results with the experimental results.

	<i>Preloading</i>	<i>Strain rate</i>	<i>Beam thickness</i>	<i>Direction</i>	<i>Displacement</i>
<i>Experiment 1</i>	$5 \pm 1 \text{ mm}$	$10 \text{ mm}/\text{min}$	$1.2 \text{ mm}$	$X +$	$30 \text{ mm}$
<i>Experiment 2</i>	$5 \pm 1 \text{ mm}$	$15 \text{ mm}/\text{min}$	$1.2 \text{ mm}$	$X +$	$30 \text{ mm}$
<i>Experiment 3</i>	$10 \pm 1 \text{ mm}$	$15 \text{ mm}/\text{min}$	$1.2 \text{ mm}$	$X + \text{ to } X -$	$43 \text{ mm}$
<i>Experiment 4</i>	$10 \pm 1 \text{ mm}$	$15 \text{ mm}/\text{min}$	$1 \text{ mm}$	$X + \text{ to } X -$	$43 \text{ mm}$

Table 4.3.4

# 5 Results and Discussion

## 5.1 Force deflection result comparison

All the experiment results are affected by noise and show fluctuation due to friction between the bearings and the sliding mass. The data post processing makes use of Zero-phase digital filtering and Polynomial curve fitting.

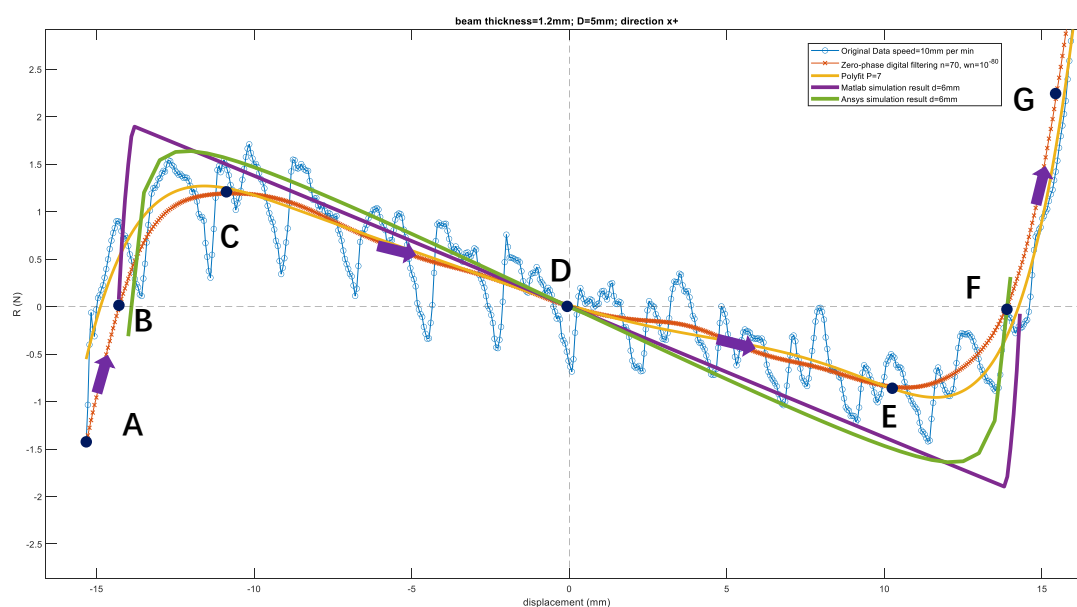


Fig 5.1.1 1.2 mm beam thickness,  $D = 5 \text{ mm}$ ,  $v = 10 \text{ mm}/\text{min}$  (Experiment 1)

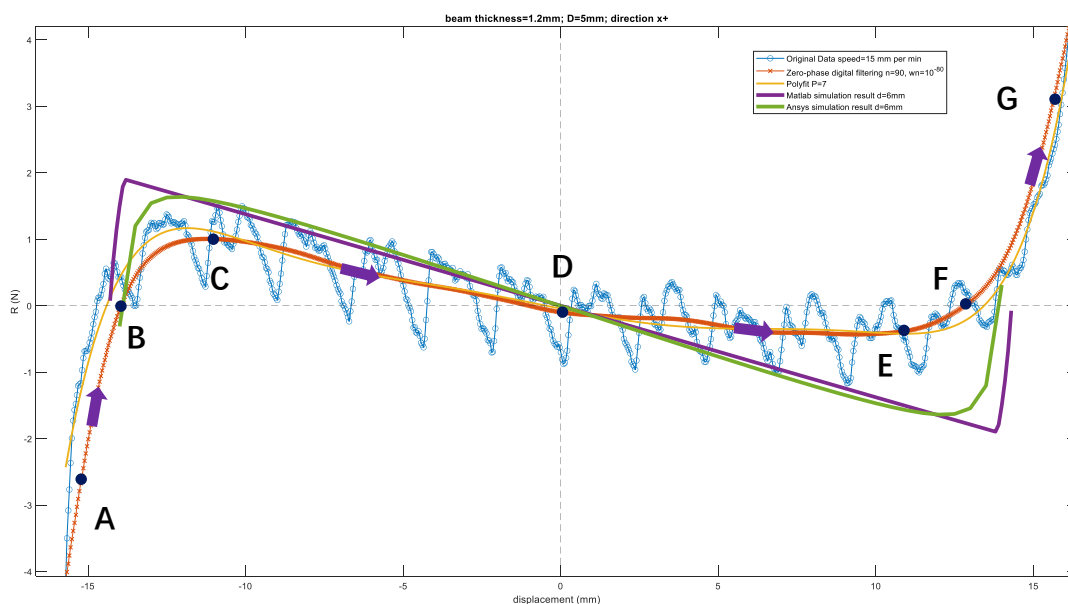


Fig 5.1.2 1.2 mm beam thickness,  $D = 5 \text{ mm}$ ,  $v = 15 \text{ mm}/\text{min}$  (Experiment 2)

For the Experiment 1 and Experiment 2 (Fig 5.1.1 and Fig 5.1.2), considering the error of preloading is  $\pm 1 \text{ mm}$ , the experimental results have a good fitting with respect to simulation at  $d = 6 \text{ mm}$ . Comparing the results of Experiment 1 with Experiment 2, the slope of the negative stiffness region for the Experiment 1 is steeper than the Experiment 2. This is mainly due to the damage of the V-shape beam. Prof. Eutioonat-Difo ([8]) have found that the Young's Modulus of PLA decreases for increasing values of elongation (Fig 5.1.3). During our experiment, the beams is already into the plastic deformation region after the 5 mm preloading. The elongation of the two beams increases during the displacement process, meaning that the stiffnesses of the beams decrease together with the Young Modulus. Based on this phenomenon, the slope of negative stiffness region of second test is more flat than the first test.

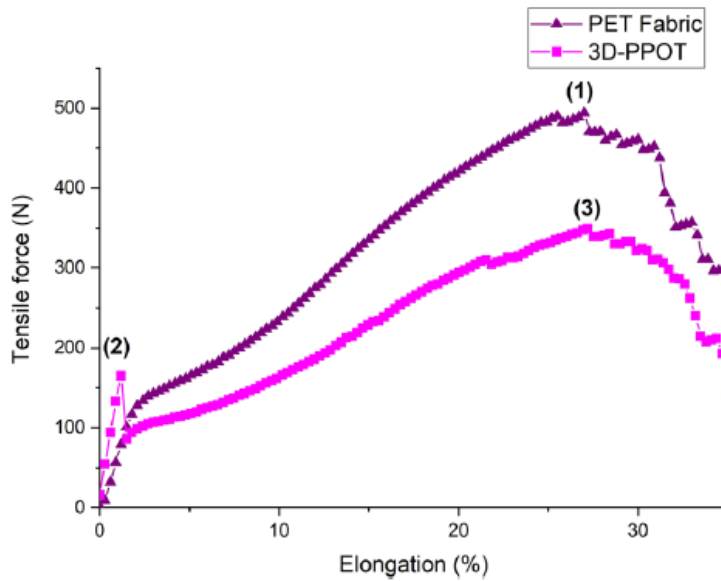


Fig 5.1.3 Tensile force–Elongation curves of PET and 3D-PPOT (using PLA filament printed) [8]

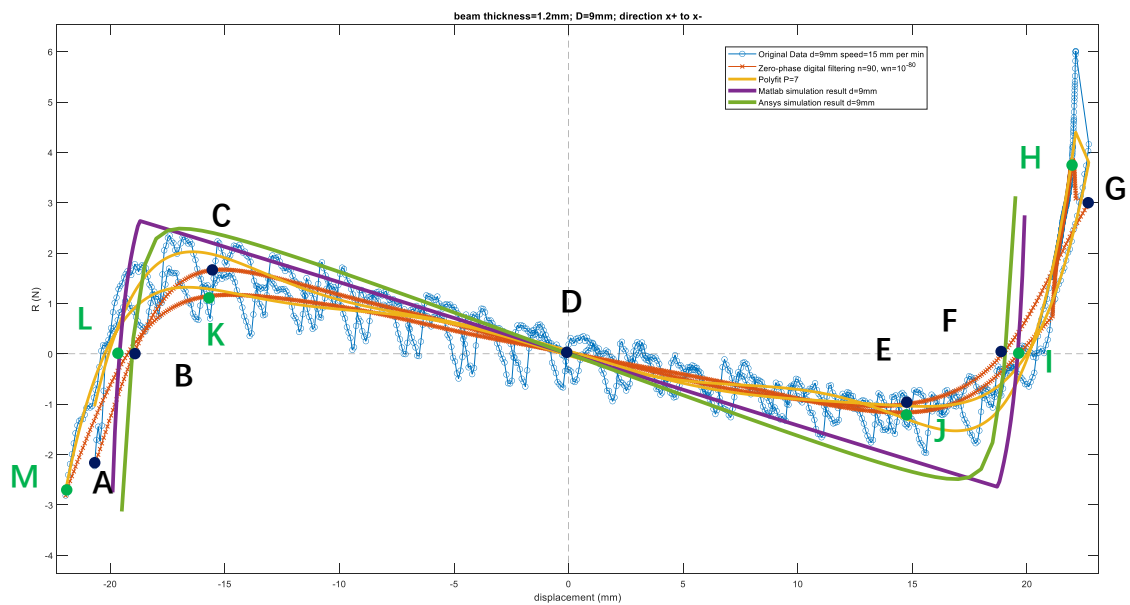


Fig 5.1.4 1.2 mm beam thickness,  $D = 9 \text{ mm}$ ,  $v = 15 \text{ mm}/\text{min}$  (Experiment 3)

For Experiment 3 (Fig 5.1.4), the pulling direction is  $x^+$  (A to G). The test is then repeated by setting the

pushing direction as  $x^-$  (H to M).

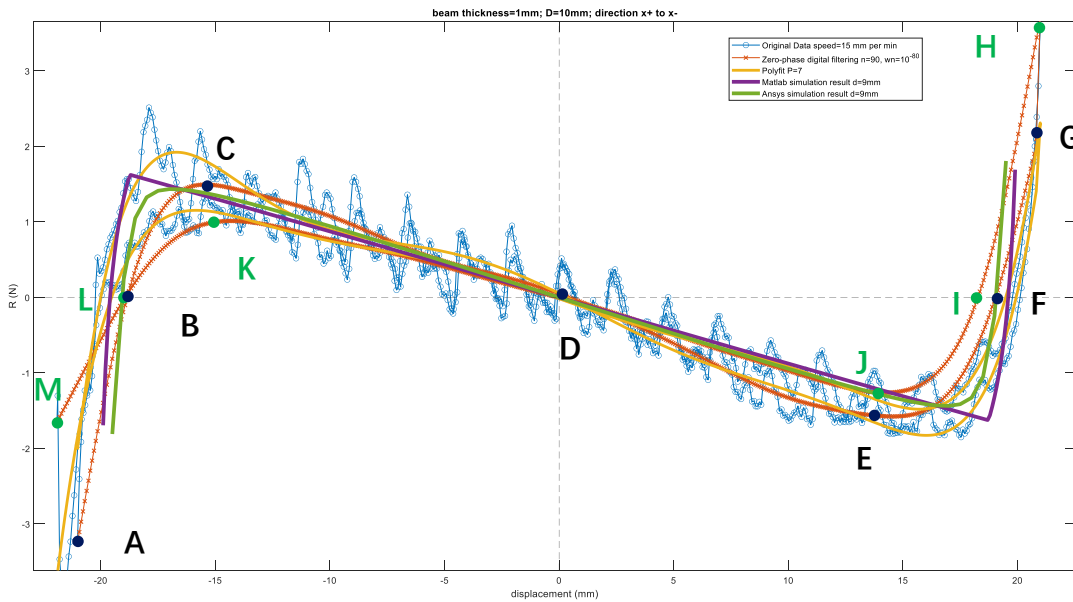


Fig 5.1.5 1 mm beam thickness,  $D = 10 \text{ mm}$ ,  $v = 15 \text{ mm}/\text{min}$  (Experiment 4)

For the Experiment 4, the direction is  $x^+$  from A to G points (Fig 5.1.5) and  $x^-$  from H to M points (Fig 5.1.5). For a brand-new V-shape beam test, the experimental result has very well fit with simulation result (Fig 5.1.5). Although the experimental results and simulation results have large differences in the range of negative stiffness, the trends exhibited in the negative stiffness region are similar. The MATLAB model and the Ansys model perfectly show the variation of the force in the negative stiffness region, and further model updating is needed to fit the experimental results in the nonlinear region (A-C, E-G, H-J, K-M).

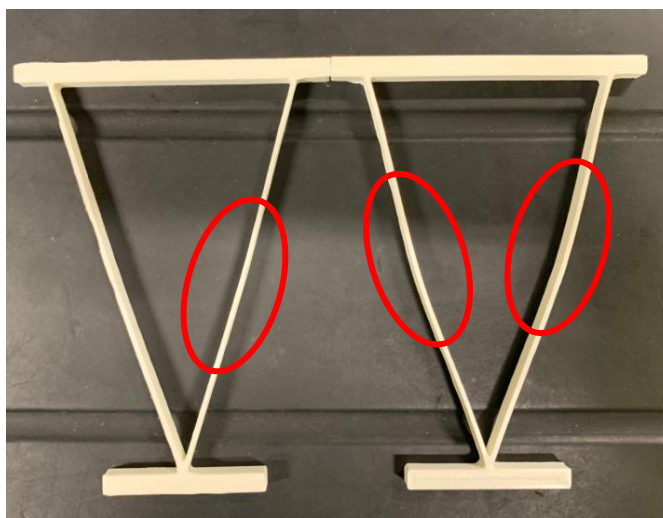


Fig 5.1.6 V-shape beam after experiment (left:  $t = 1 \text{ mm}$ ; right:  $t = 1.2 \text{ mm}$ )

After the experiment, the V-shape clearly shows a permanent deformation, and this is the main reason for the differences between the experimental results and simulation results. The developed MATLAB model can properly simulate the quasi-static behavior during the displacement process. If the material of sample is using steel or other metal instead of generic PLA, it can be expected that there will be better fitting.

$$R(u) = p_1u^7 + p_2u^6 + p_3u^5 + p_4u^4 + p_5u^3 + p_6u^2 + p_7u + p_8 \quad (\text{Eq 5.1.1})$$

For Polynomial curve fitting, let us consider the Polynomial degree equal to 7. The fitting parameter are listed in the following table:

	$p_1$	$p_2$	$p_3$	$p_4$	$p_5$	$p_6$	$p_7$	$p_8$
Experiment 1	4.35e-08	1.67e-07	-9.44e-06	-5.32e-05	5.36e-04	5.20e-03	-1.03e-01	1.62e-02
Experiment 2	6.23e-08	-1.17e-07	-1.62e-05	2.31e-05	1.30e-03	2.10e-03	-9.50e-02	-4.38e-02
Experiment 3	8.73e-09	-6.87e-08	-4.51e-06	3.33e-05	7.44e-04	-2.40e-03	-1.36e-01	5.80e-02
Experiment 4	1.04e-08	-1.34e-08	-5.12e-06	1.18e-05	7.48e-04	-2.50e-03	-1.29e-01	1.80e-02

Table 5.1.7

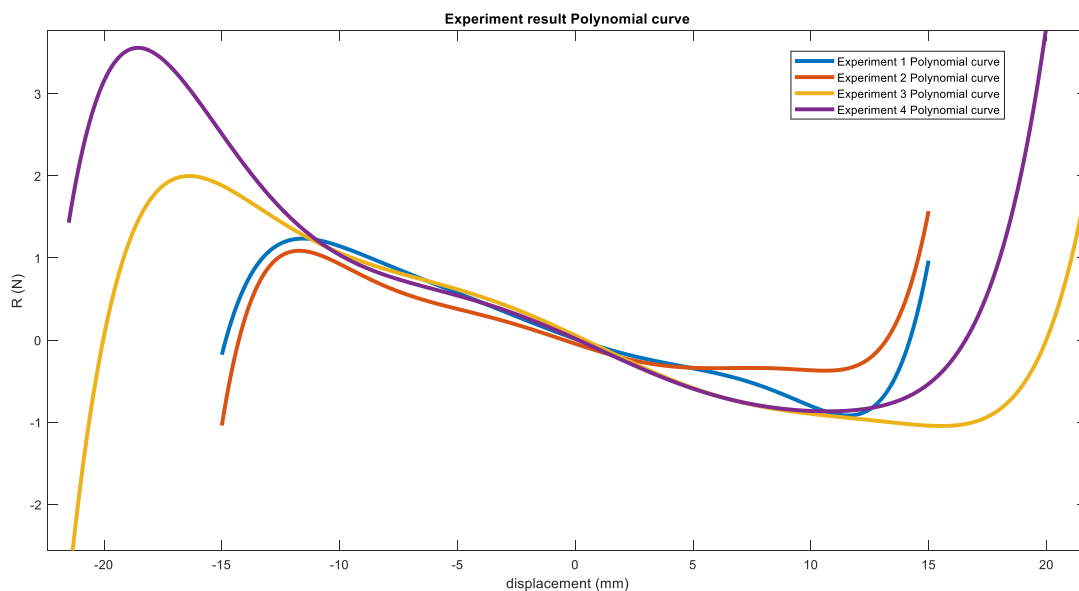


Fig 5.1.8 Polynomial curve (Polynomial degree 7)

By using polynomial equation (Eq 5.1.1) and parameter (Table 5.1.7), the force  $R$  can be represented in Fig 5.1.8.

## 5.2 Negative stiffness comparison

The stiffness can be computed by using the results of the force deflection test ( $K = dR/du$ ). Since the original experimental result are affected by noise and friction phenomena, a Zero-phase filter has been chosen to compute the stiffness along  $X$  axis.

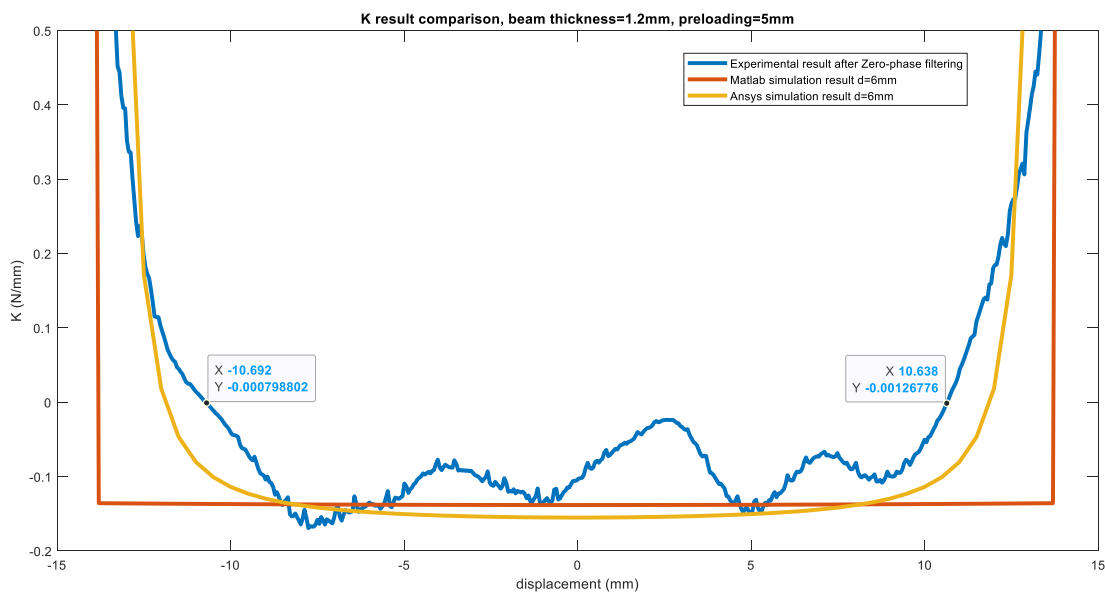


Fig 5.2.1 1.2 mm beam thickness,  $D = 5 \text{ mm}$ ,  $v = 10 \text{ mm}/\text{min}$

The stiffness comparison along  $X$  axis is shown above (Fig 5.2.1 – Fig 5.2.4). For 5 mm preloading with  $v = 10 \text{ mm}/\text{min}$  (Fig 5.2.1), in negative stiffness region, the stiffness shows fluctuation which means the stiffness is not kept constant. The range of negative stiffness is 21.33 mm (consider actual preloading is 6 mm,  $u_{lim, Prediction 1} = 23.71 \text{ mm}$ ).

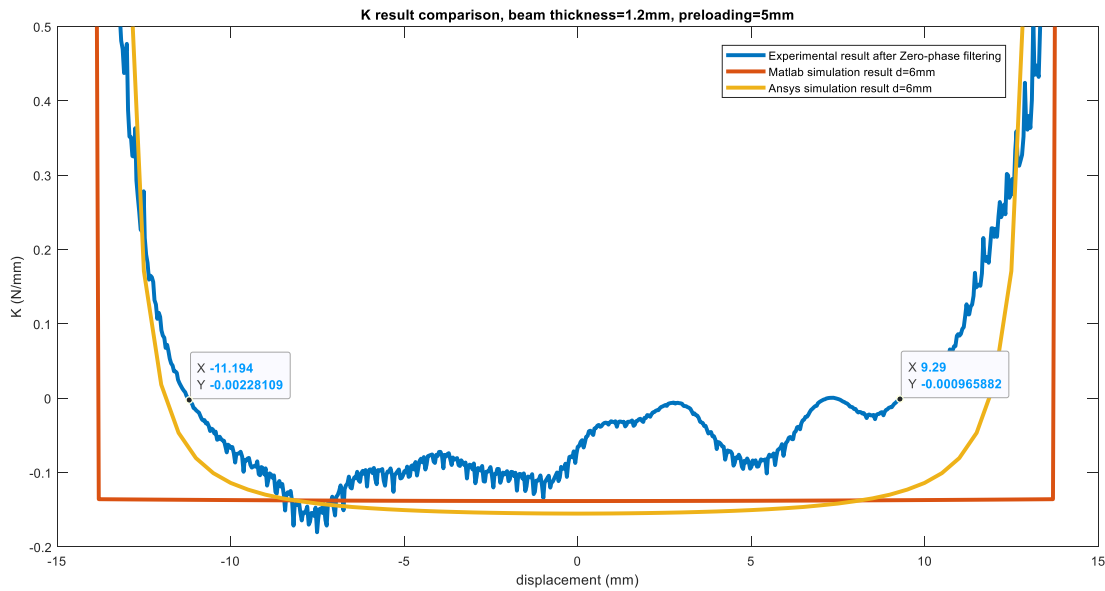


Fig 5.2.2 1.2 mm beam thickness,  $D = 5 \text{ mm}$ ,  $v = 15 \text{ mm}/\text{min}$

For 5 mm preloading with  $v = 15 \text{ mm}/\text{min}$  (Fig 5.2.2), in negative region, the stiffness shows large fluctuation, and it is also asymmetrical. This suggests two beam thicknesses are not the same due to errors of the 3D printing process. The range of negative stiffness is 20.48 mm (consider actual preloading is 6 mm,  $u_{lim, Prediction 2} = 23.71 \text{ mm}$ ) which is the same as previous results during the same preloading condition. As discussed in chapter 2.1.3, the range of negative stiffness only depends on the geometry limitation.

For 9 mm preloading with  $v = 15 \text{ mm}/\text{min}$  (Fig 5.2.3), in negative region, the stiffness is approximately kept constant around  $-0.13 \text{ N}/\text{mm}$  and the negative stiffness range is 28.80 mm (consider actual preloading is 9 mm,  $u_{lim, Prediction 3} = 32.60 \text{ mm}$ ).

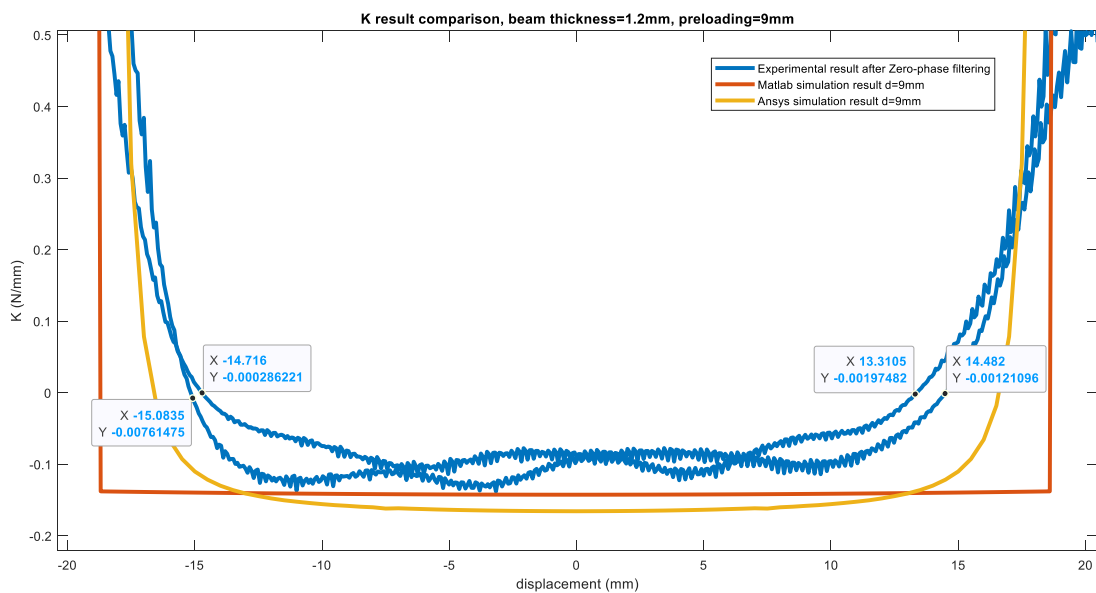


Fig 5.5.3 1.2 mm beam thickness,  $D = 9 \text{ mm}$ ,  $v = 15 \text{ mm}/\text{min}$

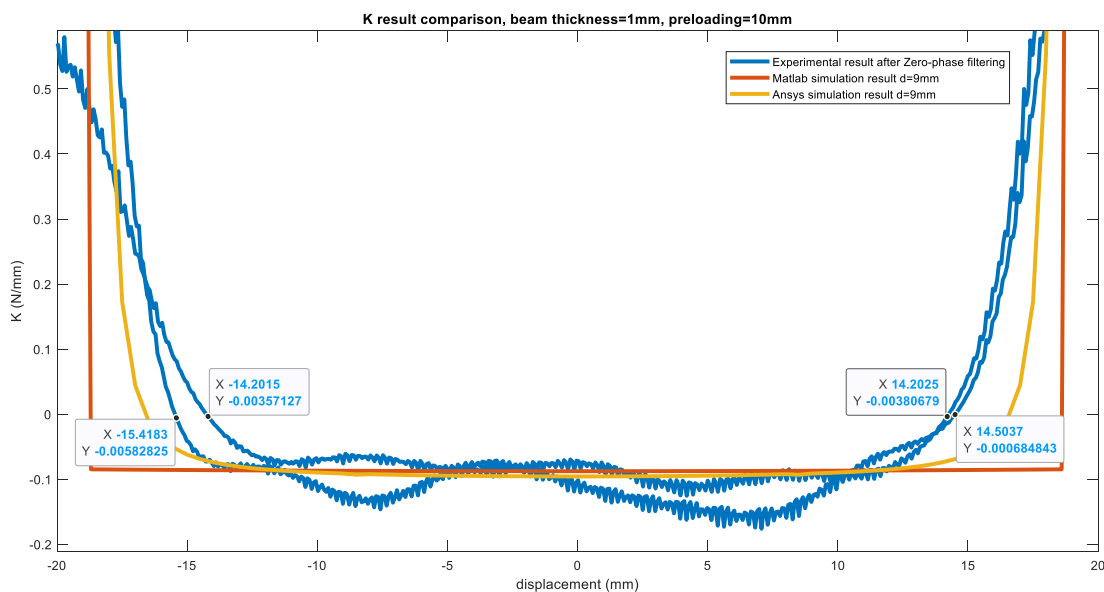


Fig 5.2.4 1 mm beam thickness,  $D = 10 \text{ mm}$ ,  $v = 15 \text{ mm}/\text{min}$

For 10 mm preloading with  $v = 15 \text{ mm}/\text{min}$  (Fig 5.2.4), in the negative region, the stiffness is almost

---

kept constant around  $-0.13 \text{ N/mm}$  and negative stiffness range is  $28.66 \text{ mm}$  (consider actual preloading is  $9 \text{ mm}$ ,  $u_{lim, Prediction 4} = 32.60 \text{ mm}$ ). In theory, this value should not be approximately equal to the one obtained with  $1.2 \text{ mm}$  beam thickness under  $9 \text{ mm}$  preloading and with velocity  $v = 15 \text{ mm/min}$ . But in our experiment, the sample with  $1.2 \text{ mm}$  beam thickness has been tested after the  $5 \text{ mm}$  preloading test, therefore the beam already had plastic deformation. As previously discussed (chapter 5.1), the Young Modulus of PLA materials decreases due to displacement and preloading.

---

## 6 Conclusion

This thesis presents the design and static behavior of a 3D printed V-shape curved beam. In particular, the feasibility of V-shape beam of different designs was discussed, and a new mathematical model (MATLAB based) has been present based on the force analysis of the V-shape beam element, to control the negative stiffness phenomenon under prestress. The mathematical model has been tested first against a FE simulation conducted on Ansys and eventually considering an experimental application. The main conclusions are drawn as follows:

1. The V-shape beam has been proven to be a successful structure to generate a negative stiffness effect. The main advantage is the capability of controlling the preloading to ensure that the negative stiffness remain constant. Future studies might exploit similar structure designs with a rotation behavior.
2. The mathematical model shows good fitting with experimental results especially in the negative stiffness region. For the V-shape beam without multiple plastic deformations, the mathematical model basically agrees with the experimental results. This model can also apply for metal materials which will have wider application.
3. As for the prediction of negative stiffness range, the prediction result is overestimated with respect to the experiment result. This suggests that the analysis of boundary conditions between the beam and the upper wall needs to be further studied.
4. The whole experimental assembly has been designed, and all engineering drawings are shown in chapter 4.1. Based on the current design configuration, the effect of the friction on the experimental results has been reduced.
5. The V-shape beam sample has been manufactured by using 3D printer. For such small scale of beam ( $t = 1 \text{ mm}$  and  $t = 1.2 \text{ mm}$ ), optimal printing setting haven been selected for UltiMaker 3 Extended with  $0.4 \text{ mm}$  nozzle diameter.

---

## 7 References

- [1] Carrella, A., Brennan, M. J., & Waters, T. P. (2007). Static analysis of a passive vibration isolator with quasi-zero-stiffness characteristic. *Journal of sound and vibration*, 301(3-5), 678-689.
- [2] Swiss Federal Institute of Technology in Zürich, Mechanics and Materials Laboratory- Negative stiffness.
- [3] Qiu, Jin; Lang, Jeffrey H.; SLOCUM, Alexander H. A curved-beam bistable mechanism. *Journal of microelectromechanical systems*, 2004, 13.2: 137-146.
- [4] Tan, X., Zhu, S., Wang, B., Yao, K., Chen, S., Xu, P., ... & Sun, Y. (2020). Mechanical response of negative stiffness truncated-conical shell systems: experiment, numerical simulation and empirical model. *Composites Part B: Engineering*, 188, 107898.
- [5] Paros, J. M. "How to design flexure hinges." *Mach des 37 (1965): 151-156*.
- [6] Yong, Yuen Kuan, Tien-Fu Lu, and Daniel C. Handley. "Review of circular flexure hinge design equations and derivation of empirical formulations." *Precision engineering 32.2 (2008): 63-70*.
- [7] Kuppens, P. R., Bessa, M. A., Herder, J. L., & Hopkins, J. B. (2021). Monolithic binary stiffness building blocks for mechanical digital machines. *Extreme Mechanics Letters*, 42, 101120.
- [8] Eutionnat-Diffo, P. A., Chen, Y., Guan, J., Cayla, A., Campagne, C., Zeng, X., & Nierstrasz, V. (2019). Stress, strain and deformation of poly-lactic acid filament deposited onto polyethylene terephthalate woven fabric through 3D printing process. *Scientific reports*, 9(1), 1-18.
- [9] Fan, H., Yang, L., Tian, Y., & Wang, Z. (2020). Design of metastructures with quasi-zero dynamic stiffness for vibration isolation. *Composite Structures*, 243, 112244.
- [10] Liu, M., Zhang, X., & Fatikow, S. (2016). Design and analysis of a high-accuracy flexure hinge. *Review of Scientific Instruments*, 87(5), 055106.